

NATIONAL BUREAU OF STANDARDS REPORT

3431

High-Temperature Thermodynamics
Technical Report II

Edited by A. M. Bass

Division of Heat and Power



U. S. DEPARTMENT OF COMMERCE
NATIONAL BUREAU OF STANDARDS

U. S. DEPARTMENT OF COMMERCE

Sinclair Weeks, *Secretary*

NATIONAL BUREAU OF STANDARDS

A. V. Astin, *Director*



THE NATIONAL BUREAU OF STANDARDS

The scope of activities of the National Bureau of Standards is suggested in the following listing of the divisions and sections engaged in technical work. In general, each section is engaged in specialized research, development, and engineering in the field indicated by its title. A brief description of the activities, and of the resultant reports and publications, appears on the inside of the back cover of this report.

Electricity. Resistance and Reactance Measurements. Electrical Instruments. Magnetic Measurements. Electrochemistry.

Optics and Metrology. Photometry and Colorimetry. Optical Instruments. Photographic Technology. Length. Engineering Metrology.

Heat and Power. Temperature Measurements. Thermodynamics. Cryogenic Physics. Engines and Lubrication. Engine Fuels. Cryogenic Engineering.

Atomic and Radiation Physics. Spectroscopy. Radiometry. Mass Spectrometry. Solid State Physics. Electron Physics. Atomic Physics. Neutron Measurements. Infrared Spectroscopy. Nuclear Physics. Radioactivity. X-Ray. Betatron. Nucleonic Instrumentation. Radiological Equipment. Atomic Energy Commission Radiation Instruments Branch.

Chemistry. Organic Coatings. Surface Chemistry. Organic Chemistry. Analytical Chemistry. Inorganic Chemistry. Electrodeposition. Gas Chemistry. Physical Chemistry. Thermochemistry. Spectrochemistry. Pure Substances.

Mechanics. Sound. Mechanical Instruments. Fluid Mechanics. Engineering Mechanics. Mass and Scale. Capacity, Density, and Fluid Meters. Combustion Control.

Organic and Fibrous Materials. Rubber. Textiles. Paper. Leather. Testing and Specifications. Polymer Structure. Organic Plastics. Dental Research.

Metallurgy. Thermal Metallurgy. Chemical Metallurgy. Mechanical Metallurgy. Corrosion.

Mineral Products. Porcelain and Pottery. Glass. Refractories. Enameled Metals. Concreting Materials. Constitution and Microstructure.

Building Technology. Structural Engineering. Fire Protection. Heating and Air Conditioning. Floor, Roof, and Wall Coverings. Codes and Specifications.

Applied Mathematics. Numerical Analysis. Computation. Statistical Engineering.

Electronics. Engineering Electronics. Electron Tubes. Electronic Computers. Electronic Instrumentation. Process Technology.

Radio Propagation. Upper Atmosphere Research. Ionospheric Research. Regular Propagation Services. Frequency Utilization Research. Tropospheric Propagation Research. High Frequency Standards. Microwave Standards.

● Office of Basic Instrumentation

● Office of Weights and Measures.

NATIONAL BUREAU OF STANDARDS REPORT

NBS PROJECT

July 9, 1954

NBS REPORT

0301-20-2674

3431

High-Temperature Thermodynamics Technical Report II

Edited by A. M. Bass

Division of Heat and Power



**U. S. DEPARTMENT OF COMMERCE
NATIONAL BUREAU OF STANDARDS**

The publication, reprint, or translation, without the express permission of the National Institute of Standards and Technology, is prohibited.

Approved for public release by the
Director of the National Institute of
Standards and Technology (NIST)
on October 9, 2015

part, is prohibited
ards, Washington
rt has been specifi-
ort for its own use.

Work of the Heat and Power Division
National Bureau of Standards
in High Temperature Thermodynamics

Foreword

For a number of years several groups in the Heat and Power Division of the National Bureau of Standards have been actively engaged in a program of research in the field of high temperature physics and chemistry. It has been the aim of this program to study the thermometric and thermodynamic properties of matter at elevated temperatures in as great detail as possible to provide the basic information that is needed in present-day technology of high temperature systems.

The first progress report on this program was issued in August 1951 (NBS Report 1123, "High Temperature Thermodynamics Technical Report"). This second report summarized the progress and accomplishments of the several groups involved in this program from that date until March 1954. The main topics discussed in this report are: studies of radiation from high temperature equilibrium and non-equilibrium systems; development of the noise thermometer; the work of the pyrometry laboratory in high temperature measurement; measurement of thermal conductivities and heat capacities at high temperatures. A number of the papers included herein have been submitted for publication in scientific journals and they are reported here for the sake of giving a complete picture of the program.

The work in this reporting period has been supported by several agencies including the National Bureau of Standards, Office of Naval Research, Office of Ordnance Research (Army), Wright Air Development Center (Air Force), National Advisory Committee for Aeronautics, and the Atomic Energy Commission.

A later report will describe studies of infrared radiation from hot gases which has been carried on as part of this program under the sponsorship of the WADC.

Dr. F. G. Brickwedde, Chief
Division of Heat and Power

A. V. Astin, Director
National Bureau of Standards

TABLE OF CONTENTS

1.	Introduction. A. M. Bass and R. D. Arnold	1
2.	A High Temperature Absorption Tube Furnace. R. D. Arnold	6
3.	Design and Construction of a "Blackbody" and its use in the Spectral Intensity Calibration of a Grating Monochromator. G. T. Lalos, R. J. Corruccini and H. P. Broida	27
4.	A Survey of Flame Spectra. N. H. Kiess	43
5.	The $\lambda 4050$ Group of Cometary Spectra in the Acetylene-Oxygen Flame N. H. Kiess and A. M. Bass	68
6.	The Decomposition of CF_4 in Flames. B. E. Squires	74
7.	Ultraviolet Absorption Spectroscopy of Spark Ignited, Low Pressure Explosions. H. P. Broida, A. J. Everett and G. J. Minkoff	91
8.	Use of a Vacuum Spectrograph for Combustion Study. W. R. S. Garton and H. P. Broida	102
9.	Development Work on the Noise Thermometer. E. W. Hogue	104
10.	The Pyrometry Laboratory. J. P. Evans	111
11.	Thermal Conductivities at High Temperatures. D. C. Ginnings and R. L. Nuttall	113
12.	Heat Capacities at High Temperatures. T. B. Douglas and E. D. West	115

1. Introduction - Radiation Studies of Systems at High Temperatures

A. M. Bass and R. D. Arnold

The High Temperature Laboratory of the Temperature Measurements Section was established in 1949 to investigate methods of determining temperatures, the accuracy of such methods, and the meaning of such temperatures in hot gases (above 1000°C). As a direct corollary to investigations of this kind, studies of non-equilibrium processes and the chemical kinetics involved in the combustion of hydrocarbon and other gaseous fuels have been of great interest. In August 1951 there was issued "Technical Report on High Temperature Thermodynamics - NBS Report 1123" which summarized the status of the program to that date.

Since that time the high temperature research program has proceeded in the direction outlined in the 1951 report. For the period since the appearance of the first report it is possible to summarize the progress made in this program in several categories.

1. The Molecule OH as a Thermometer

On the question of whether the radiation from OH in flames is of thermal or chemiluminescent origin, there are indications that in the inner cone of the acetylene-oxygen flame the radiation of OH(${}^2\Sigma^+$) is, to a large extent chemiluminescent [6]. It has also been found that in the outer cone of flames at atmospheric pressure diluted with N₂, He, or A, and also in electrodeless discharges through water vapor, the rotational distribution is abnormal [13,15]. These studies show that not only is the OH (${}^2\Sigma^+$) formed in a non-thermal distribution, but that the abnormal distribution of rotation is quite persistent ($\sim 10^4$ collisions). The theoretical calculations of the vibrational and rotational distributions in which OH is formed in certain elementary chemical reactions, using the method developed by Golden, was coded for SEAC computation, and two sample computations have been made.

In attempting to use the emission spectrum of OH as a temperature indicator, it is known that one must exercise considerable care in interpreting the results obtained. In this connection the effects of self-absorption on apparent rotational temperatures of OH in flames have been studied both theoretically and experimentally. The conditions were determined under which the errors caused by this effect are minimized [14]. Also the rotational distribution in OH in flames was found to be dependent upon the vibrational state of the emitter [11]. This is probably an indication of the effect of vibration-rotation interaction on the rotational transition probabilities which were calculated by Dieke and Crosswhite without regard to this interaction. Both the ground state (absorption) and the excited state (emission) have been investigated.

2. Studies of Other Molecules

An investigation of the use of the CH rotational intensity distribution has led to the conclusion that this molecule is unreliable as a temperature indicator [12]. In the inner cone the rotational distribution indicates that the excited CH is formed by a nonthermal process. The CH concentration in the outer cone is too small for the CH spectrum to be observed.

In addition to the visible and ultraviolet measurements described above, the program of infrared studies, as outlined in the preceding report, was continued. The detailed results will be presented in a later report, but a few items of interest may be mentioned here. The infrared emission of HF in a hydrogen-fluorine flame was observed and consistent vibrational temperatures of $4000 \pm 100^\circ\text{K}$ were measured. Rotational temperatures were erratic because of self-absorption effects [10].

A new infrared band system of FeO has been discovered and analyzed. The band extends from 0.7 to 1.4 microns and probably arises from a resonance transition of the molecule [7].

Measurements and analyses have been made on carbon dioxide and water vapor absorption in the infrared at temperatures up to 400°C and pressures up to 50 atmospheres. Observed integrated absorption coefficients are in order of magnitude agreement with calculated values. High resolution spectra in emission and absorption of water vapor and carbon monoxide have been measured and analyzed completely for several regions of the infrared [8, 9, 26].

3. Flame Structure and Combustion Reactions

Along with measurement of temperature, observations have been made leading to better understanding of flame structure and to mechanism of combustion. Polyhedral flames were obtained in burning hydrogen and oxygen and propane and oxygen diluted with argon, nitrogen, or helium. The observations tend to support the theory that cellular structure in flames is caused by spatial variation of mixture composition brought about by differential diffusion [4].

A photographic survey of the spectra of flames of various fuels (including fluorocarbons), mixture ratios, and dilutions has been completed. The purpose of the survey was to disclose flame conditions and spectral regions in which more detailed spectrophotometric studies would most likely be fruitful. The survey led directly to the first observation of the cometary bands of the C_2 molecule in hydrocarbon flame spectra. The details of these studies are given later in this report [21, 24].

Spectroscopic studies by Broida and Gaydon at Imperial College have shown that the probable mechanism for the formation of excited OH, CH, and HCO in flames is by secondary chemical reaction rather than by dissociation of larger molecules [19]. Evidence for the intermediate reaction of carbon monoxide and atomic oxygen to form excited carbon dioxide also was found [16].

A detailed study has been made of the radiation emitted by atomic flames - i.e. reactions between fuels and excited species formed in electrical discharges. The optical spectroscopic data has been correlated with chemical and mass spectrometric data and the details of this study have been described in NBS Report #3384 [27].

4. Instrumentation

Construction of the high temperature absorption tube furnace was completed, and is described in detail in this report.

Several stainless steel gas sample containers have been constructed for use in measurements of infrared absorption of gases. The vessels are designed for temperatures to 1000°C and for pressures in excess of 100 atmospheres. They provide a variety of path lengths from a few mm to about 15 cm.

Several apparatuses have been constructed for the purpose of studying atomic flames. These have provision for production of atoms by both high voltage discharge between aluminum electrodes, and high frequency electrodeless discharge. With the apparatus it is possible to sample the flame reaction optically by studying the emitted radiation, and chemically by extracting reaction products for chemical and mass spectrometric analysis.

A low pressure burner has been constructed in which it has been possible to observe the combustion of acetylene and oxygen at pressures as low as a few mm of Hg (corresponding to an altitude greater than 100,000 ft.). The burner has fused silica windows 5 inches in diameter so that it may be used for studies of emission and absorption of radiation by the molecules in the flame over the wavelength range 2000 Å to 3.5 microns.

The Perkin-Elmer spectrometer has been converted to double-pass grating operation, using a grating ruled with 7500 lines/inch. With this arrangement a resolving power of 6000 (0.6 cm^{-1} at 3600 cm^{-1}) has been achieved. Also the Leeds and Northrup grating spectrometer is being modified for infrared operation and in preliminary tests has shown a resolving power of 10,000 at 1.4 microns.

The more recent results of this program, as well as of related high temperature research in the Heat and Power Division, are presented in the balance of this report.

Publications of the High Temperature Program Since August 1951

- [1]. Rotational Temperatures of OH in Methane-Air Flames.
J. Chem. Phys. 19, 1383 (1951), H. P. Broida.
- [2]. Combustion in Bunsen Flames.
Ind. Eng. Chem. 43, 2731 (1951), F. R. Caldwell, H. P. Broida and J. J. Dover.
- [3]. Kinetics of OH Radicals, IV; Hydrogen-Oxygen Flame.
J. Chem. Phys. 20, 168 (1952), H. P. Broida and K. E. Shuler.
- [4]. Polyhedral Flames in Hydrogen and Hydrocarbons.
J. Chem. Phys. 20, 1042 (1952), W. R. Kane and H. P. Broida.
- [5]. Rotational Temperatures of OH in Several Flames.
J. Chem. Phys. 20, 1466 (1952). H. P. Broida and G. T. Lalos.
- [6]. Kinetics of OH Radicals, V; Acetylene-Oxygen Flame.
J. Chem. Phys. 20, 1383 (1952), K. E. Shuler and H. P. Broida.
- [7]. A New Infrared Band System of FeO.
Astrophys. J. 116, 652 (1952), A. M. Bass and W. S. Benedict.
- [8]. Precise Measurements in the Infrared Spectrum of CO.
J. Chem. Phys. 20, 175 (1952) E. K. Plyler, W. S. Benedict,
and S. Silverman.
- [9]. Absorption Spectrum of H₂O between 4 μ and 13.5 μ .
J. Res. NBS 49, 91 (1952), W. S. Benedict, H. H. Claassen, and J. Shaw.
- [10]. Infrared Emission of the Hydrogen-Fluorine Flame.
Phys. Rev. 87, 213A (1952), W. S. Benedict, B. W. Bullock, S. Silverman,
and A. V. Grosse.
- [11]. Effects of Vibrational State on Rotational Intensity Distributions in OH.
J. Chem. Phys. 21, 173 (1953). A. M. Bass and H. P. Broida.
- [12]. Rotational and Vibrational "Temperatures" of CH in Flames at Atmospheric Pressure.
J. Chem. Phys. 21, 340 (1953), H. P. Broida.
- [13]. Rotational "Temperatures" of OH in Diluted Flames.
J. Chem. Phys. 21, 347 (1953), W. R. Kane and H. P. Broida.
- [14]. Effects of Self-Absorption on Rotational "Temperatures" of OH in Flames.
J. Chem. Phys. 21, 1165 (1953), H. P. Broida.

- [15]. Rotational Intensity Distributions of OH and OD in an Electrodeless Discharge through Water Vapor.
Phys. Rev. 89, 1053 (1953), H. P. Broida and W. R. Kane.
- [16]. The Luminous Reaction between Carbon Monoxide and Atomic Oxygen.
Trans. Farad. Soc. 49, 1190 (1953), H. P. Broida and A. G. Gaydon.
- [17]. Use of a Vacuum Spectrograph for Combustion Study.
Fuel 32, 519 (1953), W. R. J. Garton and H. B. Broida
- [18]. A Spectrophotometric Atlas of the $2\Sigma^+ \rightarrow 2\pi$ Transition in OH.
N.B.S. Circular No. 541 (1953), A. M. Bass and H. P. Broida.
- [19]. The Mechanism of Formation of OH, CH, and HCO in Flame Spectra, Using Deuterium as Tracer.
Proc. Roy. Soc. A218, 60 (1953), H. P. Broida and A. G. Gaydon.
- [20]. Note on the Ultraviolet Spectrophotometry of Spark Ignited Low Pressure Explosions.
Fuel 33, (1954), A. J. Everett, G. J. Minkoff, H. P. Broida.
- [21]. The Decomposition of CF_4 in Flames.
J. Chem. Phys. 22, 348 (1954), H. P. Broida, D. E. Mann, B. E. Squires.
- [22]. The Herzberg Bands of O_2 in an Oxygen Afterglow and in the Night-Sky, Spectrum.
Proc. Roy. Soc., A222, 181 (1954), H. P. Broida and A. G. Gaydon.
- [23]. The Forbidden $3\Sigma^+ + u \rightarrow 3\Sigma_g^-$ Emission Bands of O_2 .
J. de Physique (1954). H. P. Broida and A. G. Gaydon.
- [24]. The $\lambda 4050$ Group of Cometary Spectra in Acetylene-Oxygen Flames.
J. Chem. Phys. 22, 569 (1954), N. H. Kiess and A. M. Bass.
- [25]. Energy Transfer in Hot Gases.
N.B.S. Circular No. 523 (1954), Edited by A. M. Bass.
This volume contains
- a. High-Resolution Studies of Infrared Flame Emission, W. S. Benedict and E. K. Plyler.
 - b. Distribution of OH Rotational Temperatures in Flames. H. P. Broida.
- [26]. The Flame Emission Spectrum of H_2O ; I. The 1.9μ Region.
J. Res. N.B.S. 52, 161 (1954), W. S. Benedict, A. M. Bass, and E.K. Plyler.
- [27]. Atomic Flames: Spectra, "Temperatures", and Products.
N.B.S. Report No. 3384 (1954), R.F. Ferguson and H. P. Broida.

2. A HIGH TEMPERATURE ABSORPTION TUBE FURNACE

R. D. Arnold

1. Introduction

As a part of a program of research on the intensity of emission and absorption spectra of flames and hot gases being carried out in the Heat and Power Division of the National Bureau of Standards [1], the high temperature absorption tube furnace described in this report has been designed and constructed.

While the object of the program is the application of spectroscopy to studies of the physical and chemical processes occurring in flames, it is advantageous to be able to observe the same molecules as are found in flames but under more controlled conditions. In even the best controlled flames there are temperature and concentration gradients, and there is uncertainty as to concentration, temperature, optical path length, and as to the degree of non-equipartition of molecular energy. For the determination of molecular properties such as transition probability and line broadening it is therefore preferable to observe molecules under known conditions of temperature, concentration, optical depth, and thermal equilibrium. In an absorption tube furnace these quantities can be much better determined than in flames.

The distinguishing features of the particular furnace described in this report are the high temperature obtainable (2000°K) and the fact that the windows of the chemically inert absorption tube are in the hot zone. Much higher temperatures (3000°K) are of course possible if a carbon tube heater is used as the absorption tube [2,3,4], but such a furnace is limited to applications in which it is allowable to have solid carbon in equilibrium with the gas under observation and in which the absence of windows (to limit the optical path to the hot zone) is permissible. Temperatures slightly higher (2200°K) than obtainable with the present furnace can be accomplished by eliminating hot-zone windows [5,6] which again leads to a reduction in versatility.

In short, the present furnace has most of the advantages of a quartz tube absorption furnace but at higher temperature. The exceptions are 1) the sample gas must be flowed through the tube, whereas a quartz tube may be sealed off, 2) the window diameter is limited and 3) the furnace is not designed for high-pressure samples.

2. The Absorption Tube

2.1 Hot Windows

The materials used in the construction of the absorption tube are high purity alundum tubing (Norton Company Mixture RA 7232) and artificial white sapphire windows. As soon as quartz is abandoned as the absorption tube material the principal problems become the sealing on of the windows and the sealing on of the gas access connections.

The window seal has been accomplished by grinding a slight taper on the edge of the window and a corresponding taper in the end of an alundum tube. Between the two is placed a one mil platinum foil (Detail "A", Fig. 2,1. At room temperature the seal is very poor but as it is heated the sapphire expands slightly more than the alundum and so improves the seal. The coefficients of expansion of the two materials are only slightly different. The sapphire window is a crystal of Al_2O_3 and the RA 7232 alundum is approximately 99% Al_2O_3 . Were the coefficients of expansion too different the expanding window would crack the tube. The platinum foil acts essentially as a gasket.

Placing the windows on probe tubes entering either end of the gas sample container (See Figs. 2,1, 2,2, 2,3) has the following advantages over simply placing windows on either end of an alundum tube sample container.

a) The sample container is easily filled through the annular space between probe and container tubes. Seals for the gas connections are outside of the furnace and can be effected with ordinary de-Khotinsky type cement.

b) Window seals of the type used are not completely tight even at high temperature and it is therefore necessary to pump continuously on the space outside of the windows so that none of the sample gas will be in the optical path outside of the hot zone. The probe tube arrangement makes the pumping simpler and also causes the pressure differential across the window to press the window more firmly into place.

2.2 Evacuation of Probe Tubes

On the outside end of each probe tube is cemented a brass piece on the end of which is affixed a quartz window with an O-ring seal. A side arm is provided to take a 5/8 in. i. d. rubber hose which connects through a dust trap to a 1 CFM mechanical vacuum pump. There is a separate pump for each end of the furnace.

2.3 Support of Probe Tube

Each probe tube is supported by a brass piece sealed to and supported by an end of the sample tube. Additional support (not shown in drawing) is

provided near the outer end of the probe tube. This outer support is adjustable so that the probe tubes may be optically aligned, using the inner support as a pivot. Inlet and outlet sample gas access tubes, in the form of quarter inch copper tubing, are provided in the brass supports.

As the furnace was assembled, and as is shown in Fig. 2.1, the optical path in the sample gas is ten inches. This length can be varied somewhat by telescoping the probe tubes, but such a change requires breaking and remaking the seal at the inner support and moving the outer support of the probe tube.

3. The Furnace

3.1 Heating Element

The heating element of the furnace consists of 0.050 inch diameter molybdenum wire wound directly on the outside of the gas sample tube. There are 100 turns in the 16 inches of the winding, 25 turns over the central 4-3/4 inches spaced at 0.19 inches per turn, 25 turns over each of two 4 inch sections adjacent to the center and spaced at 0.16 inches per turn, and 12.5 turns over each of two 1-5/8 inch outer sections spaced at 0.13 inches per turn. The diameter of the winding is 1-7/8 inches. Over the windings is a layer of Norton RA 1148 alundum cement, a high purity fused alumina cement which matures at 1300°C and is rated at 1800°C maximum temperature.

3.2 Support and Gas Seals

Surrounding the gas sample tube with an annular gap of about 3/8 of an inch, is another tube of RA 7232 alundum. This tube supports the gas sample tube by means of a brass piece cemented to either end. The outer tube is 28 inches long and the sample tube 30 inches long. In operation the inner of these two tubes is hotter than the outer and therefore expands more. To allow for this differential expansion the seal between the inner tube and the brass piece on one end is made by means of rubber sheet attached by an all-purpose liquid cement, rather than by de-Khotinsky type cement as are the other metal-to-ceramic seals. The four brass supports are water-cooled by quarter inch copper tubing soldered to their outside circumferences and each of the cement seals is cooled by an air blast.

3.3 Inlets for Electrical Power and Protective Atmosphere

Each of the two brass supports joining the ceramic tubes is pierced by two quarter-inch copper tubes. One of these is to give a protective atmosphere access to the space surrounding the heater and the other admits the heater wire itself. There are no electrical joints inside the furnace; the molybdenum wire is brought unbroken out through the copper tubes on either end. The gas seals on these tubes are effected by means of commercial (Conax) glands in which powdered talc is compressed about the molybdenum wire. These glands, the ends of which are pipe-threaded, are joined to the copper tube by

a suitable string of adapters. (Glands and adapters are not shown in the drawing.) Ceramic tubes inside of gland, adapters, and copper tube, insulate the wire electrically from the brass support pieces.

3.4 Protective Atmosphere

The purpose of the protective atmosphere is to prevent oxidation of the molybdenum winding at high temperature. While an inert atmosphere or a vacuum would accomplish this if all traces of oxygen could be excluded, an atmosphere containing a large excess of hydrogen can compensate for oxygen contamination. The protective atmosphere may be hydrogen, forming gas or, as is presently employed for this furnace, cracked ammonia. Ammonia is passed through a tube containing steel wool and heated to 900°C by a Nichrome-wire furnace, shown next to the absorption tube furnace in Fig. 2.3. At the exit end of the large furnace, the cracked ammonia passes through a device which may be used to determine its ammonia content, is bubbled through water to maintain its pressure at slightly above atmospheric and is then fed into an exhaust duct.

3.5 Thermal Insulation

The outer ceramic tube of the furnace fits into the annular transite end faces of a sheet metal cylinder 10 inches in diameter. Powdered alumina (120 mesh) fills the space between ceramic tube and metal cylinder. Glands packed with asbestos fiber prevent leakage of the powder where the tube passes through the transite faces. Leakage at the junctions of the metal cylinder with the transite faces was stopped by painting these places with Insulate cement. No cooling is provided for transite or sheet metal.

Imbedded in the alumina insulation is a stock ceramic furnace core which is supported by grooves on the inner faces of the transite end pieces. This is to hold a pair of platinum-rhodium windings far enough out from the center of the furnace that the platinum-rhodium alloy would not be above its melting point with the furnace center at 2000°C. The purpose of the outer windings is to attempt to control the temperature gradient along the axis of the furnace. They are independently manually controlled by Variacs. In practice these windings have not been used since attaching them to the laboratory power system caused interference with the bridge circuit which controls the main molybdenum winding. This effect is due to electrical conduction through the insulating parts of the furnace when these are hot.

3.6 Electrical Characteristics and Power Requirements

The electrical resistance of the furnace winding as a function of temperature is plotted in Fig. 2.4, (curve R). Resistance is measured by the control system (see S4.2) and the temperature was measured by a mercury-in-glass thermometer up to 400°C and by an optical pyrometer between 800 and 1500°C. Molded ceramic forms resting on the bottom of the absorption tube, out of the direct line of sight through the furnace but visible from off the axis, were

used as targets for the pyrometer. These forms have small deep holes in them to act as black bodies.

Curve "I" in Fig. 2.4 shows the current drawn when the furnace has reached equilibrium at the given temperature. Higher currents, up to about 30 amperes, are drawn while the furnace is heating up. Equilibrium power (W) and voltage (V) curves are derived from R and I.

For the extrapolations above 1500°C, the R-curve was taken from the known resistance versus temperature behavior of molybdenum, and the W-curve from a linear extrapolation of W versus temperature on a log log plot. This plot is close to linear over the range 250°C to 1500°C, following the equation,

$$W = 0.066 \frac{t^{1.43}}{t \text{ in } ^\circ\text{C}} \text{ Watts} \quad (1)$$

In the extrapolated region V and I are derived from R and W.

4. Furnace Control System

4.1 System Type

Control of the furnace is based upon using the main heater winding as a resistance thermometer. An electro-mechanical, time-modulated, proportional reset (integrating) type of control system adjusts the input power to maintain the furnace resistance at a value set by the operator.

4.2 Resistance Measurement

The basic control-loop circuit is shown schematically in Fig. 2.5. (A detailed electrical diagram of the chassis called "Thermoregulator" is shown in Fig. 2.6 and Fig. 2.7 in a photograph of the control rack.) A Wheatstone bridge with a 1000 to 1 ratio between its two sides contains the furnace as one of its four arms. The other arm on the low resistance side is made up of Advance ribbon (1/2 in. wide by .010 in. thick, 0.0480 ohms per foot). It has a resistance of 0.51 ohms and a very low thermal coefficient of resistance. This resistor may be seen in Fig. 2 below the furnace table on the left hand end. The ribbon is wound back and forth over pieces of ceramic tubing set in an open frame. A fan at the opposite end of the table (see Fig. 3) blows air through a chute and out over the resistor. The loops are cooled by air blowing through the ceramic tubing. Use of the fan keeps the resistance of this resistor constant within 0.2% with current up to 40 amperes.

The high resistance side of the bridge is located partly in the thermoregulator chassis and partly in the recorder. This is a modified Brown strip-chart recording potentiometer. The 20 ohm resistor is the slidewire

which comes with the instrument. Since subsequent circuitry in the control loop is arranged to make the midpoint of this slidewire the balance position for control, then at balance 10 ohms of the slidewire belong to the lower right hand arm of the bridge and 10 to the upper. The 10 ohms added to the 500 ohm resistor shown make the bridge ratio 1000 to 1. There are three decades of 10 ohms, 100 ohms and 1000 ohms per step in the decade resistor. The knob on the 10 ohm per step decade is set to read 10 ohms greater than the actual resistance to allow for the 10 ohms in the slidewire. Thus, at balance, the decade knobs read exactly 1000 times the resistance of the furnace winding.

When the winding resistance changes the bridge unbalance signal causes the balancing motor in the recorder to move the slidewire to reduce the bridge signal to zero. This happens in a time short compared to the time constant of the overall control loop, so the bridge may be considered always in balance and the instantaneous winding resistance may be read from the decade knobs and the position of the recorder pen, which follows the slider. The value of that must be added to the decade reading R_D when the pen is separated from the center of the scale by a fraction "a" of full scale is

$$\Delta R_D = a \left(\frac{R_D}{25.5} + 20 \right) \left(\frac{1}{1 - .04a} \right).$$

Since "a" is never larger than 0.5 and ΔR_D is never larger than $0.04R_D$, we may set the last factor above equal to unity and get that the furnace resistance is

$$R_f = \frac{1}{1000} R_D \left(1 + \frac{a}{25.5} \right) + 0.02a$$

The following modifications were made in the recorder. Since the bridge signal is A. C. the converter was removed and the bridge signal applied directly to the input transformer of the amplifier. In order to get a sufficient voltage for heating the furnace it is necessary to operate it from two outer arms of the laboratory 4-wire, 3-phase A.C. power system (see Fig. 2.4). Now for correct phasing of the recorder amplifier with the bridge signal it is necessary to use the same two terminals of the power system, and since this is too high a voltage for the recorder, a step-down transformer is used. The amplifier "ground", separate from the power input, is connected to the neutral (N) terminal of the laboratory system, since this is a true ground. It is apparent from this arrangement that even when the bridge is balanced there will be a potential difference between the primary and secondary windings of the amplifier input transformer. This potential is only weakly coupled capacitatively to the amplifier but is large enough to cause considerable trouble if uncompensated. The in-phase part of the pick-up is compensated by

the action of the balancing motor and causes an error in the resistance reading but this error is quite small due to the very large true bridge signal. The out-of-phase part of the pick-up, however, is completely uncompensated and gets large enough to swamp the amplifier. It is therefore necessary to compensate by adding into the secondary of the transformer an adjustable voltage 90° out-of-phase with the bridge supply voltage. This is supplied from arms N and 2 (the bridge is on 1 and 3) of the laboratory supply. The amplified signal is brought out to an oscilloscope for monitoring the out-of-phase bucking. This same arrangement also bucks out the out-of-phase signal due to the inductance of the furnace winding.

4.3 Control of the Input Power

Up to this point we have a shaft position (pen and slidewire) proportional to the difference between the true and desired furnace resistance. We want to operate on the power Variac (50 B-G2) in such a manner as to reduce this difference to zero. There is no electrical error signal since the bridge is self-balancing.

A proportional error signal in the form of a shaft rotation in the thermoregulator is generated from the shaft rotation in the recorder in the following way. The two 1000-ohm potentiometers, one in the recorder and one in the thermoregulator, and the amplifier and balancing motor in the thermoregulator form a shaft rotation follower system. The shaft of the second potentiometer assumes such a position that the input to the amplifier is zero, that is, the departure of the second slider from its midpoint is proportional to the departure of the first from its midpoint. The constant of proportionality is equal to the ratio of the voltage on the first potentiometer to that on the second and may be varied from zero to about five by the Variac marked "Prop. Control" in Fig. 2.6. The first potentiometer is geared to the recorder so that it is at its midpoint when the pen is at midscale and is at one end when the pen is at a corresponding end of the scale. We now, therefore, have a shaft rotation in the thermoregulator proportional to the furnace resistance error. The constant of proportionality may be set by the operator and is independent of the bridge voltage. A low proportionality constant makes a loose, slow control and a wide proportional band, though not wider than full scale on the recorder. A high proportionality constant makes a fast, tight control and a narrow proportional band.

Notice that a proportionality constant greater than unity may cause the second potentiometer to attempt to overrun its end. This is prevented by microswitch #3 (Fig. 2.6) which is opened when the potentiometer reaches either end and thus reduces the proportionality constant to zero. The potentiometer therefore "bounces" against the end but does not overrun it.

To complete the control loop it remains to cause the power Variac to move upward or downward at a rate proportional to the resistance error.

Connected to the Variac shaft is a reversible, constant speed motor. Control of the motor is by means of three wires which are designated R, W and B in Figures 2.5 and 2.6. When R is shorted to W the motor goes downward and when to B, upward. The switching between W and B is accomplished by relay #1, which is controlled by microswitches #1 and #2. A momentary depression of microswitch #1 causes the relay to pull up and hold up. Then a momentary depression of microswitch #2 will cause the relay to drop down and stay down, etc. Each microswitch is depressed momentarily every 6 seconds by a synchronous motor cam. Now one microswitch is fixed in position while the other rotates with the "error shaft" of the thermoregulator. The moving microswitch is originally positioned so that when the error shaft rotation is zero (recorder pen at midscale) this microswitch is diametrically opposite the fixed microswitch.

It follows from the above arrangement that at zero error the power Variac is driven upward for 3 seconds and downward for 3 seconds, thus having a net rate of zero. During the three seconds the Variac brush moves over about two windings. If there is a negative error signal (resistance less than decade setting) the upward phase of the cycle will become greater than 3 seconds and the downward phase less than 3 seconds. The net rate of the Variac will then be upward and proportional to the error signal. As has been pointed out by Nurse and Welch [7], the time modulation control of a Variac allows a continuous, rather than stepwise, variation of the average power output. When the correct control point is between two Variac windings, the brush will spend appropriate times on adjacent windings to make the average correct.

Two additional features of the system are the programmed temperature raiser and the ceiling control. The former is simply a motor-driven 10,000 ohm helipot which may be switched in to replace the decade resistor. It is raised at the rate of 1,000 ohms per hour which causes the furnace resistance to be raised at the rate of one ohm per hour. Thus the furnace is raised from room temperature to 1500°C in about four and one-half hours.

The ceiling control is shown in Fig. 2.6. It serves as a safety device to prevent the Variac from being driven above some preset voltage in case something goes wrong with the control. The Variac voltage is rectified and applied to a relay winding in series with a variable resistor. When the voltage reaches a certain point, determined by the setting of the resistor, the relay pulls up. This opens the "B" line in the Variac control circuit and thus prevents further voltage rise. The event is marked by a signal light and buzzer. Because of the hysteresis of the relay normal operation is restored only by opening the relay (SW 1, Fig. 2.6) even though the voltage has dropped below the critical value after the relay operates. Standard procedure is to set the ceiling slightly above the voltage required to maintain the desired operating furnace temperature.

Manual control of the Variac motor is provided by SW2 and SW3. When SW3 (Manual-Automatic) is in the "Manual" position then SW2 can be used to run the Variac upward or downward or to hold it stationary.

Microswitch #4 on the timing mechanism of the thermoregulator has no function in the control of the absorption tube furnace but is merely a periodic interrupter (operated by the cam on the synchronous motor) for the Sym-ple-trol pyrometer which is used to control the ammonia-cracking furnace.

5. Assembly

5.1 Thermal Insulation

Several phases of the assembly of the furnace require special attention. The large diameter 28" long ceramic tube was placed in its proper position in one of the transite end faces and the asbestos gland was packed and closed. This assembly was supported vertically and the sheet metal cylinder was attached to the transite. Then the ceramic core bearing the platinum windings was placed in its groove in the transite. Into the two concentric annular spaces so formed was poured and tamped the alumina powder. Then the other transite face was attached and the other gland packed and closed. The assembly could then be placed horizontally in its cradle. The two holes on top of the sheet metal can at either end were used only for replacement of powder that leaked out before the Insulate cement was applied to the junction of the can and the transite faces.

5.2 Heater Winding

The wire used in the heater winding is too stiff to wind directly onto the absorption tube. It was first wound on a mandril of diameter slightly smaller than that of the absorption tube and into which had been cut grooves of proper spacing. It was then heated with a torch to dull red heat (as suggested in Reference 8). When the tension was released it sprang out to a diameter between that of the mandril and that of the tube. These two were then placed end to end and the winding was transferred from one to the other by sliding turn by turn, worm fashion. This resulted in a snug fit on the tube.

5.3 Window Seal

In preparation for installing the sapphire windows in the probe tubes, the polished windows were cemented to the ends of brass rods of diameter approximately equal to that of the windows. Internal tapers were ground in the probe tubes to a depth of $1/8$ inch, the window thickness. Then, without changing the taper setting of the grinder, external tapers were ground in the window-brass rod assemblies until the outer faces of the windows would penetrate about $1/32$ inch below the outer edge of the tubes. This amount of penetration was about right to bring the windows back to flush with the tube ends with the 0.001 in platinum foil in place. Platinum foil of width greater than $1/8$ inch was wrapped around the window-rod assembly and fixed to the rod. This assembly was then placed in the probe tube and the excess foil was cut off. The rods were heated until the cement softened and the rods dropped off,

leaving the windows in place. Cement left on the windows was rubbed off with sandpaper.

6. Operation

6.1 Heating Program

The furnace is heated slowly (4 1/2 hours to 1500°C) by means of the programmed temperature raiser in order to minimize thermal shock in the ceramic parts. Operation is almost entirely automatic and only general safety monitoring is required of the operator except that the out-of-phase buckler must be occasionally readjusted. Also it is a safe practice to keep the Variac ceiling control set not far above present voltage, resetting in small increments as the alarm sounds. This is because if the voltage were to run away while the furnace temperature is low (and therefore the winding resistance is low) a very large current would flow, resulting in a very high rate of temperature rise.

6.2 Protective Atmosphere

The flow of protective atmosphere should be started while the furnace is still cold to flush out air which may have got into the system between runs. Entrance of air is minimized by running a neutral gas (e.g. dry nitrogen) through the system while the furnace is cooling after a run.

6.3 Probe Tube Pumps

It has been found advantageous to start the pumps on the probe tubes before the temperature is high enough to seal the sapphire windows. This causes the windows to be pulled firmly into their seats and seems to make the seal occur sooner after the windows are hot. At a furnace temperature of about 400°C the seals close up except for a small residual leakage which remains at all temperatures. Despite this leak the pumps used are able to maintain a probe vacuum of 75 - 300 microns at high furnace temperatures.

6.4 Temperature Profile

A rough measure of the temperature profile has been made by sighting with an optical pyrometer on black-body hole targets spaced along the bottom of the absorption tube. At a furnace temperature of 1500°C the temperature difference between the center of the furnace and the position of the windows is 40 degrees. The positions midway between the center and the windows is down 5 degrees from the center.

6.5 Optics

For absorption measurements a light source is focussed on the entrance quartz window by a mirror that subtends at least as much solid angle as does the outside end of the exit probe tube, which is therefore the aperture stop.

A lens just outside the exit quartz window refocusses the image on a spectrom-eter slit at such a distance from the lens that the light fills the aperture of the spectrometer.

6.6 Light Source

The most satisfactory source for ultraviolet absorption measurements has been a Hanovia high-pressure xenon arc lamp. It gives adequate intensity at 3000 A for the Leeds and Northrup monochromator[†][9] despite the very small

[†]Loaned to the N.B.S. High Temperature Laboratory by the Research Department, Leeds and Northrup Company on a field trial basis.

aperture of the furnace. There are sometimes fluctuations in intensity, seemingly caused by jumping of the arc, which are too large to allow quantitative absorption measurements. However, there are also periods of smooth operation of long enough duration to allow data to be taken.

6.7 Sample Spectrum

A sample spectrum of absorption in the furnace is shown in Fig. 2.8. For this measurement oxygen was bubbled through water at room temperature and the saturated mixture was flowed through the absorption tube. The furnace temperature was 1500°C and the absorption path length was 10 inches. The xenon lamp was the light source and the spectrometer was the Leeds and Northrup photoelectric recording monochromator. Shown in the spectrum is the 0,0 band head of the ultraviolet transition in OH at 3064 A.

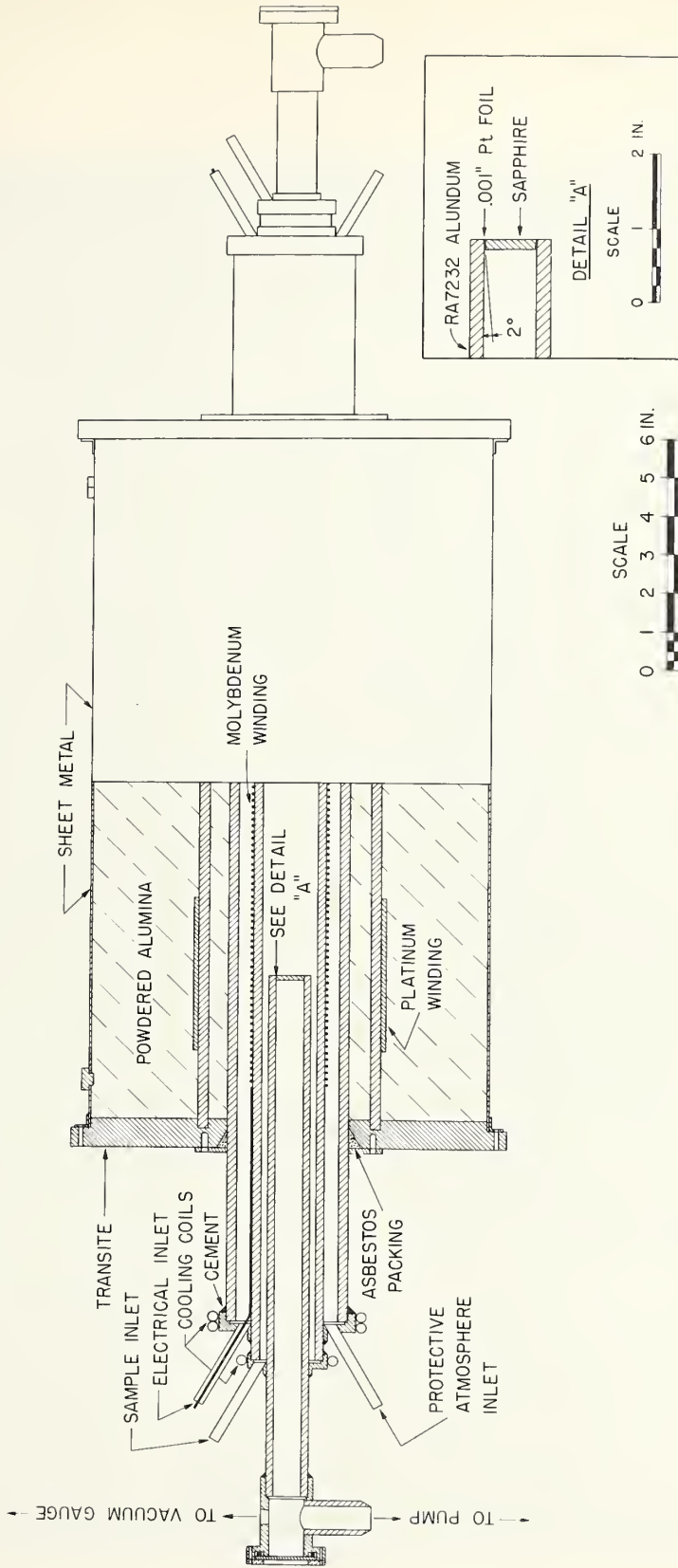
Mr. G. E. Beale, Jr. of the High Temperature Laboratory did much of the construction and assembly, and many of his suggestions were incorporated into the design of furnace and control.

References

1. N.B.S. Report 1123
2. King, A. S. *Astrophys. J.* 28, 300 (1908)
3. King, R. B. *Astrophys. J.* 108, 429 (1948)
4. Brewer, L., Gilles, P. W. & Jenkins, F. A. *J. Chem. Phys.* 16, 797 (1948)
5. Burrows, G. & Clark, F. L., *J. Sci. Instr.* 10, 248 (1933)
6. Garton, W. R. S. & Feast, M. W. *Nature* 165, 282 (1950)
7. Nurse, R. W. & Welch, J. H. *J. Sci. Instr.* 27, 97 (1950)
8. Cohn, W. M. *Z. Techn. Physik* 9, 110 (1928)
9. Broida, H. P. and Shuler, K. E. *J. Chem. Phys.* 20, 168 (1952)

Figures

- 2.1. Drawing of absorption tube furnace.
- 2.2. Front view of absorption tube furnace.
- 2.3. Rear view of absorption tube furnace.
- 2.4. Electrical characteristics of the furnace.
- 2.5. Schematic of Furnace Control Circuit.
- 2.6. Schematic of Thermoregulator.
- 2.7. Control Rack.
- 2.8. Sample Absorption Spectrum.



ABSORPTION TUBE FURNACE

Figure 2.1

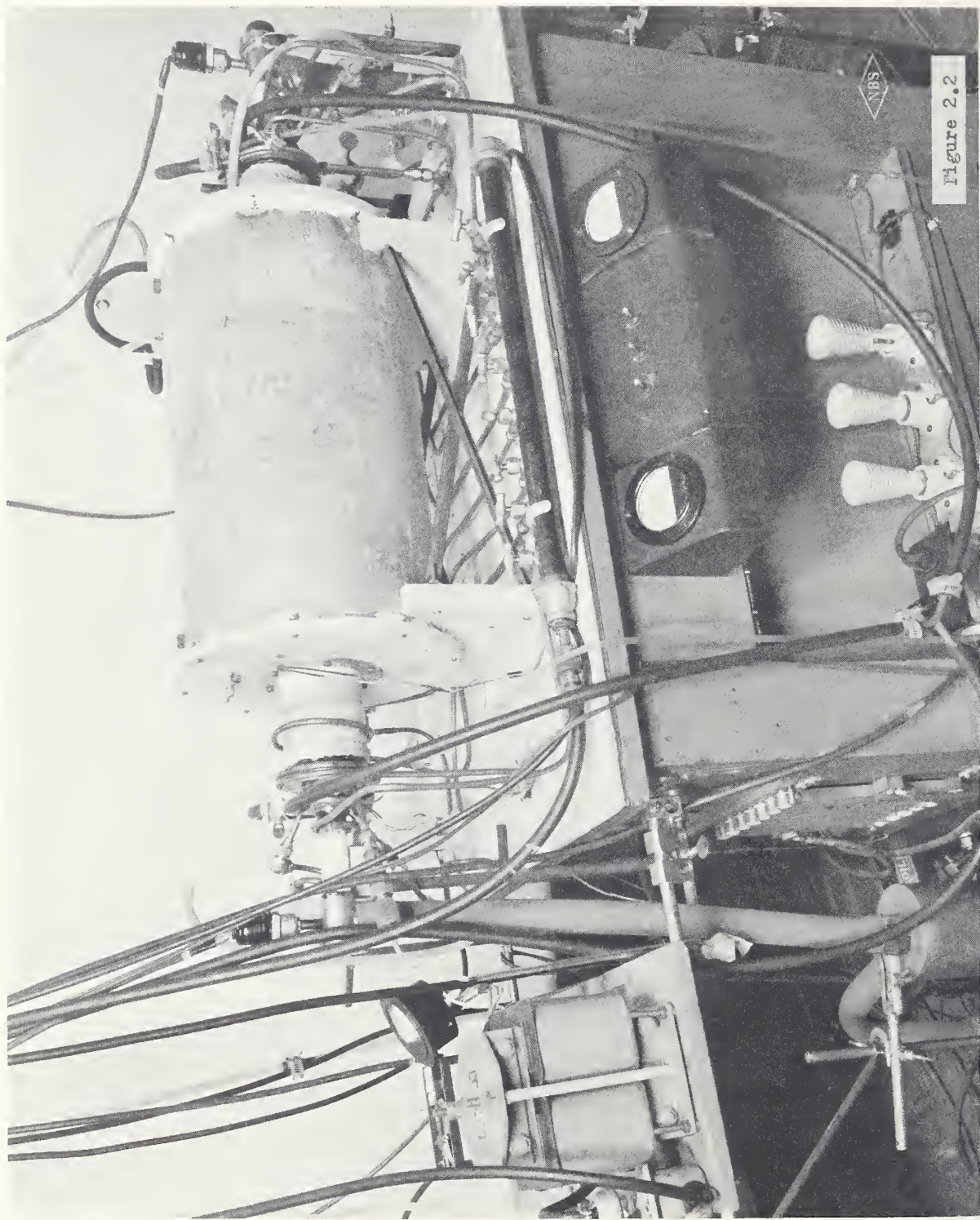


Figure 2.2

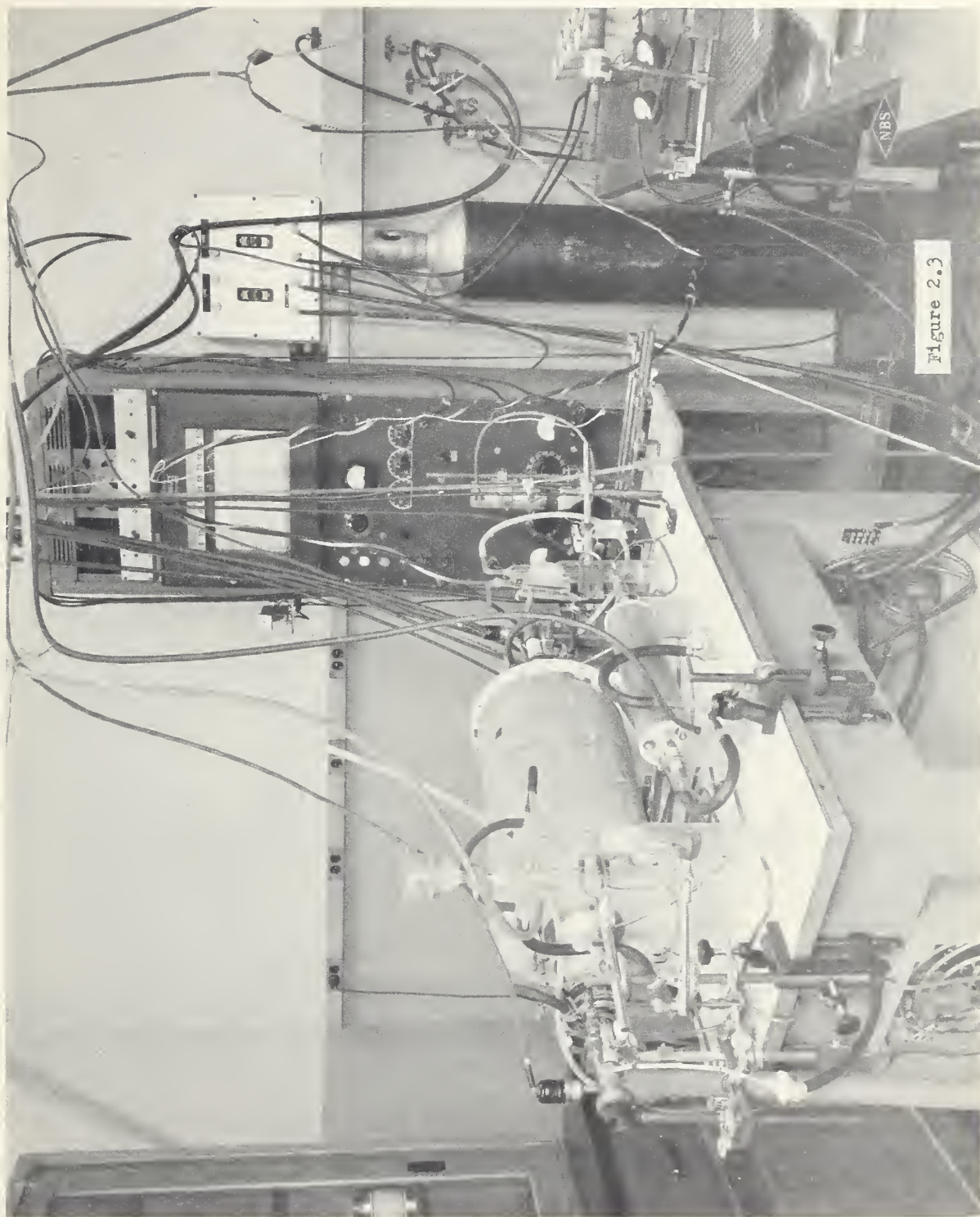


Figure 2.3

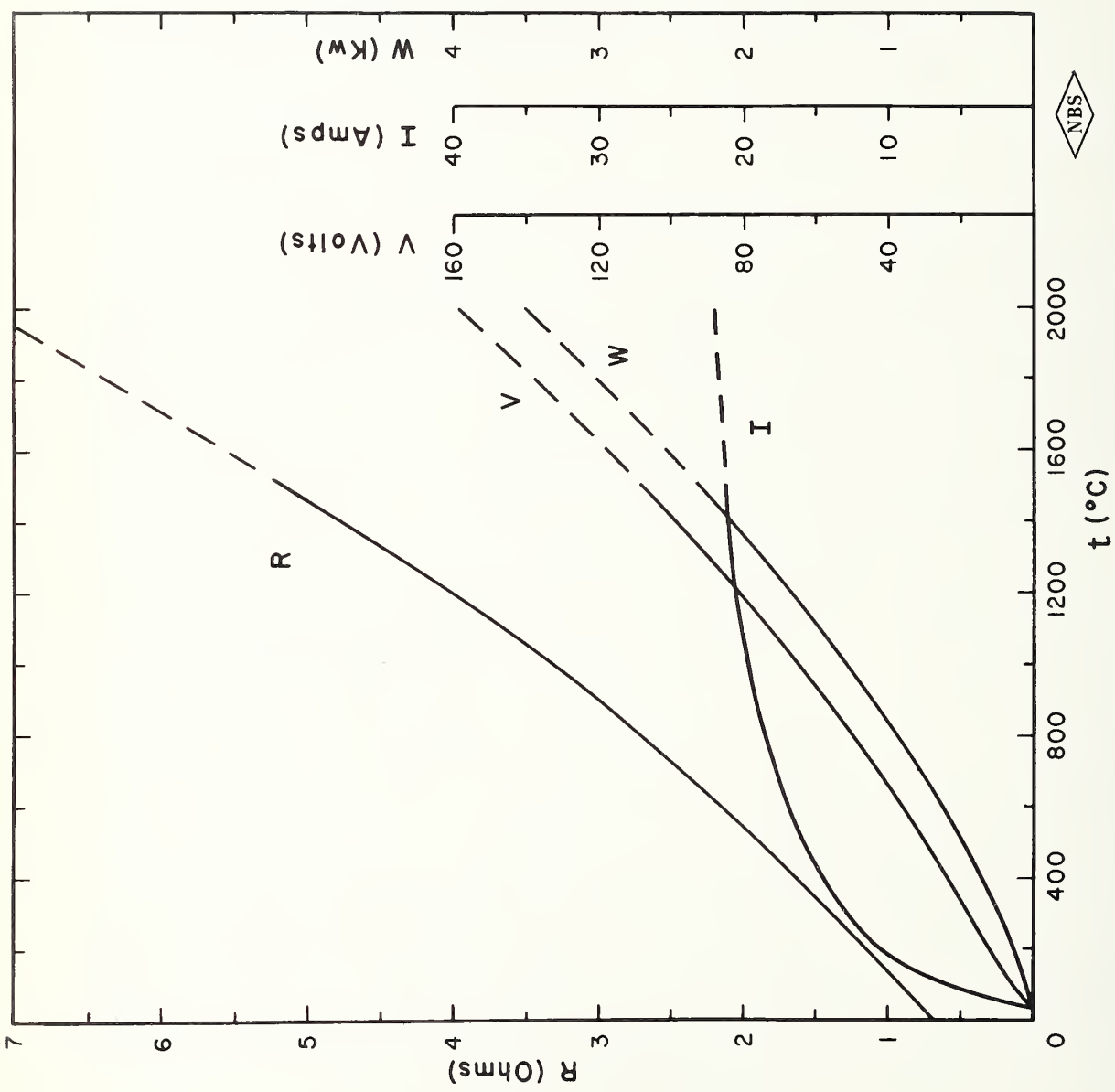
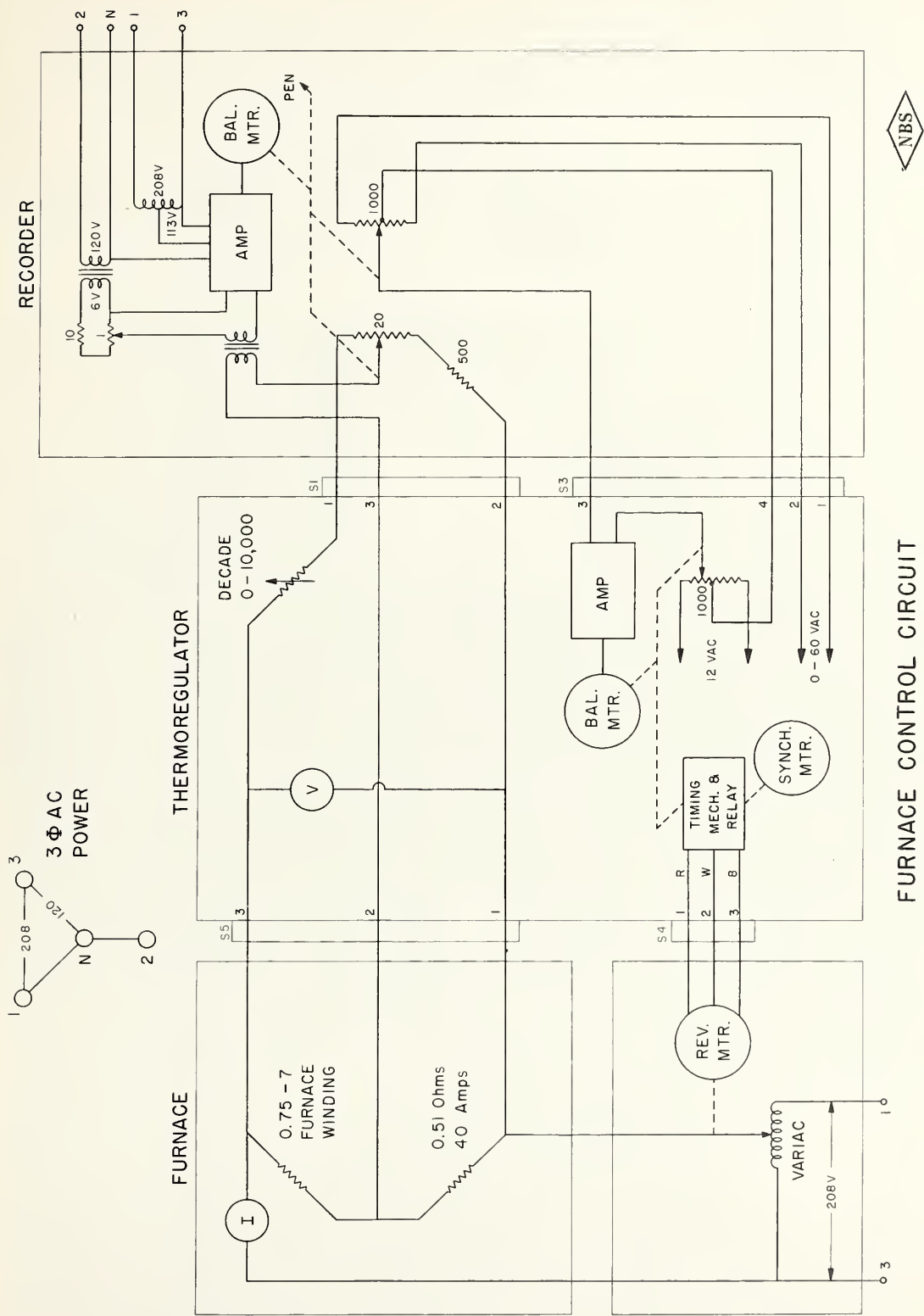


Figure 2.4



FURNACE CONTROL CIRCUIT

Figure 2.5

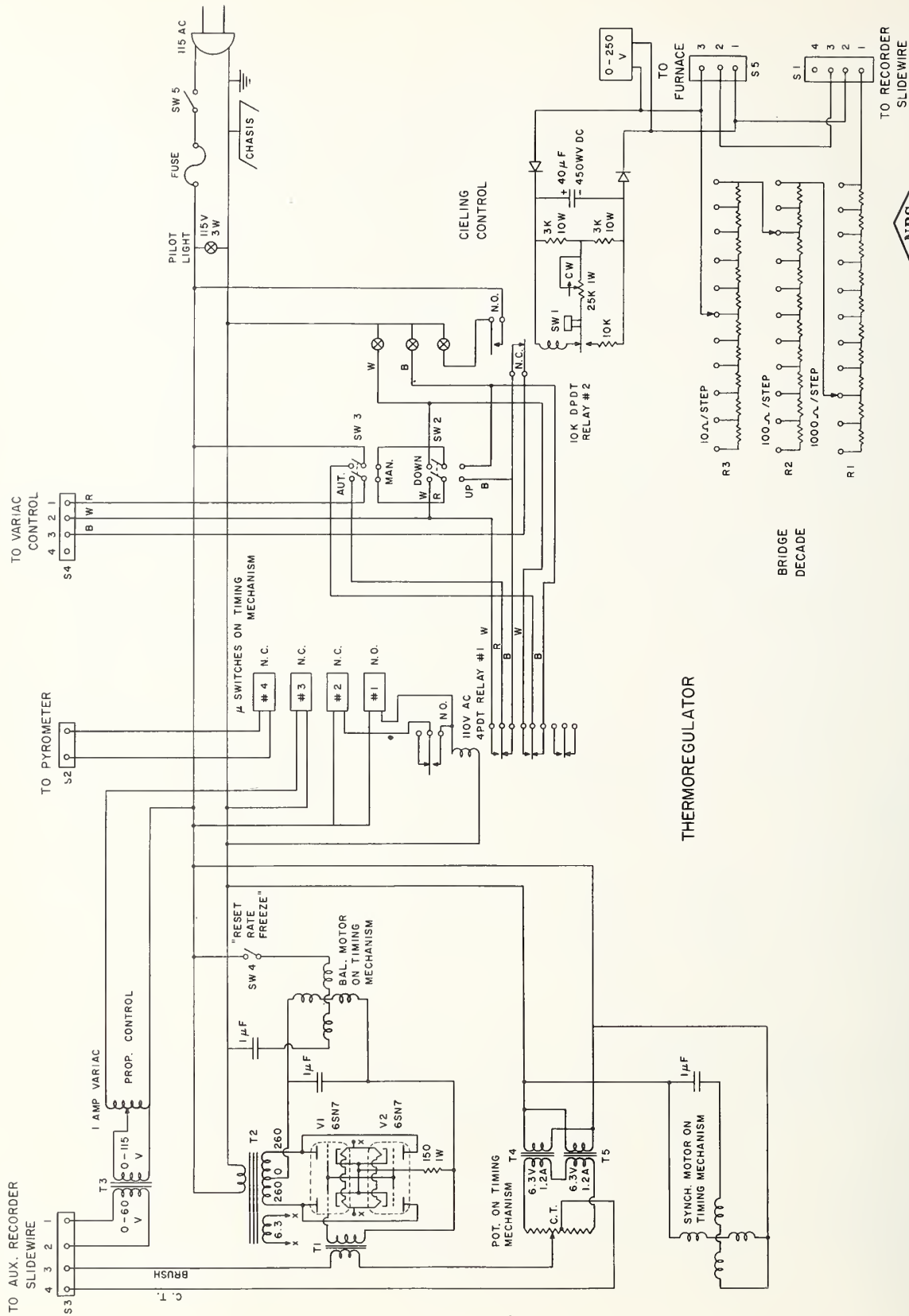


Figure 2.6



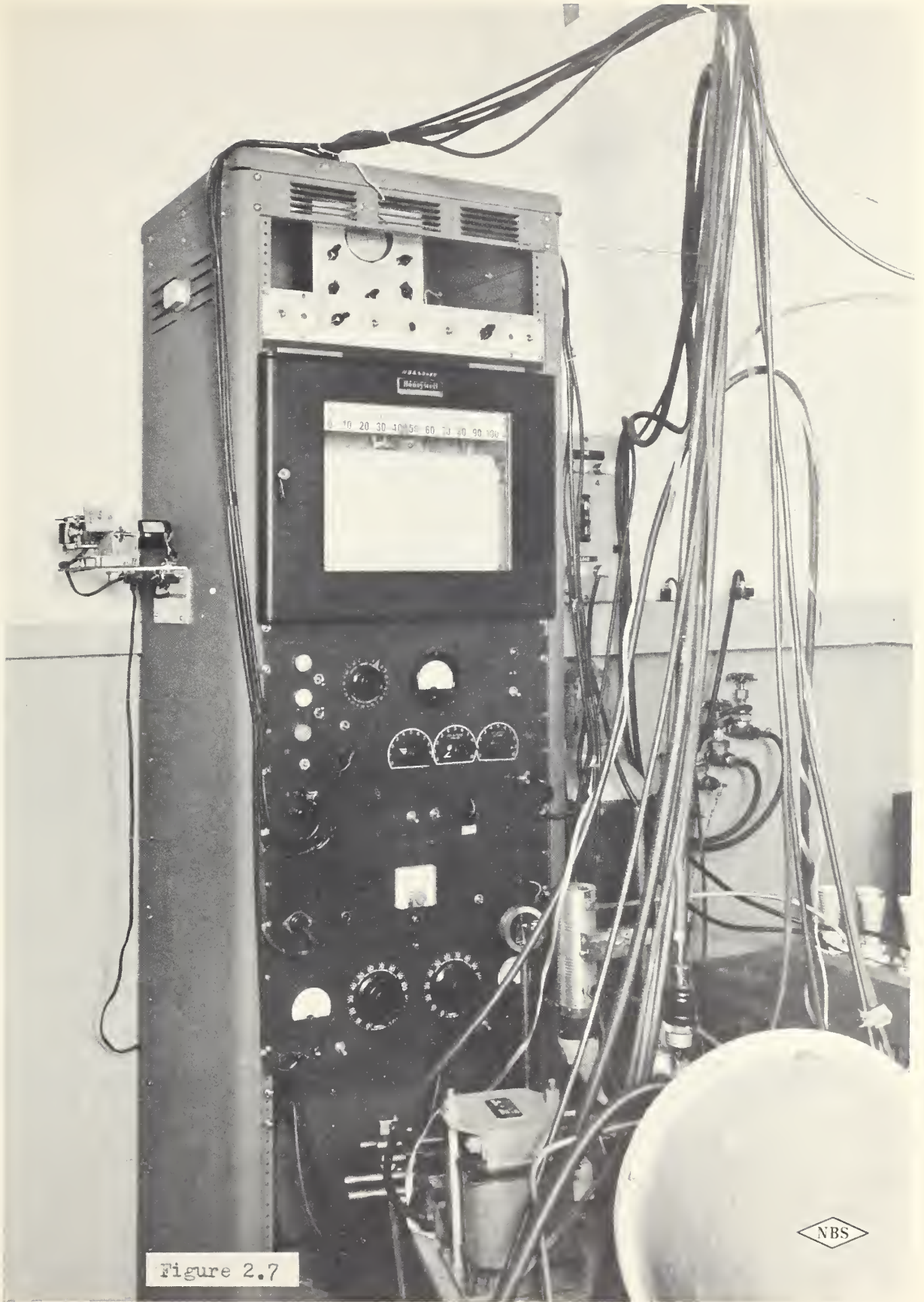
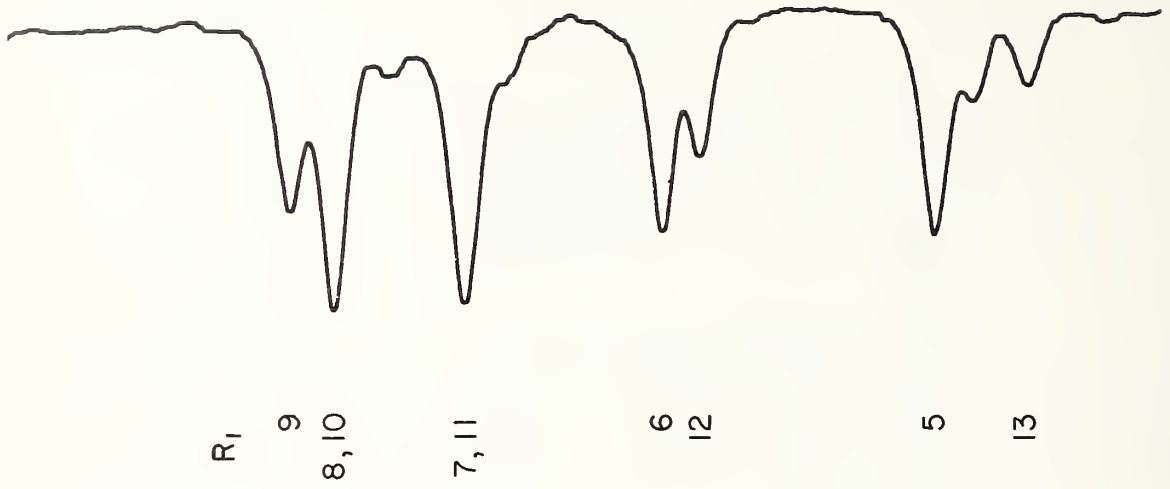


Figure 2.7

NBS



0,0 BAND HEAD OF ${}^2\Sigma - {}^2\Pi$
TRANSITION OF OH
IN ABSORPTION.

FURNACE TEMPERATURE 1500°C



————— ZERO —————

Figure 2.8

3. DESIGN AND CONSTRUCTION OF A "BLACKBODY" AND ITS USE IN THE
SPECTRAL INTENSITY CALIBRATION OF A GRATING MONOCHROMATOR*

by

C. T. Lalos, R. J. Corruccini and H. P. Broida

ABSTRACT

A "blackbody" constructed of graphite was inductively heated in an atmosphere of helium to a maximum temperature of 2700 degrees K. This "blackbody" was used as a source of radiation of known intensity as a function of temperature and wavelength in the spectral intensity calibration of a grating monochromator. The calibration was made over the spectral range of 2600 Å to 3800 Å in the second order and of 3300 Å to 7550 Å in the first order. Relative intensities were measured with an accuracy estimated to be of the order of 9% in the regions 2600 Å to 2800 Å in the second order and 7200 Å to 7600 Å in the first order, and of 5% in the regions 2800 Å to 3800 Å in the second order and 3300 Å to 7000 Å in the first order.

*Submitted for publication in The Review of Scientific Instruments

1. INTRODUCTION

Instruments that are used to measure intensity distributions accurately over large spectral ranges must be calibrated with a source of radiation of known intensity distribution over the desired spectral range. By far the best known source for this purpose is a "blackbody", i.e. a hollow cavity having its walls at a uniform temperature. This source of radiation has been studied extensively both theoretically [1] and experimentally [2], and is considered the primary standard of radiation, i.e. a source whose intensity distribution is known as a function of temperature and wavelength.

An inductively heated "blackbody" was constructed and used to calibrate a grating monochromator. Two tungsten-filament lamps also were calibrated to serve as secondary or working standards.

2. BLACKBODY

It can be shown theoretically that an enclosure of any arbitrary configuration and made of any material whose walls are at a uniform temperature emits radiation whose intensity as a function of temperature and wavelength is given by Planck's blackbody distribution equation, i.e.

$$J_{\lambda, T} = c_1 \lambda^{-5} \left(e^{c_2/\lambda T} - 1 \right)^{-1} \quad (1)$$

where $J_{\lambda, T}$ is the radiancy in ergs per second per unit area of the source at wavelength λ and temperature T , c_1 is the first radiation constant, and c_2 is the second radiation constant.

Radiation from such an enclosure may be utilized if a small opening is made in one of its walls. This radiation is essentially blackbody radiation in nature if the dimensions of the opening are small relative to the internal dimensions of the enclosure. As the opening is made larger the nature of the radiation departs more and more from blackbody radiation. For clarity we have adopted the convention of using quotation marks, i.e. "blackbody", when we refer to an enclosure containing an opening in order to utilize the radiation. This merely signifies that true blackbody radiation is not realized, and that therefore an emissivity is associated with a "blackbody" for each wavelength and temperature.

Fig. 3.1 is a cross-sectional drawing of the "blackbody" that was constructed. The inner tube or "blackbody" proper is made of graphite and was machined as shown in detail in Figure 3.2. This particular geometrical configuration was chosen because of its relative simplicity, ease of maintaining a uniform temperature, and high emissivity. Emissivity of a simplified "blackbody" of this general shape, i.e. an open-end cylinder as a function of the emissivity of the material of which it is made, is given by the expression [3]

$$\Sigma_{BB} = \frac{\Sigma_X [1 + (1 - \Sigma_X) (s/S - \sin^2 \theta)]}{\Sigma_X (1 - s/S) + s/S} \quad (2)$$

where Σ_{BB} is the emissivity of the "blackbody", Σ_X is the emissivity of the material of which the "blackbody" proper is made which is a function of temperature and wavelength, s is the area of the opening, S is the area of the enclosure, and θ is one-half of the angle subtended by the opening. It is evident from the form of this expression that Σ_{BB} does not depend critically on the value of Σ_X , especially if the ratio s/S is small. Calculations show that the percentage change in Σ_{BB} due to a variation of Σ_X from 0.6 to 0.8 and a variation of s/S from 0.05 to 0.025 is only of the order of 1-1/2 %. These assumed variations in Σ_X and s/S are larger than would be expected to be found in the use of the "blackbody" shown in Figures 3.1 and 3.2. Therefore, the calculated emissivity is not critically dependent on the assumed value of the emissivity of graphite at the operating temperature and on the physical dimensions used in the construction of this "blackbody."

The "blackbody" proper is surrounded with lampblack which serves as thermal and electrical insulation. Lampblack was chosen as the insulation after an unsuccessful attempt was made using ZrO_2 . At the high temperatures which the "blackbody" was operated, impurities in the ZrO_2 fused and formed a slag of high electrical conductivity which destroyed its use as an insulator. A fused silica tube approximately 6 inches in diameter supports the "blackbody" proper and the lampblack insulation. Water-cooled copper induction-coil leads are insulated electrically from the water-cooled metallic outer shell by means of a polystyrene window. These coils are spaced 3/4 of an inch from the 6 inch silica tube to prevent electrical breakdown between the coils and the tube. A polished quartz viewing window is located at the open end of the "blackbody" (see Figure 3.3). A shutter located directly behind the quartz viewing window serves to shield the window from the high-intensity radiation during the time that the "blackbody" is being brought up to its operating temperature and after a run during the cooling off period. The shutter is made of metal and is hand operated from the outside of the "blackbody". A small O-ring is located on the part of the shutter handle that extends out of the "blackbody" in order to keep the outside metallic shell air-tight. Helium gas regulated at a gauge pressure of a few pounds per square inch was used as the inert atmosphere and served to keep atmospheric oxygen from oxidizing the hot graphite tube. An inlet for the helium gas is located in the neck that houses the quartz viewing window. Thus the helium serves to partially keep carbon vapor from depositing on the window.

The power supply used to heat the "blackbody" was a 20 KW, 450 KC Westinghouse Radio Frequency Generator designed for industrial induction heating applications requiring up to 20 KW of radio-frequency energy. Temperature control was attained by regulating the power to the "blackbody". This was accomplished by an automatic controller [4] and an auxiliary fine power indicator and adjuster. Fig. 3.4 shows the working assembly including the induction generator, power regulator, glass system for regulating the flow of helium into the "blackbody", "blackbody", grating monochromator and its associated electronics, and the intensity recorder.

3. GRATING MONOCHROMATOR

The grating monochromator* that was calibrated has been described in detail elsewhere [5]. Briefly (see Fig. 3.5) the radiation from the source S is focused by the front-surfaced mirrors L₁ and L₂ on the entrance slit A, is then reflected and collimated by the front surfaced spherical mirror M, is diffracted by the plane reflection grating G, is then again reflected and focused by the same mirror M onto the exit slit B. The spectral energy is gathered behind the exit slit by a specially selected 1P28 photomultiplier tube P. Scattered light in this monochromator is very low; for example with a low pressure mercury discharge, scattered light in the vicinity of the 5461 A green line is less than one part in 10⁵ of the intensity of the 5461 A line. The photomultiplier-amplifier combination is known to be linear within a few percent.

*The monochromator was constructed by the Research Department of Leeds and Northrup Company and loaned to the Heat and Power Division of the National Bureau of Standards on a field trial arrangement.

The need for calibrating this monochromator results from (1) selective transmission of the external optics, (2) selective reflectance of the monochromator mirror and the grating and (3) spectral sensitivity of the photomultiplier tube.

4. CALIBRATION

A response calibration of the monochromator was made from 2600 to 7550 A. The short wavelength limit was set by the limited amount of ultra-violet energy available at the operating temperature and by the blaze of the grating (specified with a blaze near 3000 A in the second order). The long wavelength limit was set solely by the limit in sensitivity of the photomultiplier tube. Radiation was viewed in the first and second order of a 3 inch 30,000 lines per inch plane reflection grating using an entrance slit width of 20 microns

(0.4 A in the first order), and an exit slit width of 30 microns. The region 2600 to 3800 A was viewed in the second order and the region 3300 A to 7550 A in the first order. This arrangement results in an overlap region of 500 A. The temperature of the "blackbody" during the calibration was 2435°K.

The apparatus for calibrating the grating monochromator is shown in Fig. 3.5. S is the "blackbody", W is the quartz window, L₁ and L₂ are concave front-surfaced mirrors, F are optical transmission filters, and E is the grating monochromator. The "blackbody", two front-surfaced mirrors L₁ and L₂, and the grating monochromator all have an aperture of F:10.

Various combinations of Corning glass filters were used to filter out overlapping orders and to decrease scattered light. Intensity measurements in the 2nd order from 2600 to 3300 A were made using a Corning #9863 filter. This filter acted as a cut-off for the superimposed 1st order 5200 to 6600 A radiation. Measurements of intensity in the 2nd order from 3300 to 3800 A were also made using the #9863 filter but in this range the #9863 filter transmits as much as 40% of the superimposed 1st order radiation. This may possibly result in a lowered accuracy in the calibration in the 2nd order from 3300 to 3800 A.

In the 1st order intensity measurements from 3300 to 4100 A were made with a #9863 filter in order to reduce the effects of scattered light beyond 4500 A. No filters were used in the region 4100 to 6200 A. The superimposed 2nd order radiation 2050 to 3100 A was comparatively much smaller because of the nature of the blackbody radiation curve, and also because of the response characteristics of the apparatus. First order intensity measurements in the regions 6200 to 6600 A, 6600 to 7000 A, and 7000 to 7550 A were made using Corning filters #2412, #2403, and #2030 respectively. Each of these three filters served as a cut-off filter for the superimposed 2nd order radiation and also reduced scattered light from shorter wavelengths. Transmissions of all the filters were measured at each wavelength with the filters in the position they were to have for the calibration of the monochromator and just prior to the intensity measurement at that wavelength. It had been observed earlier that the transmissivity depends very critically on the angle of incidence of the radiation. The filters also were air-cooled to room temperature since temperature affects the transmissivity, especially on the low wavelength cut-off side [6]. The transmissivity of the quartz window of the "blackbody" was measured before and after the calibration. Temperatures of the "blackbody" were measured with a precision optical pyrometer calibrated at the National Bureau of Standards.

A relative spectral intensity calibration was obtained by viewing the radiation emitted by the "blackbody" with the grating monochromator over the desired spectral range and comparing these measurements with values calculated from the blackbody expression multiplied by the appropriate emissivity values as calculated from equation 2, and by the transmissivity of the quartz window of the "blackbody". Measured intensities must be multiplied by the reciprocal

of the transmissivity of any filter that is used. The multiplication factor is obtained from the ratio of the calculated intensity to the measured intensity at each wavelength and must be applied to all intensity measurements made with the grating monochromator. This multiplication factor is a function of the "transmissivity" of the grating monochromator, the reflectivity of the two mirrors L_1 and L_2 , and the sensitivity of the photomultiplier tube.

An investigation of the nature of the emission of the "blackbody" was made preparatory to the actual calibration, at a time when nitrogen rather than helium was used as the inert atmosphere in the "blackbody". This was done by scanning continuously the spectral interval over which the calibration was to be made. Records thus obtained showed the smooth form of the "blackbody" radiation curve and the high wavelength cut-off of the photomultiplier. In addition these records showed that some absorption was present. On closer examination a strong absorption at about 3900 Å was identified as the $0,0$ band of the $2\Sigma - 2\Sigma$ electronic transition of CN with a head at 3883 Å. Two very strong absorption lines at 5890 and 5896 Å indicated the presence of sodium as an impurity in the graphite. Various other absorption lines and bands also were observed. With the exception of the sodium lines the absorption was eliminated by substituting helium for nitrogen as the inert atmosphere in the "blackbody".

Intensity measurements during the actual calibration were taken at intervals of 200 Å in the 1st order and every 100 Å in the 2nd order. Temperature readings were made after each 3 readings, i.e. approximately every ten minutes.

Figure 3.6 is a plot of the multiplication factor on a logarithmic scale versus wavelength for the grating monochromator. The multiplication factor increases from an arbitrarily assigned value of unity at 4900 Å to approximately 60 at 2600 Å and 25,000 at 7550 Å. The shape of the curve at longer wavelengths is determined primarily by the response of the photomultiplier while that at the shorter wavelengths by the blaze of the grating.

The accuracy of an intensity response calibration over a large wavelength interval is limited by several possible sources of error - the temperature of the "blackbody", transmissivity of filters, wavelength, linearity of the photomultiplier or associated electronics, and scattered light in the monochromator. Temperature of the "blackbody" is the largest single source of error. For a small change in temperature, ΔT , the relative change in intensity from a blackbody in the region of the Wien Law approximation is $C_2 \Delta T / \lambda T$ where C_2 is the second radiation constant, λ the wavelength and T the absolute temperature. At 4850 Å and 2435°K a one degree change or error in temperature causes a 1/2% change in the intensity. During the course of the calibration the temperature of the "blackbody" was held within a slowly fluctuating $\pm 6^\circ\text{C}$ and corrections were made for changes in temperature. The transmissivity of the filters is known to better than 1%. Since the wavelength interval is less than 1 Å and the wavelength is known to better than 1 Å, there is only a negligible error in the present calibration (at 7000 Å an error of 1 Å causes less than 0.1% error in the calculated intensity). Scattered light caused no error except in those

regions of very low light intensity. Also the linearity of the electronics caused no error except for the highest amplification (i.e. low light intensity).

The accuracy of the calibration was estimated to be of the order of 5% in the region of 2800 to 3800 A in the 2nd order and in the region 3300 to 7000 A in the 1st order. A somewhat lower accuracy of the order of 9% is estimated for the region 2600 to 2800 A in the 2nd order because of the low energy available. In the 1st order from 7200 A to 7550 A the accuracy is probably of the order of 9% because of the low sensitivity of the phototube in this region. The high wavelength cut-off of the LP28 photomultiplier tube occurs at approximately 7800 A. At the shorter wavelengths the low accuracy can be improved by operating the "blackbody" at a higher temperature and by using a grating with a more appropriate blaze, and at longer wavelengths by using a detector of relatively higher sensitivity in this region.

Measurements of the ratio of intensity of the "blackbody" at two arbitrarily chosen wavelengths (4000 A and 5200 A) using three different slit widths (10 to 80 microns) resulted in the same value of the ratio. This observation indicates that the calibration is independent of the slit width of the monochromator, and that therefor the slit width can be changed subsequent to the calibration without changing the multiplication factor. A similar test was made with the temperature of the "blackbody" as the variable instead of the slit width of the monochromator. Results of this test indicated that the calibration of the monochromator is independent of the temperature of the "blackbody" during the actual calibration.

Two tungsten-filament lamps to serve as secondary or working standards also were calibrated. The procedure used essentially was to measure the intensity as a function of wavelength of a lamp at some measured temperature with the monochromator and to correct these readings by the proper multiplication factor from Fig. 3.6. The result was the spectral energy emitted by the lamp at that temperature. Comparison of these corrected values of intensity with the blackbody distribution curve at the same temperature is a measure of the emissivity of tungsten thus obtained between 2800 and 7400 A agree within 2% to the corresponding values given in reference 2. This close consistency indicates that our accuracy was considerably better than that estimated from the various possible errors.

5. CONCLUSIONS

With the present response calibration of the monochromator in conjunction with the known spectral emission characteristics of the calibrated tungsten strip lamps it will be possible to compare and to accurately measure radiation intensities over a broad spectral range. An effort will be made to use these known response characteristics to determine the vibrational transition probabilities of molecules such as C_2 , CH and OH.

The "blackbody" will be useful for calibrating response characteristics in other spectral regions and as soon as the instrumentation is completed, an infra-red secondary standard will be calibrated. It is planned also to use the "blackbody" to calibrate total radiation pyrometers.

6. REFERENCES

- [1] Forsythe, W. E., The Measurement of Radiant Energy, McGraw-Hill.
- [2] De Vos, J. C., The Emissivity of Tungsten Ribbon - The Tungsten Strip Lamp as a Standard Source of Radiation, Ph.D. thesis, Univ. of Amsterdam, Holland.
- [3] Michaud, M., Compt Rend. 226, 999 (1948).
- [4] Theron, J. J., Rev. Sci. Instr. 24, 281 (1953).
- [5]a-Fastie, W. G., J. Opt. Soc. Am. 42, No. 9, 641 (1952).
b-Broida, H. P. and Shuler, K. E., J. Chem. Phys. 20, 168 (1952).
- [6] Gibson, S., Spectrophotometry, NBS Circular 484 (1949).

7. FIGURE LEGEND

- 3.1. "Blackbody" for monochromator calibration.
- 3.2. Detail of carbon tube for "blackbody".
- 3.3. Photograph of front of "blackbody". I - leads to water-cooled copper induction coil; S - shutter for protecting window; Q - quartz window.
- 3.4. Photograph showing end of monochromator, recorder and "blackbody".
- 3.5. Schematic diagram of optical arrangement of calibration apparatus. S - "blackbody"; W - quartz window; M_1 and M_2 - front surfaced aluminum mirrors; F - filters; A - entrance slit of monochromator; M - spherical mirror; G - grating; B - exit slit; P - photomultiplier; and E - monochromator housing.
- 3.6. Multiplication factor for the grating monochromator.

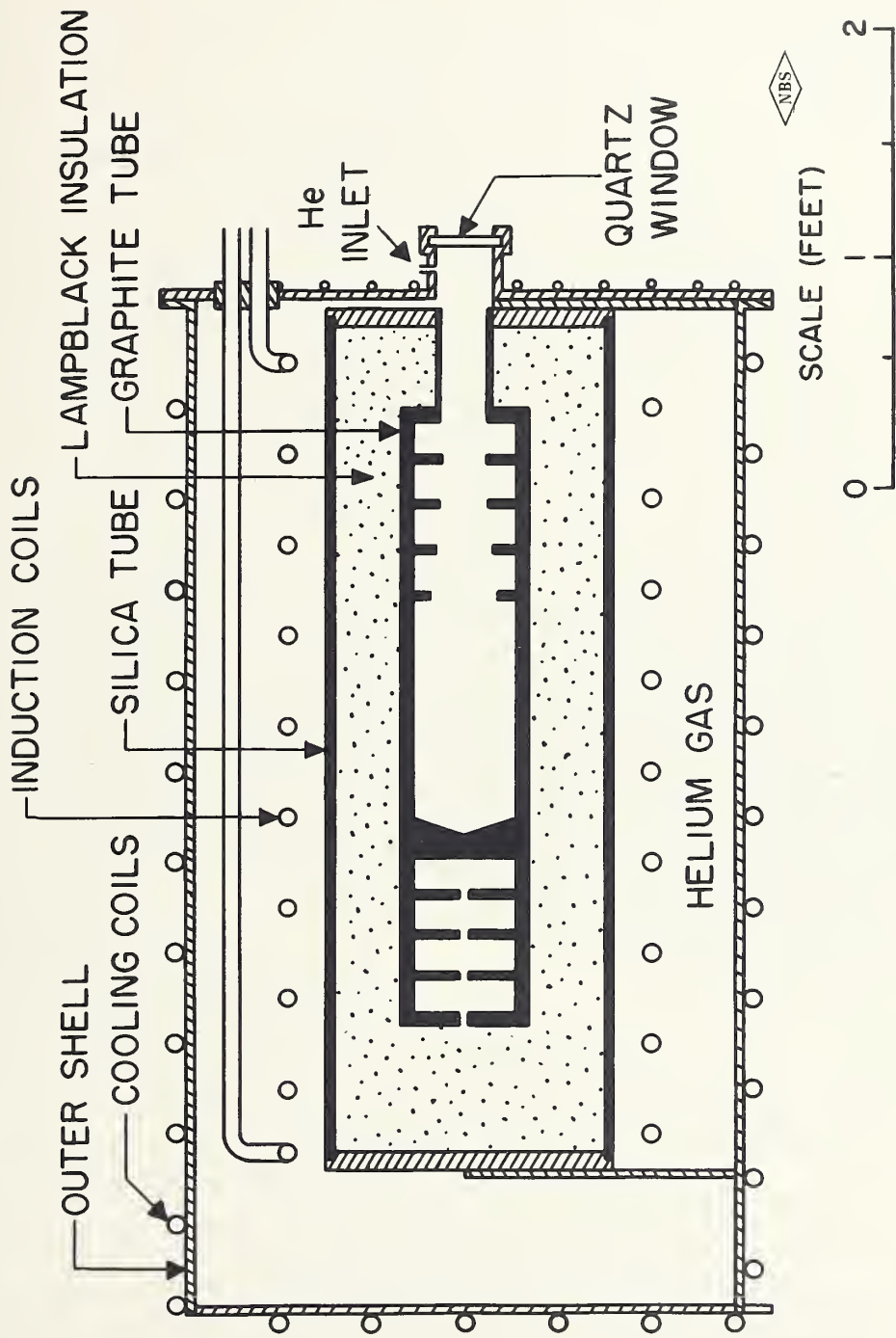
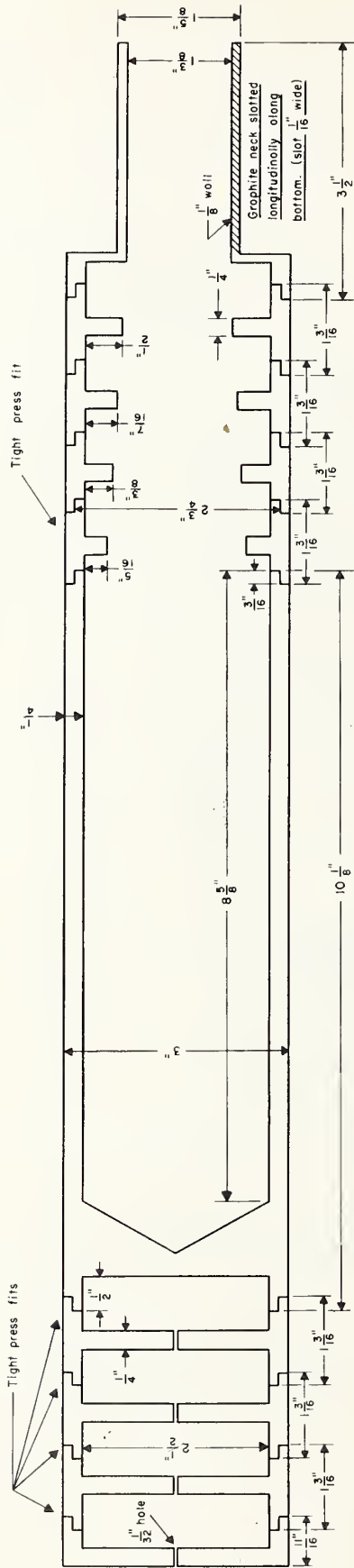


Figure 3.1



Note: — Keep clean and free of oil



Figure 3.2

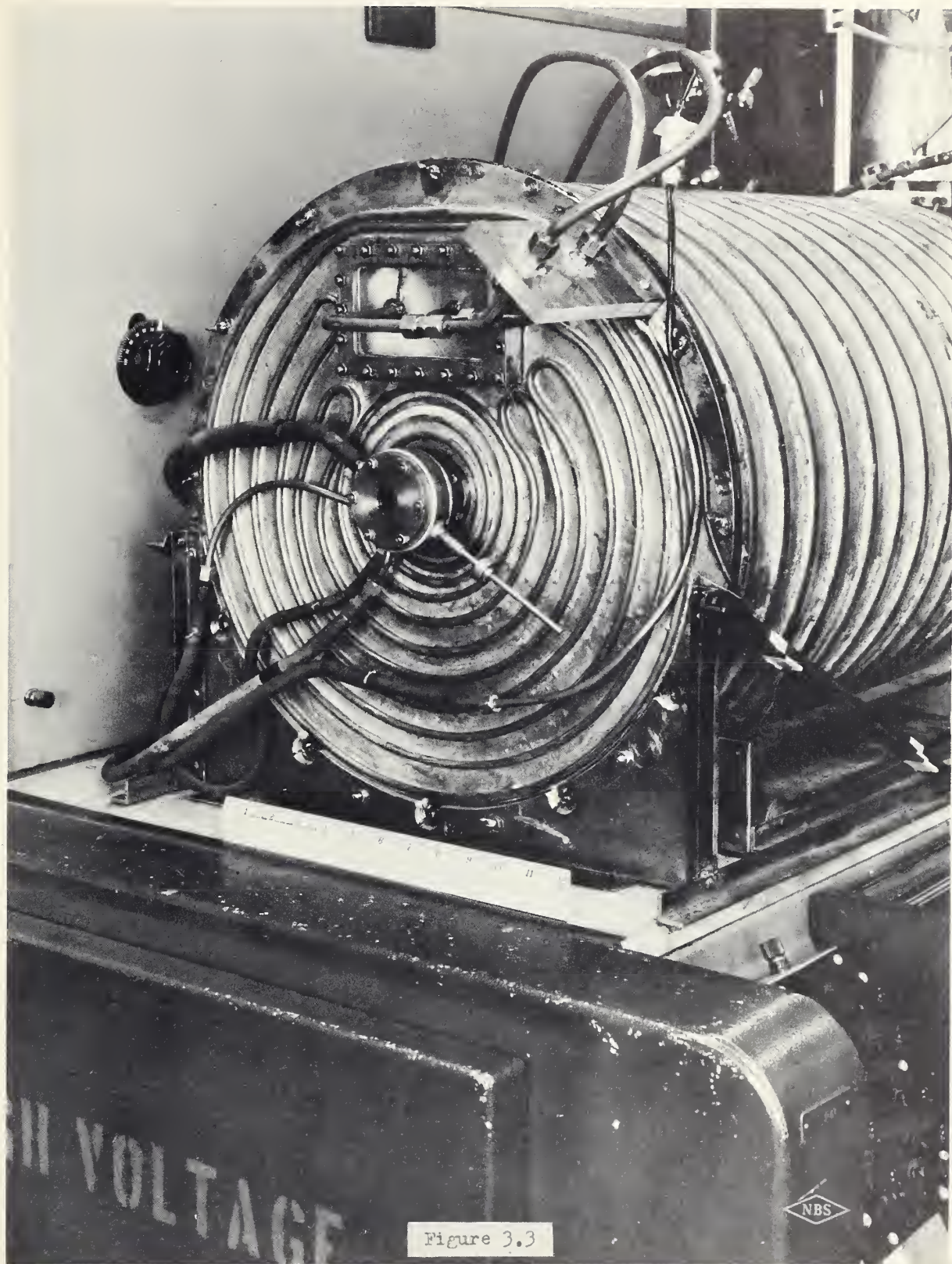


Figure 3.3



Figure 3.4

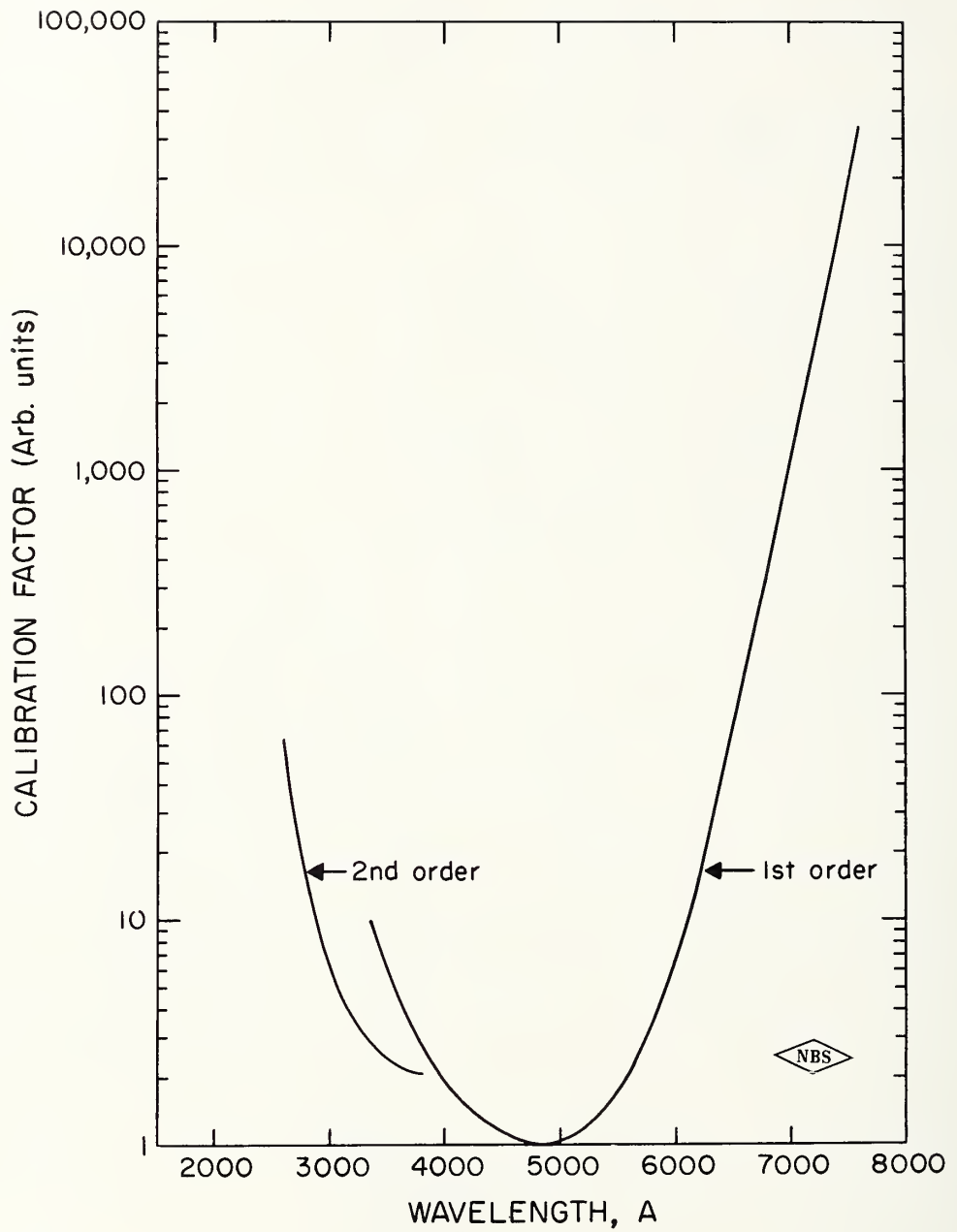


Figure 3.6

4. A Survey of Flame Spectra

N. H. Kiess

A photographic survey of flame spectra was undertaken for the purpose of guiding more specialized study of the problems of combustion. A large number of plates were taken. This report attempts to present the information on these plates in a systematic manner.

The spectra were photographed on Kodak plates. For each of the following prints, the type of plate used and the exposure time are given. In some cases it was necessary to mask the print in order to compensate for the large gradient in plate blackening. The spectrograph used is the Hilger E-2, with interchangeable glass and quartz optics. The dispersion of the glass is about three times that of the quartz. Commercial grade tank gases - fuel and oxygen, sometimes with an inert diluent - were burned on commercial welding torches with port diameters ranging from 0.040 in. to 0.148 in. The flows were regulated and measured to an accuracy of ± 2 per cent. The burner port diameter, total gas flow, and fuel-to-oxygen ratio are given for each figure. To express the latter, the parameter α is used, where

$$\alpha \equiv \frac{\text{fuel/oxygen}}{\left(\text{fuel/oxygen}\right)_{\text{stoichiometric}}}$$

Thus if $\alpha < 1$, the mixture is lean, while if $\alpha > 1$, the mixture is rich.

Figure Legend

Acetylene - Oxygen Flame

- $\alpha = 1.00$: burner port diameter 0.041 in., total flow 35cc/sec.
- Fig. 4.1: quartz optics, plate type 33, exposure time 10 sec. The features include OH extending with uniform intensity over the whole slit. The 0,0 head is at 3064A and the 1,0 head is at 2811A. They also include three CH systems appearing only in the inner cone. The heads of these systems are at 4315A, 3871A, and 3143A. Some of the bands of the C₂ Swan system are visible before the plate sensitivity falls off at the long-wavelength end. These are the 1,0 sequence at 4737A and the 2,0 sequence at 4383A, the latter being superimposed on a branch of the 4315A system of CH.
- Fig. 4.2: quartz, 33, 2 min. The increased exposure brings out the 0,1 and 2,0 sequences of OH, with heads at 3428A and 2608A, respectively. The 1,1 and 1,0 bands of the 3871A CH system, with heads at 4025A and 3628A, respectively, are present. The 0,0 sequence of the C₂ Swan system at 5165A is strong, despite the low plate sensitivity in this region. Between this and the 1,0 sequence appear the 0,1 band of the 4315A CH system, with head at 4890A, and some of the "tail bands" of the Swan system. The Deslandres-d'Azambuja system of C₂ appears, with the 0,0 head at 3852A. The 0,1 head at 4102A is faint, as is the 1,0 head at 3607A. In the region of 3300A to 3700A, where the OH is weak, there appear some of the Schumann-Runge bands of O₂, with best contrast in the outer cone. Also in the outer cone is a continuum at longer wavelengths.
- Fig. 4.3: quartz, II-0, 30 min. It was necessary to mask the print because of the several factors which cause the plate blackening to fall off at short wavelengths. The most important of these is the decrease in radiation from the flame, but absorption by air, gelatine, and quartz also have an effect. In this region the atomic carbon line at 2479A and the 4th positive system of CO are prominent features. The latter extends from about 2800A to 1000A. The Schumann-Runge O₂ bands are in the outer cone, and overlap with the 3,0 sequence of OH, whose head is at 2444A. At 2320A there is a trace of the Mulliken system of C₂.
- Fig. 4.4: quartz, 103-0-UV sensitive, 1 hour. No new systems are brought out, but the 4th positive CO and the Schumann-Runge O₂ bands are extended to the short-wavelength end of the instrument. The print was masked.

[1]



OH 1,0 λ 2811

CH λ 3141

OH 0,0 λ 3064

OH 0,1 λ 3428

O₂ Schumann - Runge →

CH λ 3871

CH and C₂ Swan 2,0 λ 4315

C₂ Swan 1,0 λ 4737

[2]



OH 2,0 λ 2608

CH λ 3134

C₂ D-D 1,0 λ 3607

OH 3,0 λ 2444

OH 2,0 λ 2608

O₂ Schumann - Runge →

CH C₂ D-D 0,1 λ 4025

C₂ D-D 0,0 λ 3852

CH and C₂ Swan 0,0 λ 5165

C₂ tail bands OH 1,0 λ 2811

[3]



← CO 4th Positive

C₂ Mulliken λ 2320

C λ 2479

[4]



← CO 4th Positive

C₂ Mulliken λ 2320

C λ 2479



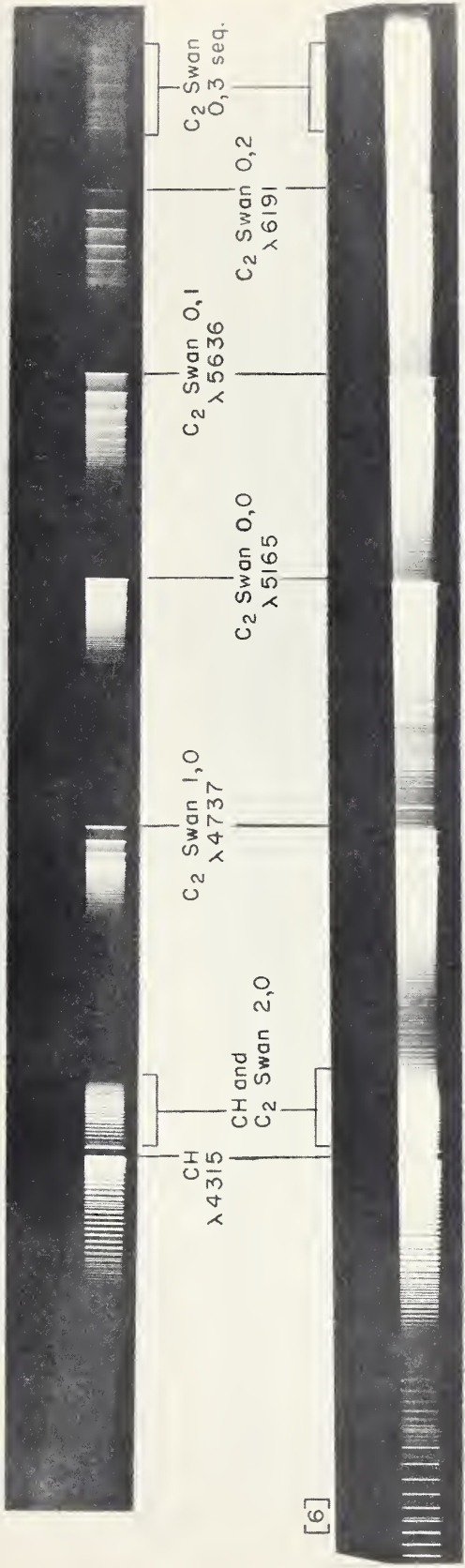
Figure 4.1 - 4.4

Fig. 4.5: glass, II-F3, 10 sec. The CH bands at 3871A and 4315A, and the C₂ Swan system, are shown with a dispersion approximately three times that by using quartz optics. The 3871A CH band is weak because of the cut-off in the transmission of glass in that region. The heads of the Swan bands are: 2,0 sequence, (superimposed on CH), 4383A; 1,0 sequence, 4737A; 0,0 sequence, 5165A; 0,1 sequence, 5636A; 0,2 sequence, 6191A; 0,3 sequence, about 6677A.

Fig. 4.6: glass, II-F3, 100 sec. More of the fine structure of the Swan bands, as well as the "tail bands" of the Swan system, and the 4890A band, are brought out.

Fig. 4.7: glass, I-N, 5 min. There is a complex band system on the long wavelength side of the 0,3 sequence of the Swan system. Masking was necessary because of the high intensity of the complex structure.

[5]



[6]

C2 Swan tail band and CH

[7]

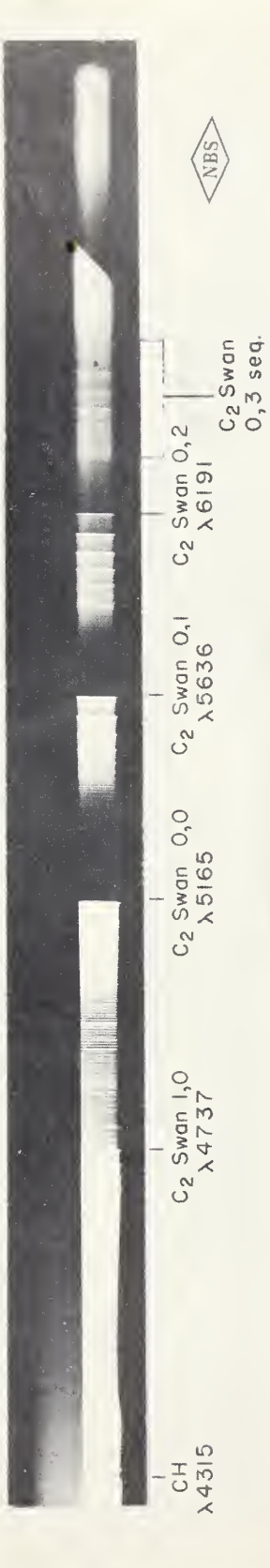


Figure 4.5 - 4.7

$\alpha = 2.00$: port diam. 0.041 in., total flow 45cc/sec.

Fig. 4.8: quartz, 33, 10 sec. This exposure is to be compared with Fig. 4.1, the corresponding exposure for $\alpha = 1.00$. It is seen that the C_2 bands are stronger here, both the Swan system and the Deslandres-d'Azambuja system. The 2,0 sequence of the C_2 Deslandres-d'Azambuja system, with head at 3400Å appears. The 3143Å CH system is enhanced, as are the 4025Å and 3628Å bands of the 3871Å CH system and the "tail bands" of the Swan system.

Fig. 4.9: quartz, 33, 2 min. The increased exposure shows that the Schumann-Runge O_2 bands are absent in this region.

Fig. 4.10: quartz, II-0, 30 min. The C_2 Mulliken bands are comparatively strong in this flame. The atomic carbon line and the CO 4th positive bands are strengthened, while the O_2 bands are faint in this region. Masking was necessary.

Fig. 4.11: quartz, 103-0-UV sensitized, 1 hour. The CO 4th positive bands are extended to the short wavelength end of the instrument (2100Å). Masking was necessary.

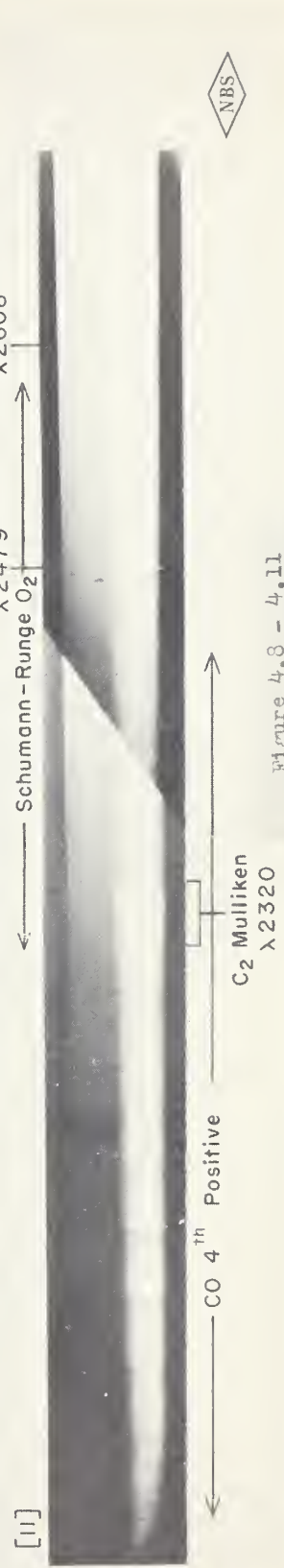
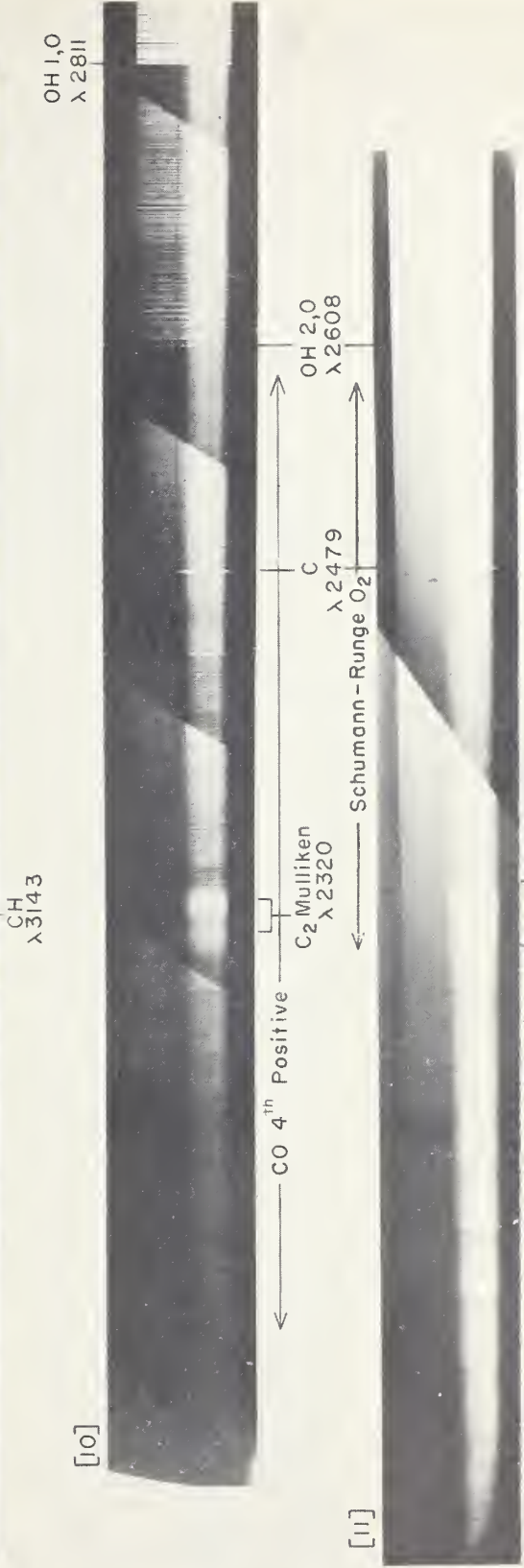
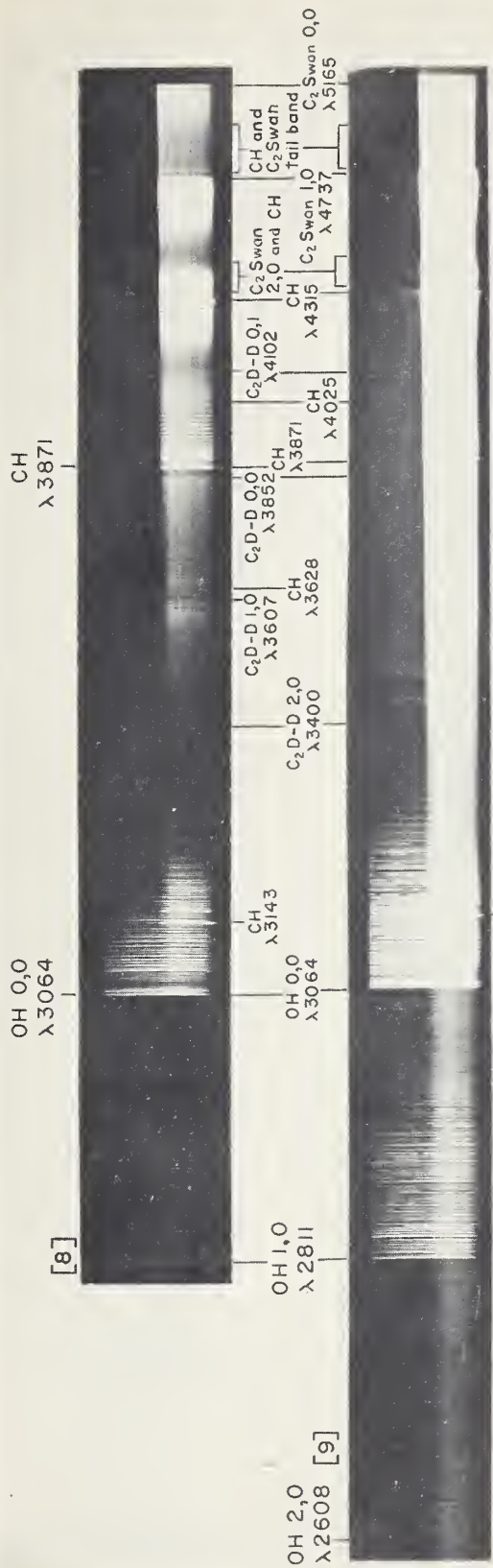


Figure 4.8 - 4.11

Fig. 4.12: glass, II-F3, 10 sec. The Swan system is stronger with respect to the CH bands than for $\alpha = 1.00$.

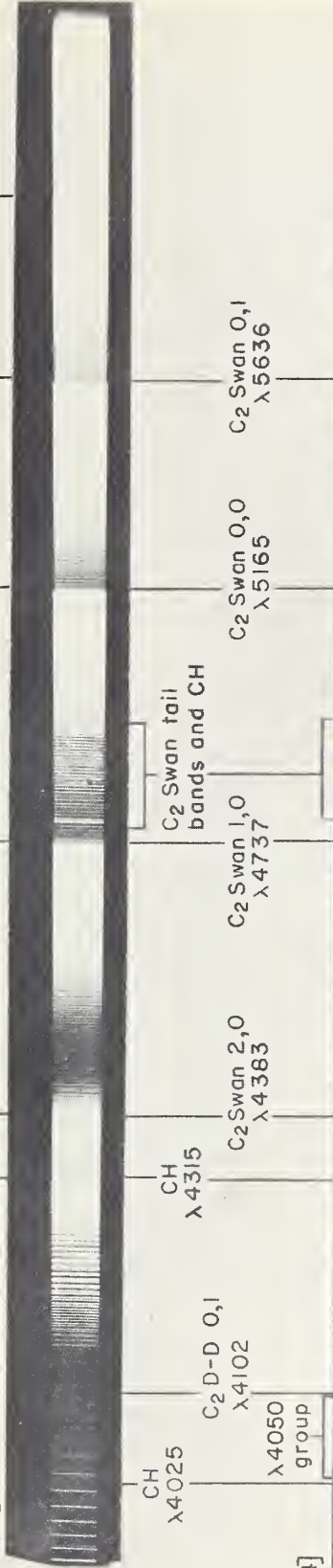
Fig. 4.13: glass, II-F3, 100 sec. The tail bands are brought out, along with more fine structure.

Fig. 4.14: glass, II-F3, 100 sec. The new features are the strong continuum, which becomes stronger toward the red end, and the band systems in the mantle. The C_2 and CH bands, while much weaker than in the inner cone, are nevertheless quite strong. The 4050A group appears equally strong in the inner cone and in the mantle. CN appears as an impurity (3883A). Masking was necessary.

[12]



[13]



[4]

CN O,0 λ 3883



CH λ 3871



Figure 4.12 - 4.14

$\alpha = 3.00$: port diam. 0.041 in., total flow 55cc/sec.

Fig. 4.15: quartz, 33, 10 sec. This mixture burns with a luminous white mantle around the inner cone. The features of the inner cone differ somewhat from those for $\alpha = 2.00$. The OH bands are much weaker and the CH bands are somewhat weaker, while the C_2 bands remain very strong. The 3143A CH band is now rather free from overlapping OH. The mantle contains C_2 and CH, both much weaker than in the inner cone, and OH. CN appears in the mantle alone, the 0,0 head being at 3883A. This is the result of diffusion of air into the flame. Also in the mantle is the "4050A group", attributed to C_2 . It maintains uniform intensity in both the inner cone and the mantle. At medium quartz dispersion it appears as several broad, diffuse lines, one of which is at 4050A. Masking was necessary.

Fig. 4.16: quartz, 33, 2 min. The increased exposure brings out the 1,0 sequence of CN, head at 3590A, and the NH band at 3360A, both resulting from diffusion of air into the flame. Because of the weakness of the OH, a portion of the Fox-Herzberg bands of C_2 appears on the short wavelength side of 3064A. There is a strong continuum over the whole exposure. Masking was necessary.

Fig. 4.17: quartz, II-0, 30 min. In this region also there is a strong continuum. The 2,0 sequence of OH is very weak. The Mulliken C_2 bands are comparatively strong, though not as strong as for $\alpha = 2.00$. The atomic carbon line and the CO 4th positive bands are weak. Masking was necessary.

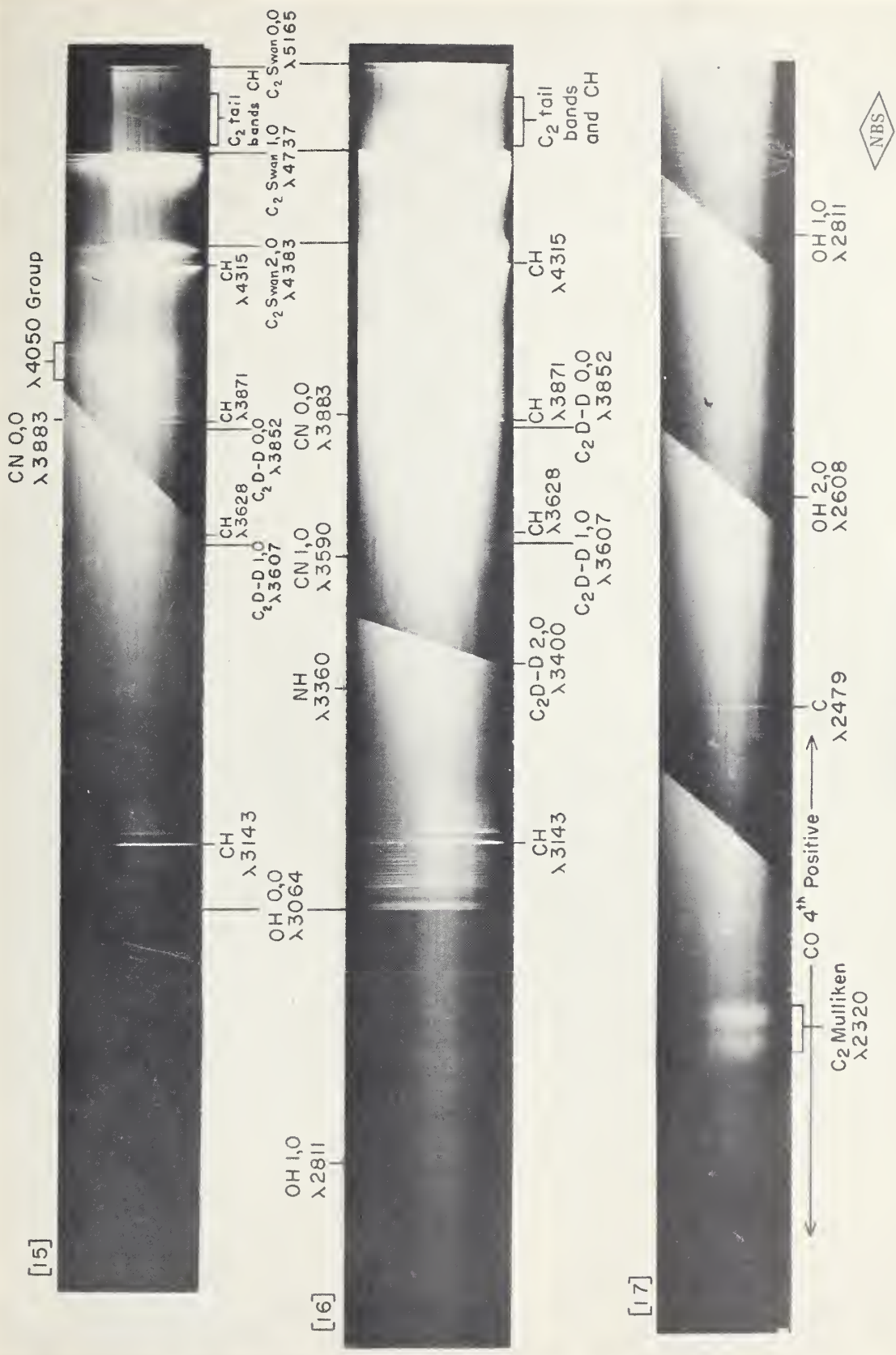


Figure 4.15 - 4.17

$\alpha = 0.400$: port diam. 0.041 in., total flow 36cc/sec.

Fig. 4.18: quartz, 33, 10 min. The intensity of the flame as a whole is much less than for $\alpha = 1.00$. However, it is the intensities of the bands with respect to each other that is of primary interest. Relative to the OH bands, the Swan bands are much reduced in intensity. The 3143A CH system is also much reduced, as are the higher transitions (1,0 and 1,1) of the 3871A CH system. The 0,0 bands of the 3871A and 4315A systems are slightly reduced. The Deslandres-d'Azambuja system of C_2 is absent. In the outer cone, the Schumann-Runge O_2 bands appear with good contrast. In the inner cone there is an extensive band system, between 4000A and 2500A, appearing as a wavy background. These are the "hydrocarbon flame bands", believed to be emitted by CHO. They begin to appear as the flame becomes lean, and are strong in this flame.

Fig. 4.19: quartz, II-0, 30 min. The increased exposure brings out the CH, O_2 , and hydrocarbon flame bands below 3064A.

Fig. 4.20: glass, 103-F3, 15 min. Because of the decrease in intensity of the Swan bands, the CH band at 4890A stands out. Fine structure at the long-wavelength end appears not to belong to the Swan system. Schumann-Runge O_2 bands are in the outer cone, weak, up to about 5000A. There is a fairly strong continuous background in both inner and outer cones, which extends to shorter wavelengths.

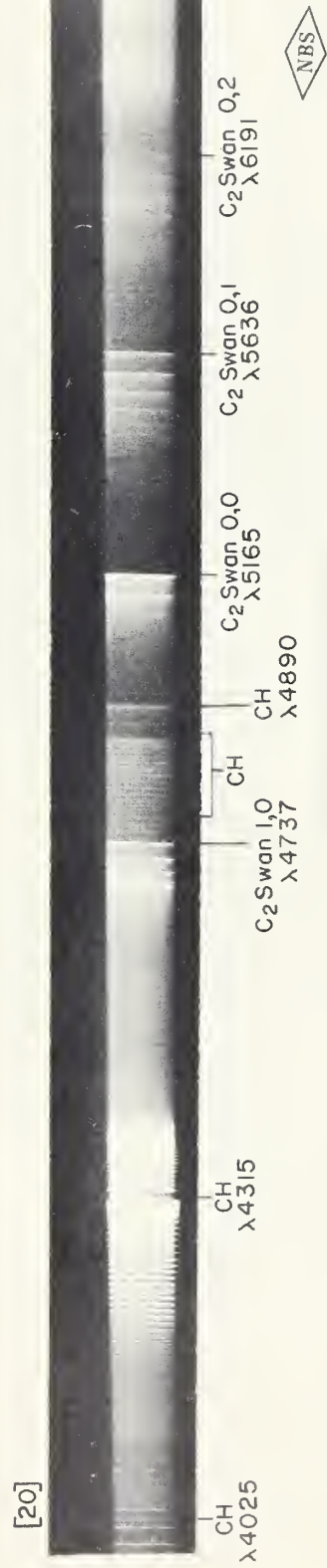
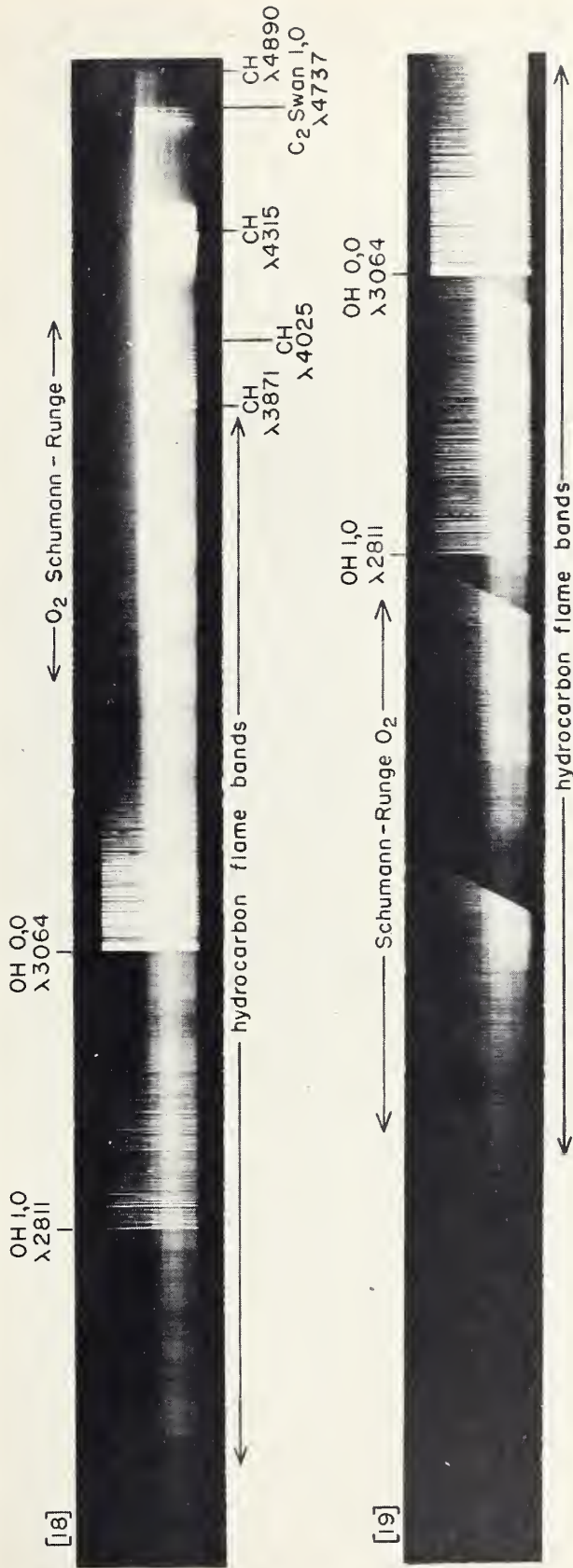


Figure 4.18 - 4.20

$\alpha = 0.200$: port diam. 0.088 in., total flow 54cc/sec.

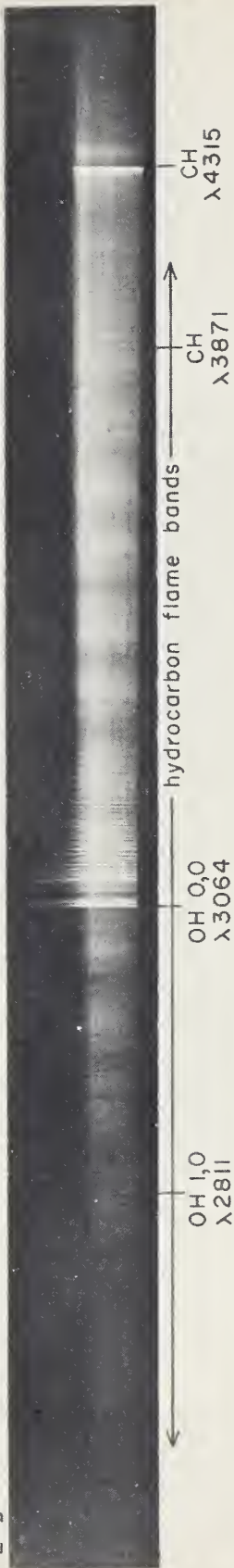
Fig. 4.21: quartz, 103-0, 10 min. There are no other band systems than the hydrocarbon flame bands, OH, and CH. The latter two are highly suppressed, while the former is now the prominent feature of the flame.

$\alpha = 0.191$: port diam. 0.072 in., total flow 40cc/sec.

Fig. 4.22: quartz, 103-0-UV sensitive, 2 hours. The long exposure brings out the hydrocarbon flame bands at shorter wavelengths than 2500A. There are no other OH bands than the 0,0 and 1,0.

Fig. 4.23: glass, 103-D, 30 minutes. In this region there is only a slight trace of the Swan system - the 0,0 head at 5165A. A weak, wavy structure between the CH bands at 4315A and 4890A is the "carbon monoxide flame bands", the emitter of which is believed to be CO_2 . A continuous background is evident.

[21]



[22]



[23]



Figure 4.21 - 4.23

$\alpha = 0.126$: port diam. 0.127 in., total flow 27cc/sec.

Fig. 4.24: quartz, 103-0, 10 minutes. No outer cone appears. The only diatomic bands are the 0,0 OH and the 4315A CH. These are very weak. The rest is hydrocarbon flame bands.

Hydrogen-Oxygen Flame

$\alpha = 1.12$: port diam. 0.072 in., total flow 98cc/sec.

Fig. 4.25: quartz, 103-0, 90 sec. The 0,0; 1,0; 2,0; and 0,1 sequences of OH are strong. The 3,0 sequence, with head at 2444A, and the 0,2 sequence, head at 3920A, are weak. There is a continuum at the long-wavelength end.

$\alpha = .331$: port diam. 0.072 in., total flow 66cc/sec.

Fig. 4.26: quartz, 103-0, 20 min. Strong OH, with O₂ mixed in.

OH O,0
 λ 3064

CH
 λ 4315

[24]



[25]



OH 3,0
 λ 2444

OH 2,0
 λ 2608

OH 1,0
 λ 2811

OH O,0
 λ 3064

OH O,1
 λ 3428

OH O,2
 λ 3920

[26]



NBS

Figure 4.24 - 4.26

$\alpha = 2.00$: port diam. 0.041 in., total flow 35cc/sec.
Fig. 4.27: quartz, 103-0, 20 min. This flame is comparatively weak in overall intensity. The C_2 bands are relatively stronger than for $\alpha = 1.00$. There is slight evidence of hydrocarbon flame bands.

Propane-Oxygen Flame

$\alpha = 1.00$: port diam. 0.041 in., total flow 24cc/sec.
Fig. 4.28: quartz, 103-0, 20 min. The band systems here are all found in the acetylene-oxygen flame. The difference is that the carbon-containing bands, especially C_2 , are relatively weaker compared to OH than in the acetylene oxygen flame. This is true for all values of α . Furthermore, the overall intensity is less. In the inner cone is a trace of the hydrocarbon flame bands. There is a continuum at longer wavelengths.

$\alpha = .261$: port diam. 0.127 in., total flow 42cc/sec.
Fig. 4.29: quartz, 103-0, 20 min. No Swan bands. OH and the hydrocarbon flame bands are relatively strong. CH is relatively weak.

[27]



OH 2,0 λ 2608
 OH 1,0 λ 2811
 OH 0,0 λ 3064
 CH λ 3143
 OH 0,1 λ 3428
 C₂D-D 1,0 λ 3607
 CH λ 3628
 C₂D-D 0,0 λ 3852
 CH λ 3871
 CH λ 4025
 CH λ 4315
 CH end C₂
 C₂ Swan 1,0 λ 4737
 C₂ Swan 0,0 λ 5161
 CH λ 4890

[28]



OH 1,0 λ 2811
 OH 0,0 λ 3064
 CH λ 3143
 CH λ 3871
 CH λ 4315

[29]



hydrocarbon flame bands
 Hg (impurities)

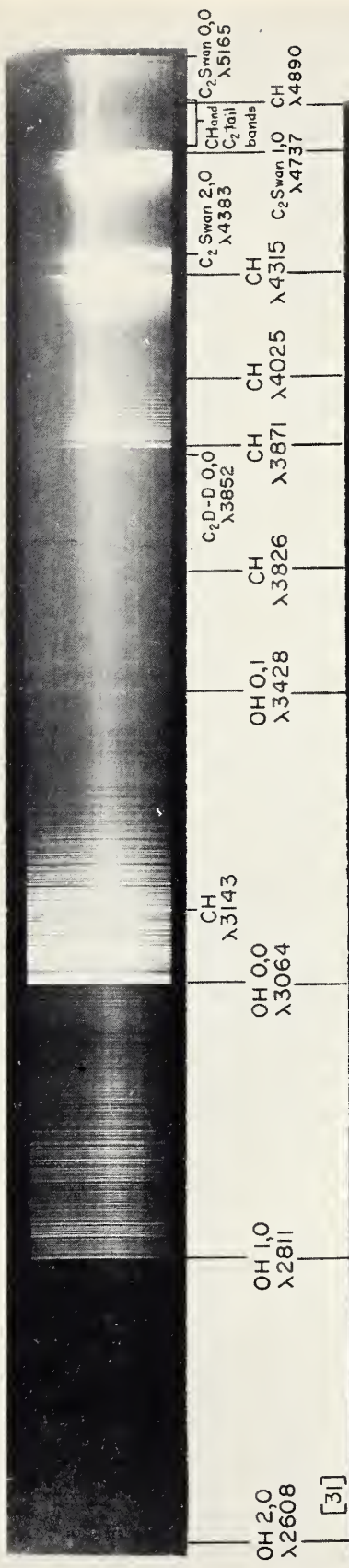


Figure 4.27 - 4.29

Methane-Oxygen Flame

- $\alpha = 2.00$: port diam. 0.041 in., total flow 20cc/sec.
Fig. 4.30: quartz, 103-0, 1 hour. This flame is weak in overall intensity. As in the rich flames of acetylene and propane, the C_2 bands are strong compared with the other bands, but here the Deslandres-d'Azambuja system of C_2 is very weak, only the 0,0 head at 3852A showing.
- $\alpha = 1.00$: port diam. 0.041 in., total flow 30cc/sec.
Fig. 4.31: quartz, 103-0, 10 min. The overall intensity is much less than that of the acetylene-oxygen flame of same α . Relatively, however, the OH remains strong, while the CH is weaker and the C_2 is very much weaker. There is a trace of the hydrocarbon flame bands, and a continuum at long wavelengths.
- $\alpha = .500$: port diam. 0.041 in., 25cc/sec.
Fig. 4.32: quartz, 103-0, 10 min. This flame differs from other hydrocarbon flames of comparable values of α in that OH is by far the strongest feature. The Swan bands are absent and the CH and hydrocarbon flame bands are weak.

[30]



[31]



[32]



Figure 4.30 - 4.32

Acetylene-Oxygen Flame Diluted with Carbon Dioxide

$\alpha = 2.00,$

50% CO₂ : port diam. 0.148 in., 54cc/sec.

Fig. 4.33 : quartz, 33, 8 min. Diatomic spectra, hydrocarbon flame bands, and carbon monoxide flame spectra are all present.

$\alpha = 1.00,$

64% CO₂ : port. diam. 0.148 in., total flow 58 cc/sec.

Fig. 4.34 : quartz, 103-0, 2-1/2 min. The diatomic spectra are suppressed, while the hydrocarbon flame bands are by far the strongest feature. The characteristics of the carbon monoxide flame-continuum and wavy band structure - are present.

$\alpha = .400,$

50% CO₂ : port diam. 0.148 in., 35cc/sec.

Fig. 4.35 : quartz, 33, 10 min. The outer cone is too weak to register. Diatomic spectra are highly suppressed, while the hydrocarbon flame bands show up with great strength and high contrast.

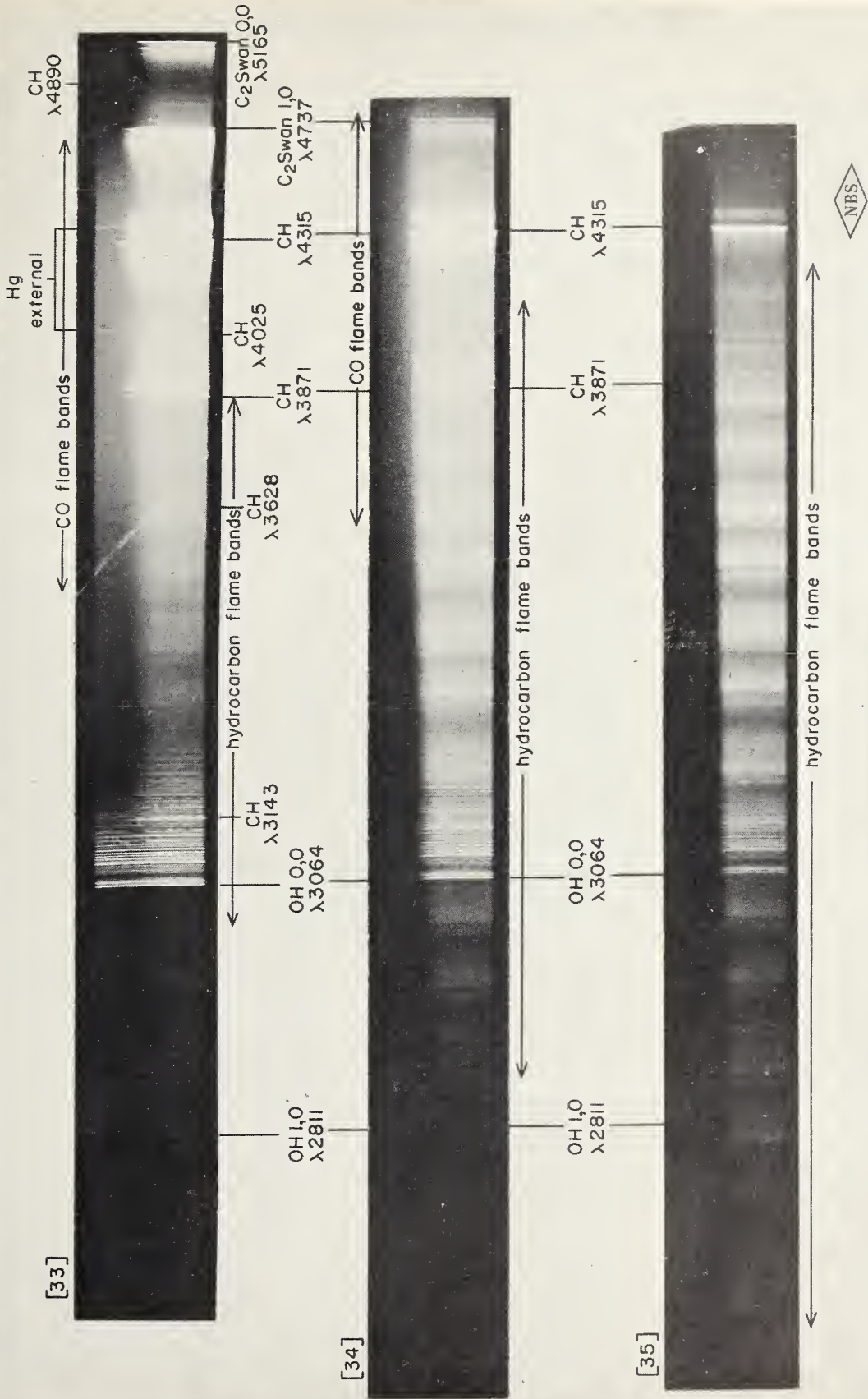


Figure 4.33 - 4.35

fig. 36: This graph gives estimates of the intensities of the principal band systems in the acetylene-oxygen flame as a function of \mathcal{L} . The intensities are graded on a scale from 1 to 1000, and the units are completely arbitrary. They are based on visual impressions from examining and inter-comparing plate blackenings, compensating, if necessary, for differences in exposure time and plate type. They are intended to serve as a rough guide as to what fuel to oxygen ratios to use to bring out these band systems.

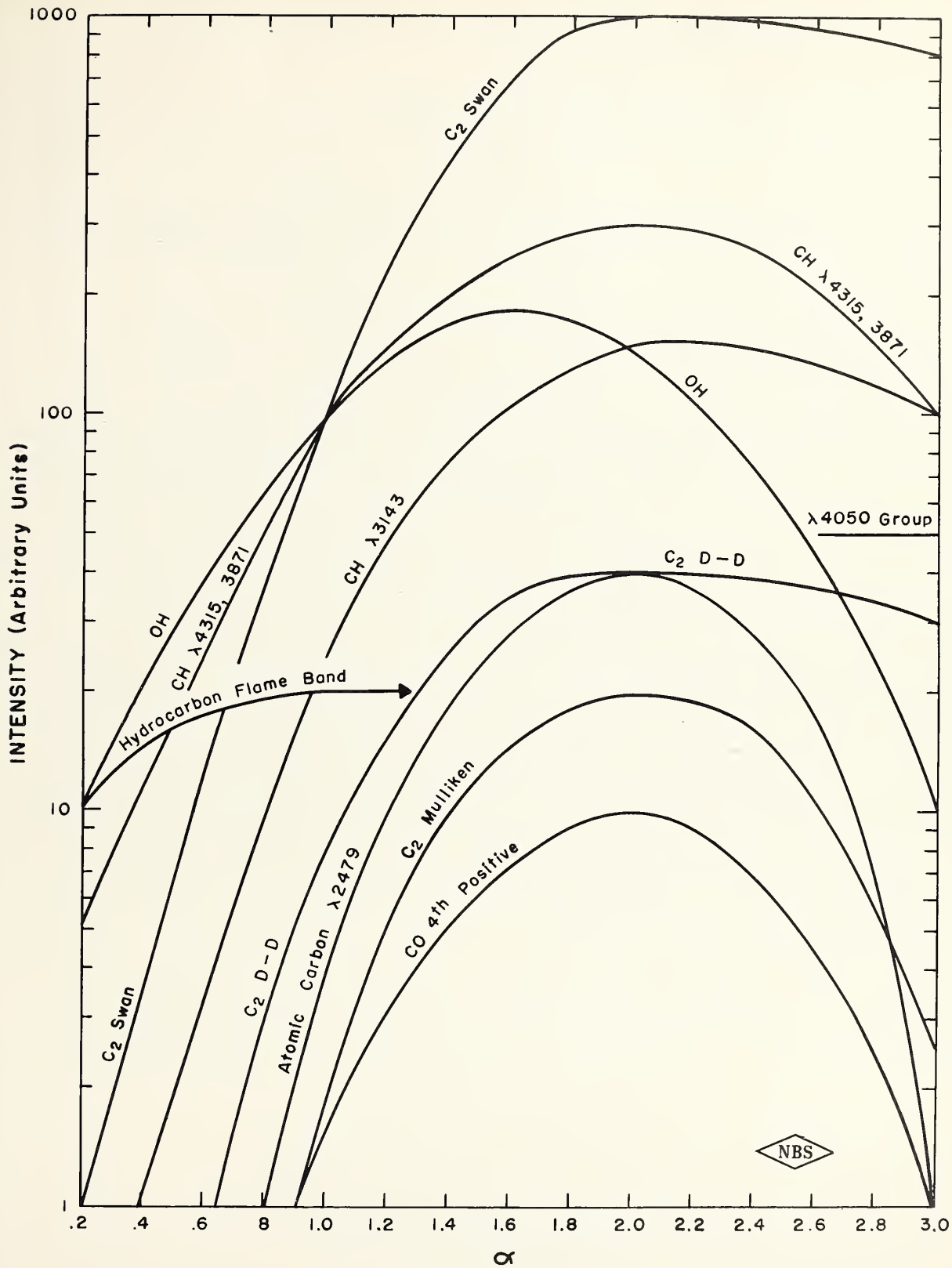


Figure 4.36

5. The $\lambda 4050$ Group of Cometary Spectra in the Acetylene-Oxygen Flame*

Norman H. Kiess and Arnold M. Bass
(National Bureau of Standards, Washington, D. C.)

The group of emission bands which has been observed in spectra of comets and late class N-stars, in the region of $\lambda 4050$, has been produced recently in the laboratory in a number of sources.¹ Durie² has observed the $\lambda 4050$ emission in the flame reaction of fluorine with organic compounds, but to the best of our knowledge these bands have not been observed before in flames burning in oxygen. We have recently observed a band emission in the $\lambda 4050$ region in the radiation from the luminous zone of a fuel-rich acetylene-oxygen flame. This luminous zone appears at a fuel-to-oxygen ratio of about 2.6 times stoichiometric, and remains in the flame well beyond the ratio of 4 times stoichiometric. The low dispersion spectrum in this region shows a group of bands similar to that observed by Durie² and Herzberg³. Figure 5.1 is a reproduction of the spectrum as photographed with a Hilger E-2 spectrograph with glass optics. The source for this exposure was an acetylene-oxygen flame, of fuel to oxygen ratio three times stoichiometric, burning on a welding torch with a port diameter of 1 mm. The exposure time was 1 minute on a spectrum analysis No. 1 plate. The bands of the $\lambda 4050$ group are clearly discernible as they extend unchanged over the whole slit, while the other features of the spectrum (which are mostly CH) show a marked decrease in intensity in going from the inner cone to the outer cone. Through the cooperation of the Spectroscopy Section of this Bureau, these bands were photographed in the second order of a 21 foot grating spectrograph with dispersion of 0.88A/mm. The spectrum at this high resolution resembles that described by Douglas⁴ as obtained in a discharge between carbon electrodes. Our spectrum is much richer in lines, as would be expected by considering the much higher temperature of our source. Fig. 5.2 is a reproduction of a densitometer tracing of the spectral region between 4050 and 4075 A. This tracing was taken from a spectrum analysis No. 1 plate exposed for 4 1/2 hours by using as a source a three times stoichiometric acetylene-oxygen flame burning on a rectangular slot burner of dimensions 50 mm by .076 mm. The region of the flame selected for this trace lies above the reaction zone.

Douglas has suggested that these bands may be explained as arising from a $\Sigma-\pi$ transition of a linear C_3 molecule, and he has presented an analysis of the rotational structure of the band which forms a head at 4050A. For most of the lines of this band our measurements agree with those of Douglas to better

*Submitted for publication in The Journal of Chemical Physics

1. For a recent complete review of this problem see B. Rosen and P. Swings, *Ann. d'Astrophys.*, 16, 82 (1953).
2. R. A. Durie, *Proc. Roy. Soc., Lond.*, A211, 110 (1952)
3. G. Herzberg, *Astrophys. J.*, 96, 314, (1942)
4. A. E. Douglas, *Astrophys. J.* 114, 466 (1951).

than 1 cm^{-1} in the spectral range in which the data overlap. Because of the higher excitation temperature which we used, we have been able to extend the analysis suggested by Douglas to higher rotational quantum numbers. The extended analysis is presented in Table 5.1. The lines for J less than 48 are omitted since the wavelengths which we measured are essentially the same as those reported by Douglas. For the type of transition postulated by Douglas, our measurements lead to the following constants:

$$B' = 0.413 \text{ cm}^{-1}$$

$$B'' = 0.430 \text{ cm}^{-1}$$

$$D' = 0.45 \times 10^{-6} \text{ cm}^{-1}$$

$$D'' = 0.90 \times 10^{-6} \text{ cm}^{-1}$$

$$\nu_0 = 24675.75 \text{ cm}^{-1}$$

These values for B'' , B' , and D'' are in very close agreement with those of Douglas. For D' Douglas reports a value of $0.26 \times 10^{-6} \text{ cm}^{-1}$ which is considerably smaller than that which we found.

TABLE 5.1

Extended analysis of the $\lambda 4050$ band of C_3

J	P(J)	Wave number cm^{-1}		R(J)
		Q(J)		
48	24598.61		24678.44	
49		24637.45		
50	94.20			77.09
51		34.59		
52	89.58			75.96
53		31.58		
54	84.90			74.63
55		28.51		
56	80.03			73.20
57		25.45		
58	75.46			71.61
59		22.28		
60	70.74			70.17
61		19.06		
62	65.84			68.37
63		15.62		
64	60.87			66.52
65		12.38		
66	55.82			64.38
67		08.81		
68	50.75			62.18
69		05.27		
70	45.49			
71		01.71		
72	40.29			
73		598.08		
74	34.83			
75		94.38		
77		90.65		
79		86.76		
81		82.87		
83		78.88		
85		74.83		
87		70.74		
89		66.54		
91		62.32		
93		58.13		
95		53.74		
97		49.38		
99		44.85		
101		40.29		
103		35.72		
105		31.11		
107		26.22		
109		21.60		
111		16.60		

Figure Legends

Figure 5.1. Emission spectrum of acetylene-oxygen flame as photographed with Hilger E-2 glass prism spectrograph.

Figure 5.2. Densitometer trace of the $\lambda 4050$ band in emission from acetylene-oxygen flame. Original plate photographed with 21 foot grating spectrograph, dispersion 0.88 A/mm.

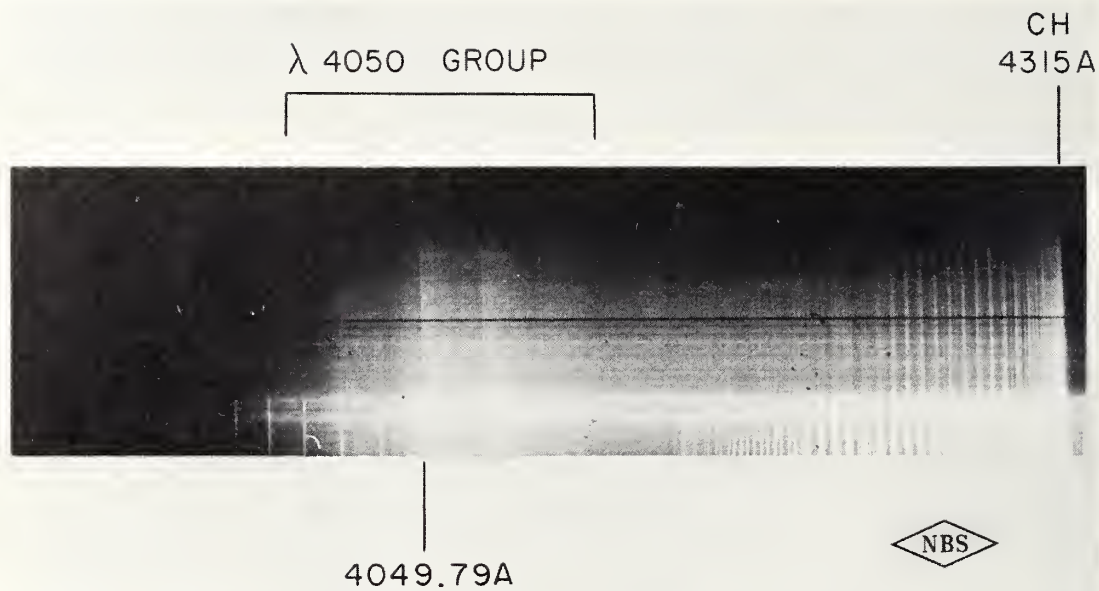
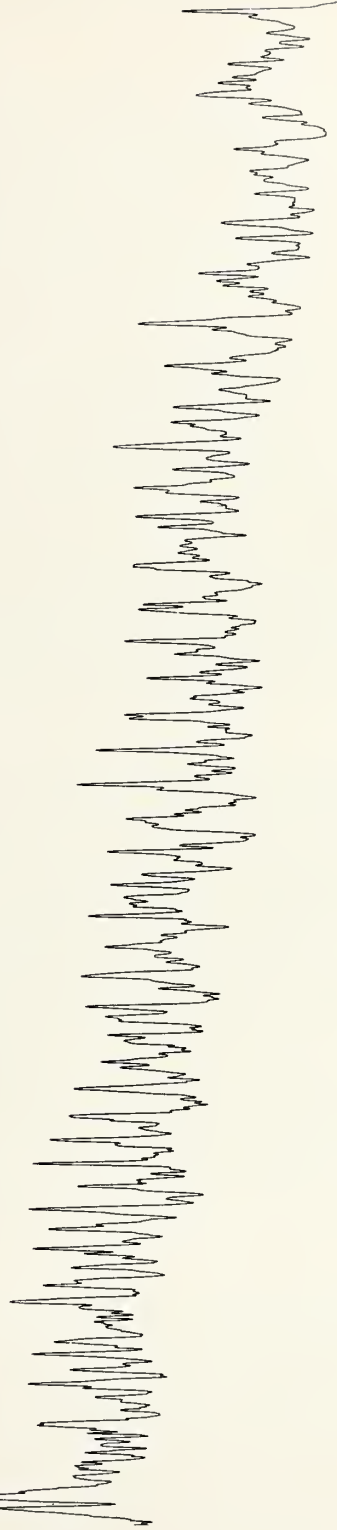


Figure 5.1

40 50 60
R

Q 21 31 41 51 61 71 81 91 101

CH P 20 30 40 50 60 70



24675 24625 24575 cm⁻¹
4050 4060 4070A

Figure 5.2

6. THE DECOMPOSITION OF CF_4 IN FLAMES

B. E. Squires

Recent studies of discharges through fluorocarbon vapours have led to the discovery and partial analysis of several band systems ascribed to emission by electronically excited CF and CF_2 molecules¹⁻³. The thermal decomposition of CF_4 in a graphite furnace has permitted the observation of the same band systems in absorption⁴. It seemed of interest to explore other convenient

¹Andrews and Barrow, Nature, 165, 890 (1950).

²Laird, Andrews, and Barrow, Trans. Faraday Soc. 46, 803 (1950).

³Venkateswarlu, Phys. Rev., 77, 676 (1950).

⁴Andrews and Barrow, Proc. Phys. Soc., 64, 481 (1951).

means for studying the breakdown of CF_4 . The admixture of the stream of the vapour of this fluorocarbon in an acetylene-oxygen flame results in a many-banded spectrum in which new bands belonging to the previously found $2\Sigma - 2\Pi$ transition of CF have been identified. The CF_2 bands found in earlier work^{1,2,5} do not seem to be present.

⁵Margrave and Wieland, J. Chem. Phys., 21, 1552 (1953).

Spectrograms were taken with a Hilger E-2 instrument using glass optics from 8700 to 4000 A and quartz optics from 5000 to 2100 A. Eastman plates were used of emulsions 103 and I variously sensitized from 2100 to 9000 A. Iron comparison spectra are shown on most plates. Because of the limited time, photographs were first taken only when a flame showed visible changes by the addition of fluorocarbons, either by the naked eye or with the use of a pocket spectroscope. These boundaries were extended when it seemed desirable to bring out some weak aspect of the spectra in the invisible portions of the spectrum. The acetylene-oxygen flame was not photographed using glass optics. Ordinary welding torches and a slot burner 5 cm. long and .075 or .15 mm wide were used. The prints in this report are those which show nearly all of the observed spectra.

Introduction of CF_4 deepens the color of the blue outer cone of the acetylene-oxygen flames. For a fuel to oxygen ratio of 2.0, the 1-0, 0-0, 1-1, 0-1, 0-2, and 0-3 bands of the CF system A-X were observed in the inner cone. The 0-2 and 0-3 bands with heads at 2479 and 2559 A were not reported by Andrews and Barrow^{1,3}, and may have been missed because of overlapping by the CF_2 bands found in the discharge. The 0-4 and possibly the 0-5 bands also were present in the flame but were obscured by overlapping bands of CS, which were strong in the region between 2494 and 2715 A. CCl bands between 2777 and 2790 A

also were prominent, and a few copper lines were observed. The usual acetylene flame spectra of C_2 , CH, CN, CO, and OH were not appreciably altered (see plates 6.1 to 6.10, 6.17 and Table 6.1).

The appearance of the A-X system of CF seemed to be favored for a fuel to oxygen ratio of 2.0. A lower fuel to oxygen ratio produced a flame slightly brighter visibly but somewhat smaller and less favorable for the appearance of the C_2 Deslandres-D'Azambuja system. A higher ratio produced a flame less bright visibly with a larger orange mantle and somewhat less stable. The amount of CF_4 added was adjusted to produce the maximum intensity of the CF bands; greater amounts apparently cooled the flame and lesser amounts reduced the population of CF. A sharp band head was observed at 2781.9 Å which has not been positively identified; it is probably due to CCl. No evidence was found of the B-X²Π system attributed to CF; this is most probably due to the greater intensity of the CO fourth positive system in this region.

The appearance of hydrogen-oxygen flames is markedly changed by the addition of CF_4 . The nearly colorless flame appears blue with a tinge of red. For a fuel to oxygen ratio of 1.0, spectra due to the impurities Cu, CuCl, CuF, CuO, K and Na were observed with the addition of CF_4 . The usual OH spectra of hydrogen-oxygen flames was not appreciably altered (see plates 6.11 to 6.16, Table 6.2). An extensive system of bands was observed for wavelengths greater than 7000 Å but it has not been identified; it would require more extensive study than has been made. Other than the usual OH bands, no radiation was observed below 3000 Å with exposures as long as 1.5 hours.

The CuF bands (see plate 6.13) have been observed in flames, probably for the first time. Both the CuF and CuCl bands (see plate 6.15) were fairly intense even with a few minutes exposure, showing several vibrational transitions not listed in the compilation of Pearse and Gaydon.⁶ The copper as an impurity in

⁶Pearse and Gaydon, The Identification of Molecular Spectra, Second Edition, Chapman and Hall, London (1950).

the spectra comes from the tip of the brass burner which showed definite signs of erosion after several hours of use with these flames, particularly with hydrogen. Possibly this erosion is caused by the action of atomic fluorine or hydrogen fluoride which may be formed in the lower portions of the flame, although their spectra were not observed. The cooling of the burner also makes possible the condensation of water and the consequent formation of hydrofluoric acid if hydrogen fluoride is present. The chlorine is a known impurity in the CF_4 gas in the form of $FCl_2C:CCl_2F$ in quantities up to 6%. The sources of sodium, potassium, and sulphur are not known, but they are common impurities in flames. It appears likely that a very small amount of CS_2 was in the CF_4 , and also the intensity of the CS bands were greater in the first sample of CF_4 than in the second.

This study of these spectra has encouraged us to investigate such "mixed" flames, partly in order to search for new bands or spectra, and partly to obtain spectra under higher resolution so that detailed analyses may be made.

TABLE 6.1. Compilation of bands and lines observed in an acetylene-oxygen-carbon tetrafluoride flame. Intensities listed are relative, estimated on a scale of 1000. Bands with an asterisk (*) are estimated wavelengths and most probable assignments.

<u>System</u>	<u>Wave Length</u>	<u>v', v''</u>	<u>Intensity</u>
C ₂ Swan	5165.2	0,0	500
	5129.3	1,1	300
	5097.7	2,2	200
	4737.1	1,0	900
	4715.2	2,1	800
	4697.6	3,2	800
	4684.8	4,3	800
	4382.5	2,0	500
	4371.4	3,1	500
	4365.2	4,2	700
Deslandres-D'Azambuja's	3852.2	0,0	200
	3607.3	1,0	90
	3592.9	2,1	90
	3587.6	3,2	100
	3399.7	2,0	80
CCl	2789.8	0,0	70
	2788.3	1,1	70
	2782.3	0,0	60
	2778.8	0,0	70
	2777.6	1,1	70
CF A-X	*2551.5	0,3	30
	*2558.8	0,3	30
	*2475.0	0,2	50
	*2479.3	0,2	50
	*2404.1	0,1	40
	*2400.2	0,1	40
	2331.8	0,0	10
	2327.8	0,0	10
	2308.7	1,1	10
	2304.6	1,1	10
	2242.2	1,0	10
	2238.2	1,0	8
CH 4300 A	4312.5	0,0	1000

TABLE 6.1. (Cont.)

<u>System</u>	<u>Wave Length</u>	<u>vⁱ, vⁱⁱ</u>	<u>Intensity</u>
CH 3900 A	3889.0	0,0	300
	3871.1	0,0	400
	3628	1,0	40
CH 3143 A	3143.4	0,0	1000
	3156.6	1,1	100
CN Violet	3883.4	0,0	400
	3871.4	1,1	200
	3861.9	2,2	100
CO Fourth Positive	2311.5	7,16	8
	2286.1	6,15	10
	2261.7	5,14	9
	2238.3	4,13	2
	2221.5	7,15	9
	2196.8	6,14	10
	2173.0	5,13	9
	2150.2	4,12	8
	2137.0	7,14	2
	2128.3	3,11	3
	2113.1	6,13	4
	2107.2	2,10	3
	CS	2708.9	3,4
2693.2		2,3	20
2677.0		1,2	30
2662.6		0,1	30
2621.6		3,3	20
2605.9		2,2	20
2589.6		1,1	50
2575.6		0,0	60
2538.7		3,2	40
2523.2		2,1	30
2507.3		1,0	20
2493.7	5,3	8	
NH	3360	0,0	200

TABLE 6.1. (Cont.)

<u>System</u>	<u>Wave Length</u>	<u>v', v''</u>	<u>Intensity</u>
OH	3063.6	0,0	200
	2945.2	3,2	10
	2875.3	2,1	20
	2811.3	1,0	60

<u>Element</u>	<u>Wave Length</u>	<u>Intensity</u>
Copper	3274.0	100
	3247.6	100
	2247.0	5
	2242.6	4
	2238.5	4
	2236.3	4
	2230.1	6
	2227.8	2
	2225.7	5
	2214.6	2
	2199.8	2
	2199.6	2
	2192.3	2
	2181.7	4
	2178.9	4
2169.5	1	
2165.1	2	

TABLE 6.2. Compilation of bands and lines observed in a hydrogen-oxygen-carbon tetrafluoride flame. Intensities listed are relative, estimated on a scale of 1000. Bands with an asterisk (*) are estimated wavelengths and most probable assignments.

<u>System</u>	<u>Wave Length</u>	<u>v', v''</u>	<u>Intensity</u>	
CuCl "B"	4982.2	0,1	50	
	4881.5	0,0	500	
	4788.5	1,0	200	
	"D"	*4773	0,5	40
		*4686	0,4	80
		*4600	0,3	300
		4515.9	0,2	500
		4433.8	0,1	700
		4353.9	0,0	900
		4280.9	1,0	600
4211.0	2,0	300		
*4146	3,0	100		
"E"	*4745	0,5	40	
	*4658	0,4	70	
	*4575	0,3	300	
	4493.8	0,2	500	
	4412.4	0,1	700	
	4333.2	0,0	900	
	4258.9	1,0	600	
	4187.9	2,0	400	
	4119.9	3,0	100	
	*4157	4,0	50	
CuF "A"	5694.3	0,0	100	
	5685.7	1,1	90	
	5677.2	2,2	80	
	*5669	3,3	50	
	*5660	4,4	30	
	*5652	5,5	10	
	*5644	6,6	5	
	"B"	5061.1	0,0	200
5052.3		1,1	100	
*5043		2,2	50	
*5034		3,3	20	

TABLE 6.2. (Cont.)

<u>System</u>	<u>Wave Length</u>	<u>v', v''</u>	<u>Intensity</u>
CuF "C"	4932.0	0,0	800
	4926.8	1,1	600
	*4922	2,2	700
	*4916	3,3	300
	*4911	4,4	100
CuO	6161.5	1,1	100
	6146.8	0,0	20
	6059.3	2,1	40
	6045.1	1,0	10
H ₂ O	8097		400
	7164.5		50
OH	3428.1	0,1	400
	3184.8	2,2	700
	3121.7	1,1	800
	3063.6	0,0	1000
	2945.2	3,2	400
	2875.3	2,1	500
	2811.3	1,0	600
	2677.3	3,1	100
	2608.5	2,0	200
<u>Element</u>			
Copper	5105.6		400
	3274.0		1000
	3247.6		1000
Potassium	7699.0		1000
	7664.9		1000
Sodium	5890.0		200
	5895.9		200

Figures 6.1 - 6.10, 6.17

Spectrograms of an acetylene-oxygen-carbon tetrafluoride flame with a fuel to oxygen ratio of about 2.0. Prints were made from type 103-0 and 103-0 U. V. Eastman Kodak spectrographic plates with exposures ranging from 5 sec. to 50 minutes. Relative intensities are tabulated in Table 6.1.

Figures 6.11 - 6.14

Spectrograms of a hydrogen-oxygen-carbon tetrafluoride flame with a fuel to oxygen ratio of about 1.0. Prints were made from type 103 F-3 and 1-N Eastman Kodak spectrographic plates with exposures ranging from 2 to 20 minutes. Relative intensities are tabulated in Table 6.2.

Figures 6.15, 6.16

Spectrograms of a hydrogen-oxygen-carbon tetrafluoride flame with a fuel to oxygen ratio of about 1.0. Prints were made from type 103-0 Eastman Kodak spectrographic plates with exposures ranging from 10 to 30 minutes. Relative intensities are tabulated in Table 6.2.



Figure 6.1 - 6.2

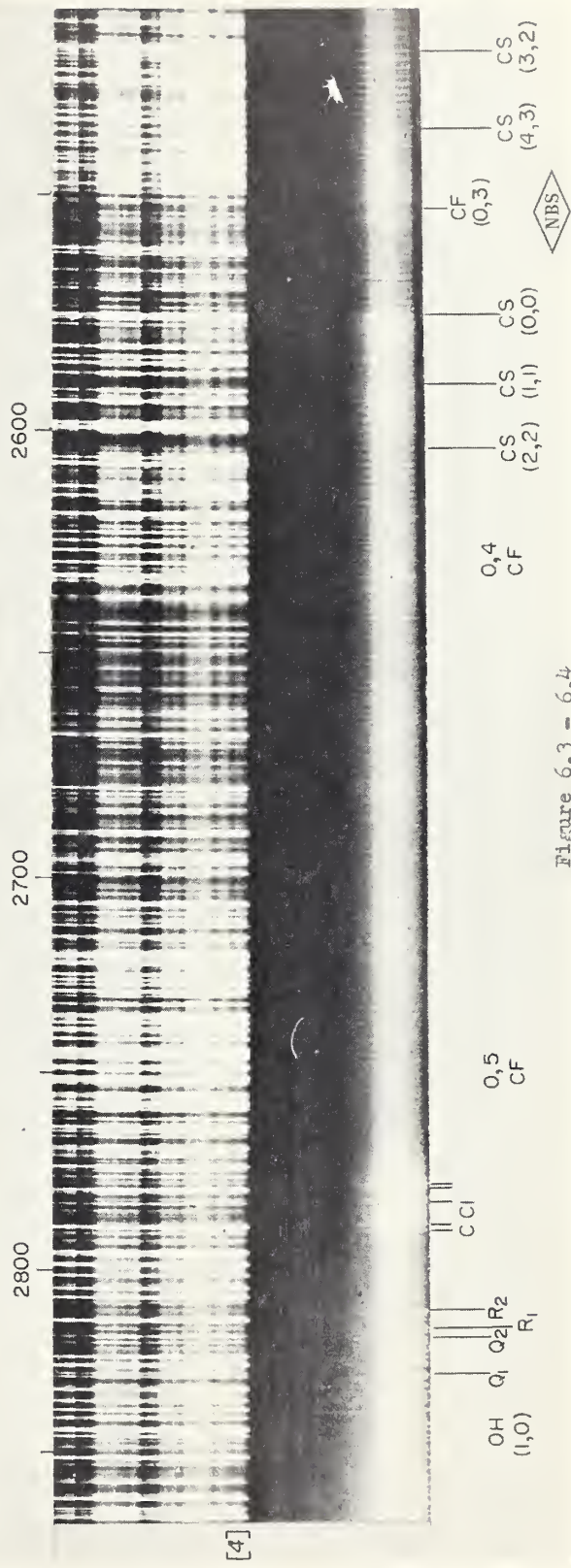
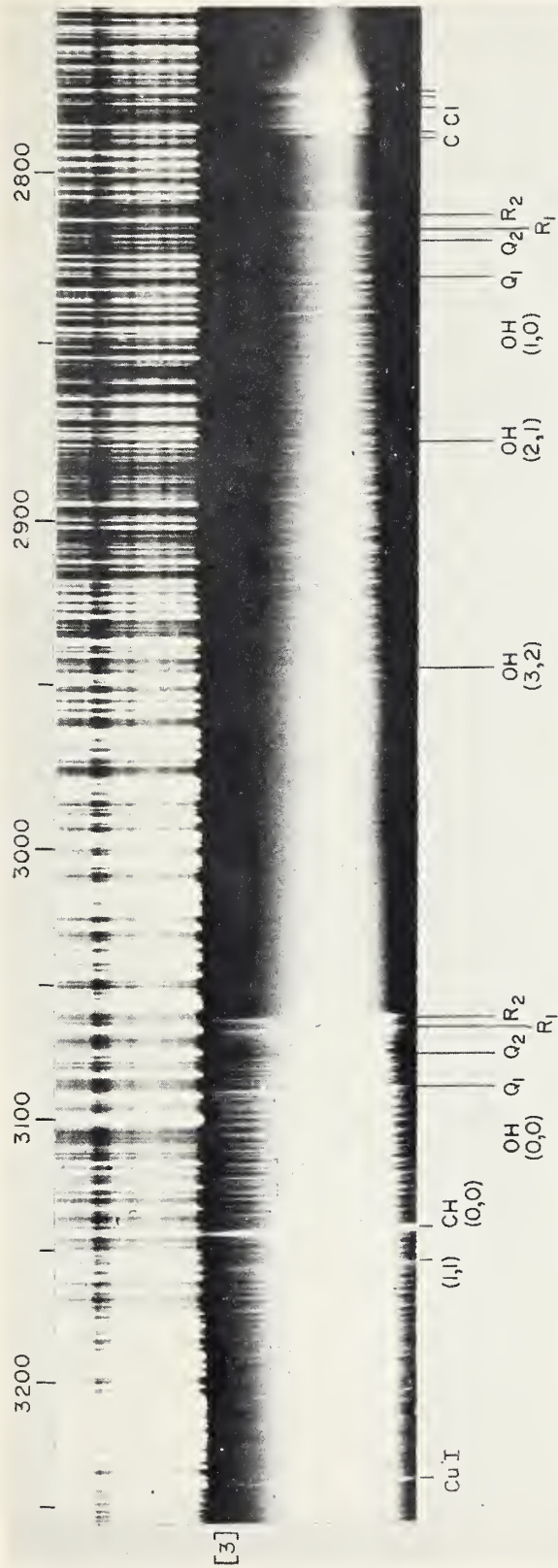


Figure 6.3 - 6.4

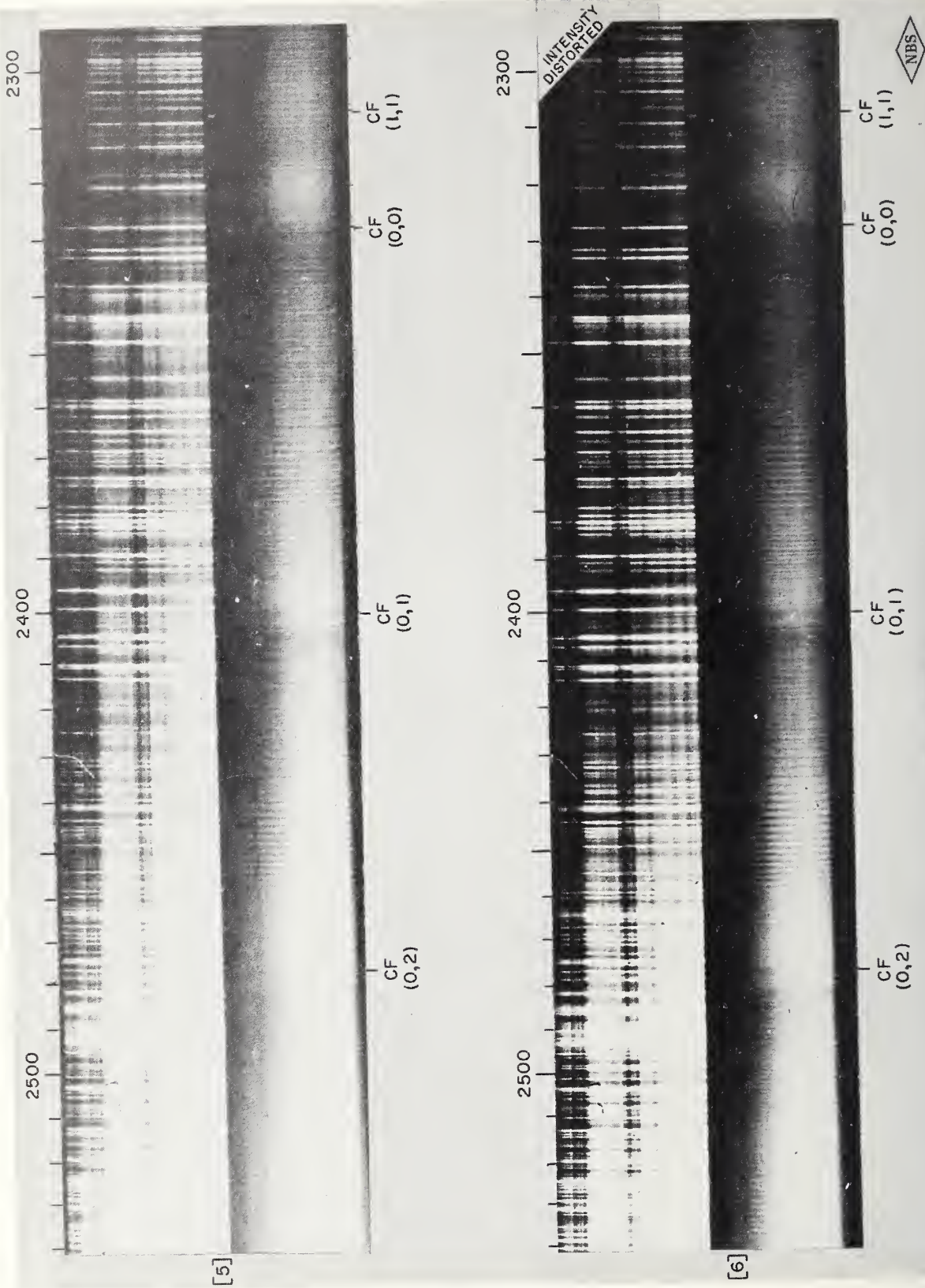


Figure 6.5 - 6.6

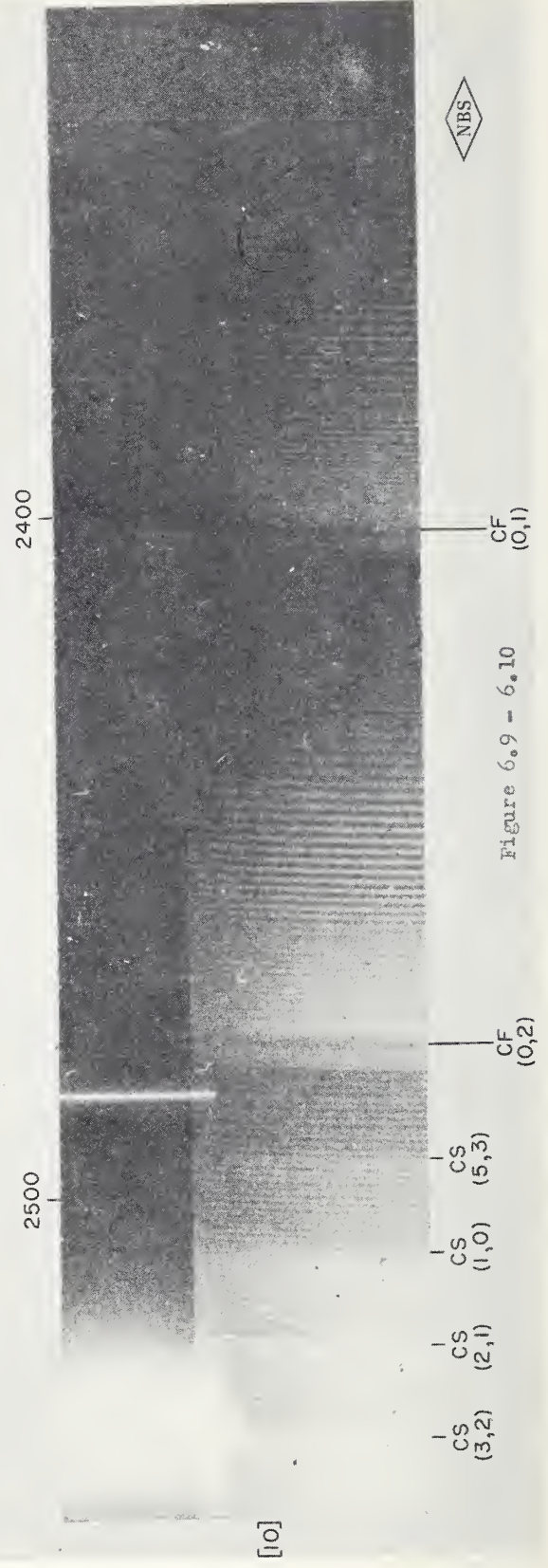
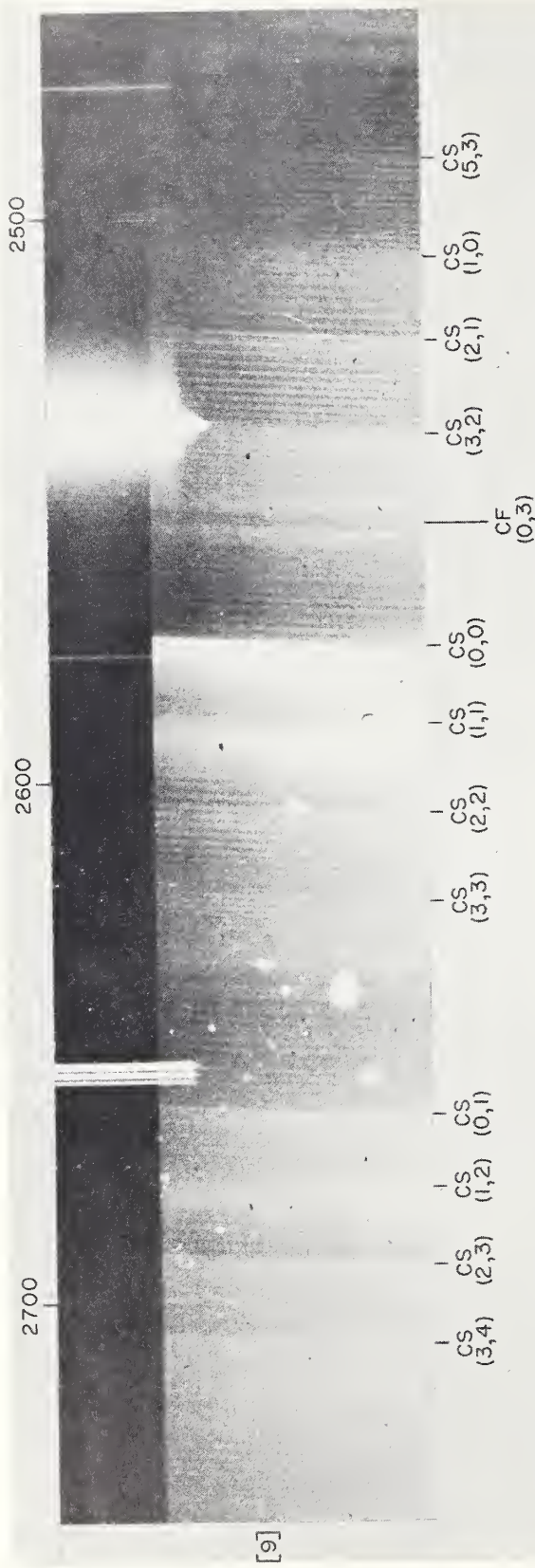


Figure 6.9 - 6.10

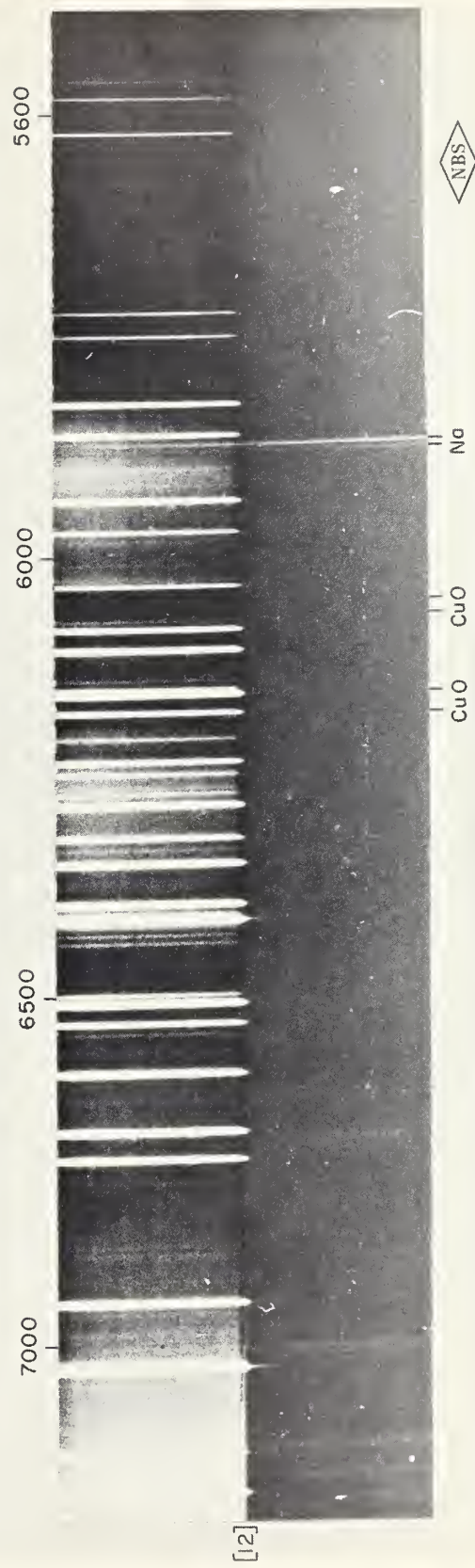
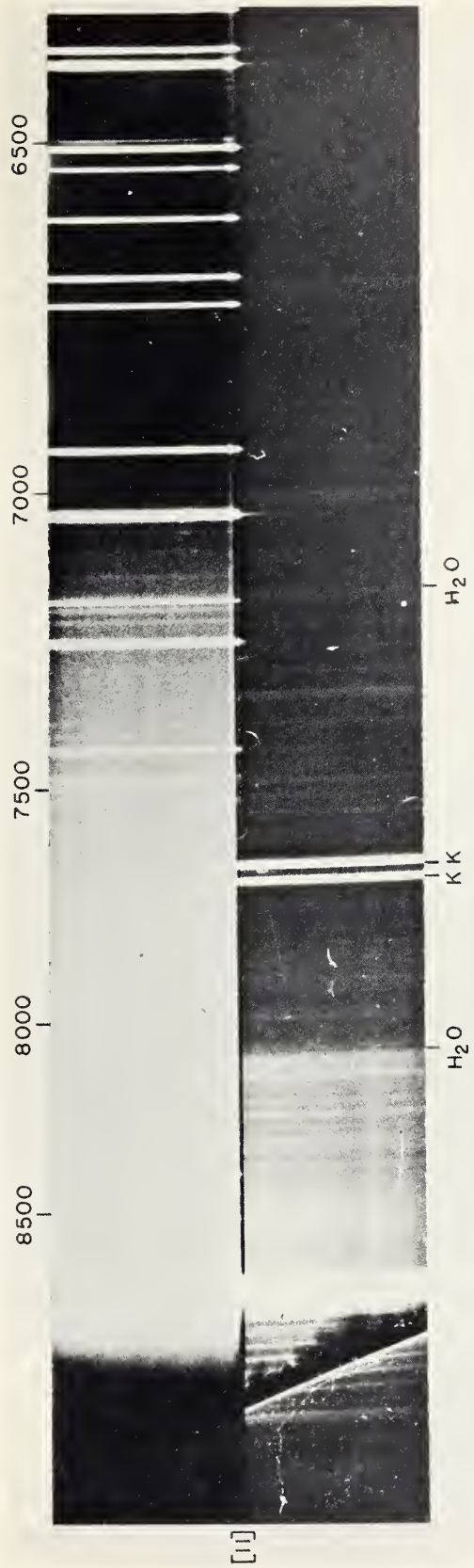


Figure 6.11 - 6.12

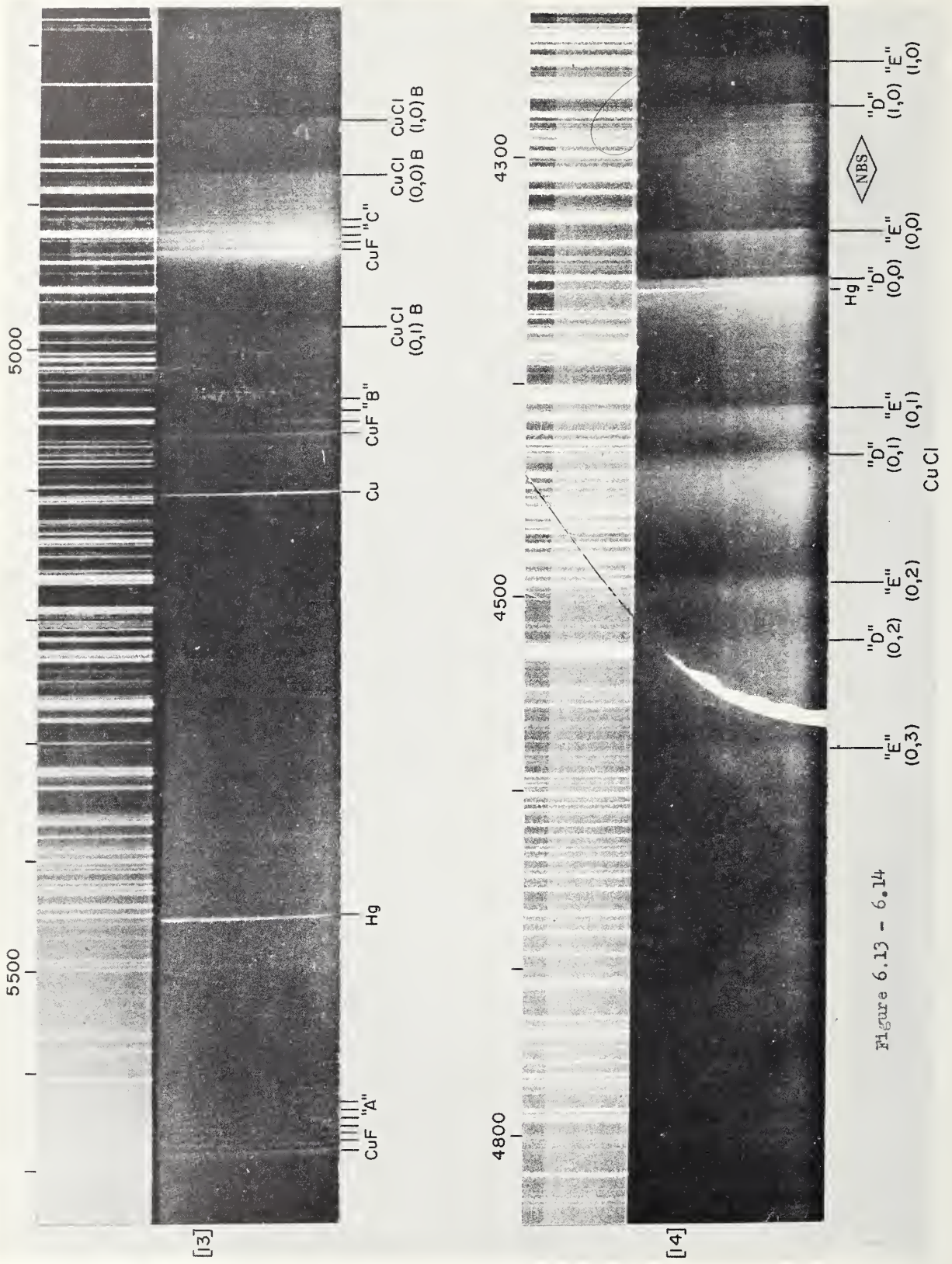


Figure 6.13 - 6.14

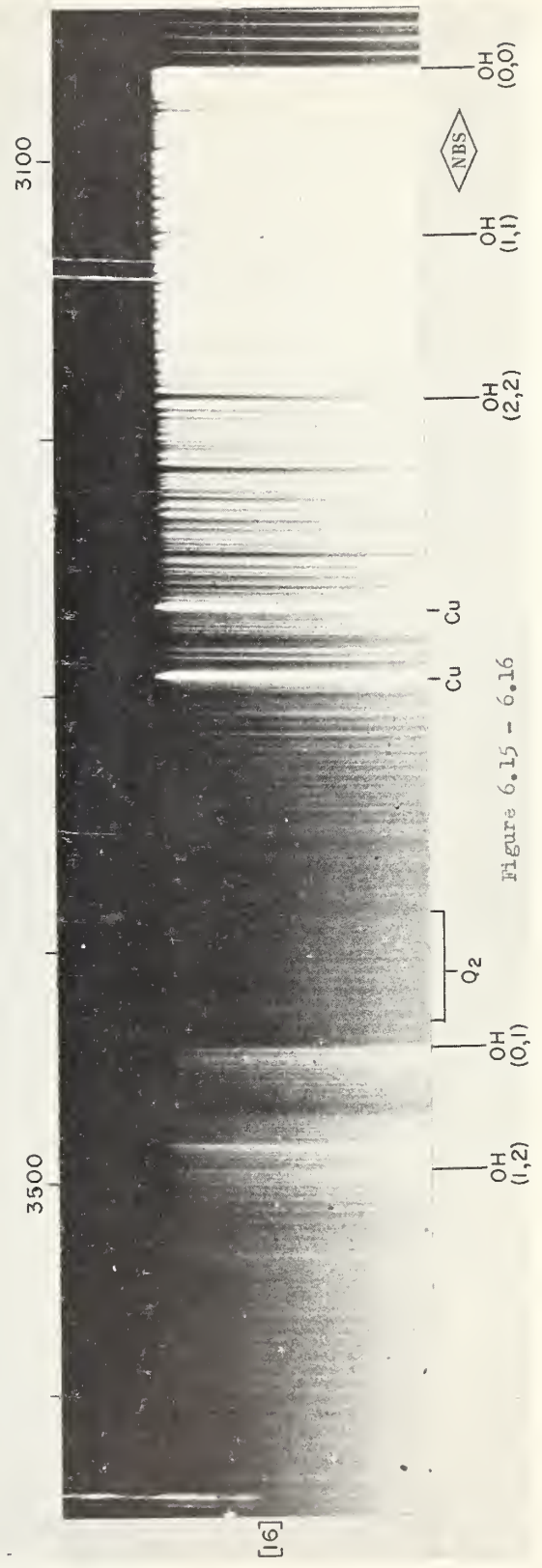
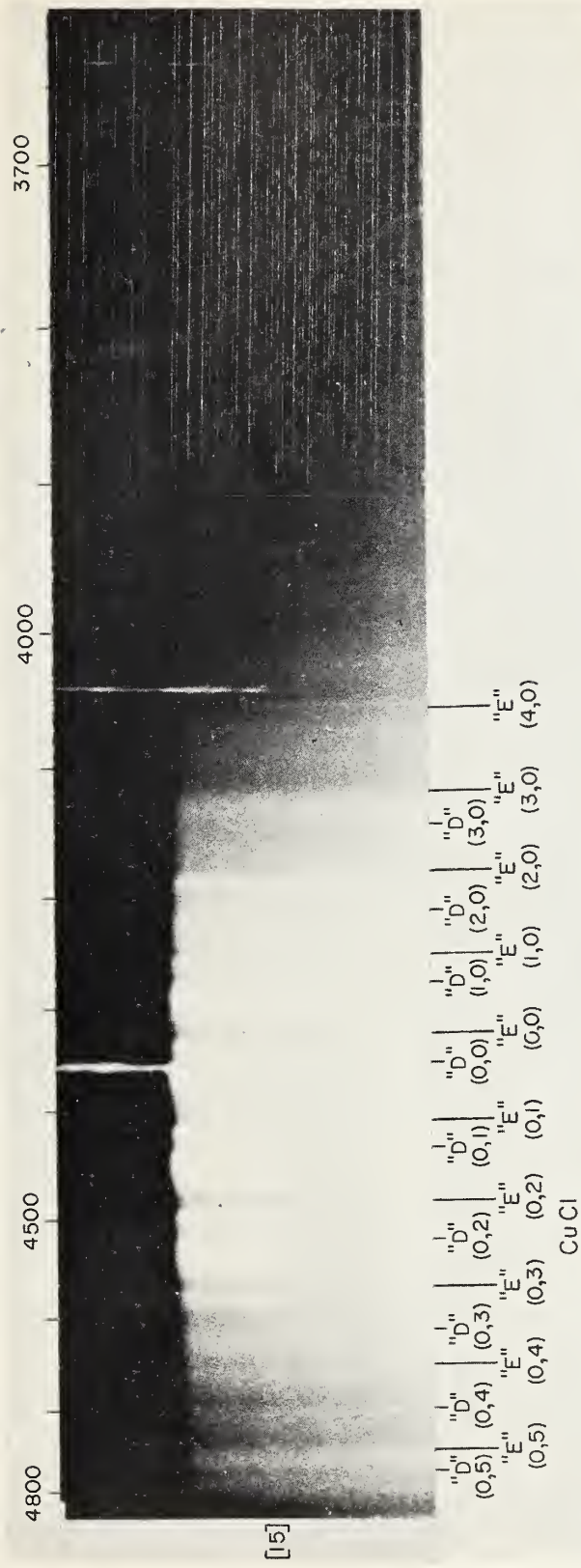


Figure 6.15 - 6.16

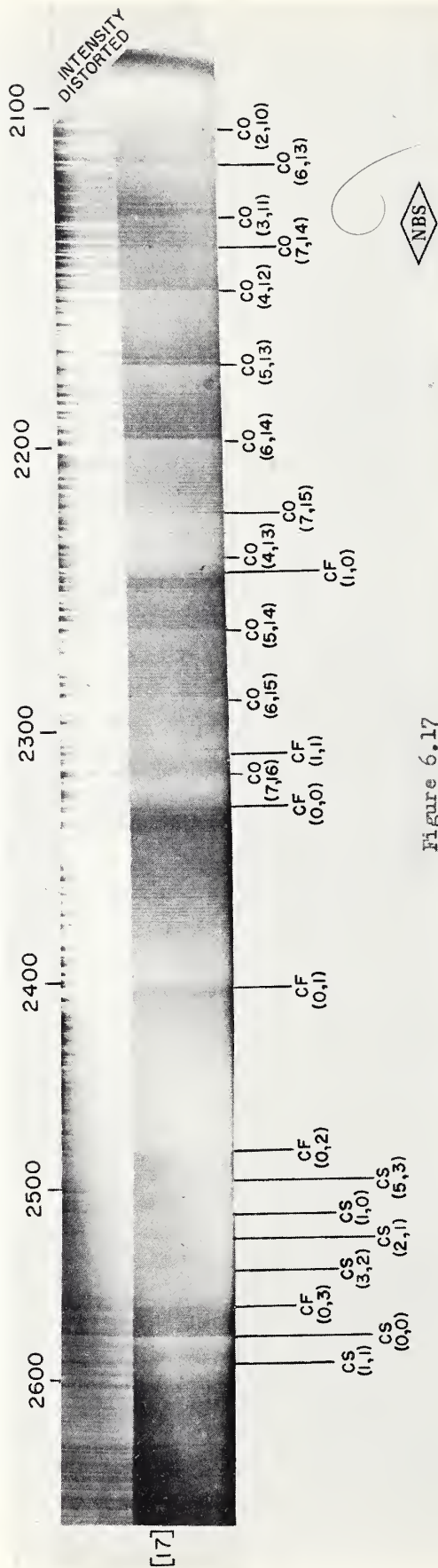


Figure 6.17

7. ULTRA VIOLET ABSORPTION SPECTROSCOPY OF
SPARK IGNITED, LOW PRESSURE EXPLOSIONS*

by

H. P. Broida¹, A. J. Everett and G. J. Minkoff²

ABSTRACT

Preliminary studies have been made of the absorption of ultra-violet radiation at selected wavelengths as a function of time by spark-ignited explosions in low-pressure mixtures of hydrogen and oxygen, of methane and oxygen, and of carbon-monoxide and oxygen. Plots of the logarithm of the optical density versus frequency between 3000 Å and 2100 Å for the three mixtures at various pressures were linear with a slope of $1.51 \times 10^{-14} \text{ cm}^{-1}$. The results have been compared to previous work on determinations of hydrogen peroxide formed by explosions in similar vessels. No evidence for the existence of hydrogen peroxide in the gas phase was found. Also ozone was not detected (less than 0.03 percent of the original free oxygen) in the main reaction but some may have appeared about 10 milliseconds later. Formic acid was found during the main absorption. The present experiments in cylindrical vessels did not permit a clear separation between absorption due to the flame front and that due to the hot gases behind the flame.

The isolation of hydrogen peroxide from liquid-air cooled, spark-ignited explosions of hydrogen and oxygen has been reported by Egerton and Minkoff (1947), who described U. V. absorption tests on the source of formation of the hydrogen peroxide. When methane explosions were studied later in the same apparatus, hydrogen peroxide and ozone were isolated (Everett and Minkoff, 1949). Further work on the U. V. absorption of the explosions (Everett, 1953) showed that the results of Egerton and Minkoff were rendered doubtful by the presence of condensed droplets on the windows. Another difficulty was due to the duration of the flame travel, which was much shorter than had been expected (Egerton, Everett and Minkoff, 1953). This meant that unless the explosions were accurately synchronised with very short exposures, the photographs with absorption would receive so much light, extraneous to the explosion time, that the absorption would be masked. It was therefore decided to investigate the phenomenon by using photomultiplier detection.

¹National Bureau of Standards, Washington, D. C.

²Chemical Engineering Department, Imperial College, London S.W. 7

*In preparing the manuscript for inclusion in this report, copies of the figures were not available. The text is presented without the figures since the procedures and results are of importance in studies of combustion. This paper will be presented at the Fifth Symposium on Combustion, Pittsburgh, September 1954.

The method was to pass U. V. light axially through the cylindrical explosion tube, and to allow a selected wavelength to fall on a photomultiplier. This gave a signal which was sent to a cathode ray oscillograph and recorded as a single sweep, at a rate which produced a time-intensity curve for the duration of the explosion.

One reference only has been found to the use of the photomultiplier method of following the U. V. absorption of explosions. This briefly describes the results obtained by Norrish, Porter and Thrush (1953) with flash ignited explosions of acetylene-oxygen mixtures. The results obtained by Norrish and Porter (1952) with a high-speed photographic technique on hydrogen explosions have some relevance to the present work and will be discussed later. In the infrared, Bullock and Silverman (1953) have studied the progress of light emission in a carbon monoxide-oxygen explosion, and they also report a few absorption experiments. These results will be discussed in a later publication in connection with the U. V. emission of explosions.

Experimental

Apparatus. The spectrograph used was a large aperture, Raman-type Hilger E-518 with quartz optics, having a dispersion of 50 A/mm. at 3000 A, 30 A/mm. at 2500 A and 15 A/mm. at 2100 A. With entrance and exit slits set at 0.25 mm., it was possible to resolve 12.5 A, 7.5 A and 3.8 A at the corresponding wavelengths. The photomultiplier was a specially selected R.C.A. type 1P28, with an ultraviolet transmitting envelope. It was enclosed in a light-tight housing mounted on a continuously moveable rack fitted with a fine adjustment. The position could be read to ca.0.01 mm. with a vernier. Wavelengths were calibrated daily with a low-pressure mercury lamp, and were reproducible to approximately 0.03 mm.

A simple photomultiplier power supply was used, which consisted of four small 300 volt batteries with a voltage divider giving any voltage between 300 and 1200 v. The very simple and robust circuit has been described elsewhere (Oldenberg and Broida, 1951).

The cathode ray oscilloscope was a Furzehill instrument, type 1684/D with blue screen and mark II camera. The instrument could be set for single-sweep operation, the spot being kept just off the left side of the screen. When two contacts were broken, the spot traversed the screen at velocity which had been chosen according to the requirements of the experiment. The shortest duration of the overall phenomena was such as to require the spot to cross the screen in 6 - 7 milliseconds. It was then possible to resolve in time events occurring in 2 percent of this, i.e. about 10^{-4} secs.

The source of light was a M. S. Co. hydrogen arc, type HFW1, which was water-cooled and ran on 1 amp. The D. C. mains could not be used to supply this (except in preliminary experiments) because the background light, instead

of appearing as a straight line, had a strong, 150 c/s ripple superimposed. The H.T. was therefore supplied by six heavy-duty 12V accumulators. Due to the wandering of the arc, small fluctuations of intensity (not more than 3%) were sometimes observed.

The reaction vessel consisted of a pyrex tube, 2 cm. wide and 30 cm. long, with flanged ends on which quartz windows had been fixed with Araldite cement. The gas mixture was introduced through a stopcock, lubricated with silicone grease, in a narrow glass tube which entered the vessel at a central position. The electrodes were tungsten wires fused in pyrex capillaries so that only the cross-section of the wire (0.1 mm.) was exposed to the hot gases. The 1/4 inch spark gap was situated in a small chamber fused to one side of the center of the explosion vessel. This was designed to reduce light from the spark from entering the spectrometer. In order to prevent the condensation of products on the windows, the explosion vessel was surrounded by a steam jacket, which kept the temperature at ca.70°C. The spark itself was obtained by the rapid opening of a switch in the primary of a 4000 V. transformer, the secondary of which was connected to the electrodes. The firing switch also triggered the oscilloscope sweep.

Optical Alignment. The light from the hydrogen arc was focused on the slit of the spectrometer by one quartz lens, between the arc and the explosion vessel. The reaction vessel was traversed by a slowly converging beam of light, which reduced any errors due to reflection or channelling inside the walls of the vessels. Such errors were also diminished by using a stop on the lens, and so confining the light to the central part of the tube. In order to test for the possibility of changes in light intensity due to overall changes in refractive index of the gases (due to variation of temperature or of composition), experiments were repeated using both parallel and diverging beams of light as well as convergent. However, there was no change in percentage absorption. This does not eliminate the possibility of scattering of light by pockets of burning gas, cellular flames, and similar phenomena which might reduce the amount of light reaching the spectrometer.

Materials. Hydrogen and oxygen were of normal commercial purity. The only impurity in methane, from Point of Ayr Colliery, was 2% nitrogen. Commercial carbon monoxide was freed of moisture and iron carbonyls by passage through liquid nitrogen. The hydrogen content was shown to be not greater than 3 parts in 10,000 by mass spectrometer analysis. Mixtures were made up in 5 l. flasks at least one day before they were required, to ensure thorough mixing. The compositions used were: $2 \text{ CO} + \text{O}_2$; $1.6 \text{ H}_2 + \text{O}_2$ and $\text{CH}_4 + 2.0_2$.

Procedure. The explosion vessel had been originally washed with dilute hydrofluoric acid, rinsed and dried. Between explosions, the vessel was evacuated with a metrovac pump, to ca.0.01 mm, for one minute, and the gas mixture then introduced; its pressure was measured with a mercury manometer, which was then separated from the vessel by two stopcocks. Fifteen seconds after filling,

the mixture was exploded. For absorption experiments the zero position was obtained on each photograph by opening the trigger and firing switch with the spectroscope slit closed.

The time scale was obtained on every 10th exposure by recording a 50 c/s signal at the same scanning speed. After developing, fixing and drying the films each frame was projected, with tenfold enlargement, and both the explosion curve and the zero line were traced on a sheet of paper. The distance from the explosion peak to the zero line represents the transmitted light (I), while the distance from the zero line to the line traced out by the spot before the explosion indicates the incident light (I_0). These distances are illustrated in Fig. 6(a). The function which is used to describe all the absorption results is the optical density (D), given by $\log_{10}(I_0/I)$.

With each gas, several series of experiments were carried out. The effect of pressure at one or two selected wavelengths was investigated, and the dependence of optical density on wavelength was also observed at selected pressures.

Results

Wavelength Dependence. The explosions of hydrogen-oxygen, carbon monoxide-oxygen and methane-oxygen mixtures all showed absorption beginning below 3000 Å and increasing more rapidly as the wavelength decreased to 2100 Å. It was found that with all three gases, straight lines were obtained by plotting $\log_{10} D$ against the frequency (wave number) of the absorbing light. The slopes of five such lines, which include two pressures each of hydrogen and of carbon monoxide and one of methane, are identical within the experimental error, as is shown in Fig. 1, and have a value of $1.51 \times 10^{-4} \text{ cm}^{-1}$.

Fig. 1

The interpretation of these facts, and their relation to the detection of hydrogen peroxide, will be referred to in the Discussion. Although the slopes have a common value, the amount of absorption depends both on the gas and on the pressure. Thus, at 2300 Å, at a pressure of 10 cm., hydrogen explosions had an optical density of 0.28, carbon monoxide 0.34, while methane had the strongest absorption, with $D = 0.65$. If the absorbing species had a concentration which was proportional only to the pressure (p) (for example, one of the reactants), then plot of D/p against p should be straight lines parallel to the pressure axis. A relation of this type was only exhibited by methane explosions above 4 cm. pressure. Hydrogen showed a slow, linear increase passing through the origin, while carbon monoxide was associated with a steeper rise beginning at a higher pressure than hydrogen. (Fig. 2)

Absorption by OH. The comparatively low resolving power of the spectro- scope made it impossible to attempt to resolve the banded absorption spectrum of OH in the region 2900 - 3200 A. Nevertheless, by measuring the absorption at 2900, 3000, 3100 and 3200 A, it was shown that absorption over this range had a maximum value of 10% at 3100 A, corresponding to the 3064 (0,0) band of OH. This was observed in both hydrogen and methane explosions.

Absorption by Formaldehyde. This was only observed in the preliminary experiments in which the vessel was not heated. The light received by the photomultiplier appeared as a steady signal on the oscilloscope, and absorp- tion was indicated by a transient movement of the line, which was observed visually. There was then some indication, in the explosions of methane, of absorption from 2800 A to ca. 3600 A, the region in which formaldehyde absorbs most strongly.

Absorption Due to Formic Acid. Formic acid has a banded absorption system with the most intense maxima at 2285, 2295, 2340 and 2400 A (Pearse and Gaydon, 1953). During the main part of the work, some evidence was obtained of the presence of absorption peaks at 2340 and 2400 A, with optical densities only about 0.06 above the values of the main absorption slope. In the preliminary series of experiments to which reference has just been made, peaks were detected at the four wavelengths corresponding to formic acid within the accuracy of our measurements; there, however, the optical densities were much greater in relation to neighboring absorption, as is evident from fig. 3, in which the observations in this part of the spectrum are plotted on an extended wavelength scale.

Fig. 3

The discrepancy was not due to the effect of heating the vessel, since the more intense absorption did not return when the heating was stopped.

Absorption by Ozone. Ozone has an absorption system with a maximum at 2550 A (Fabry, 1950). Many readings were taken between 2350 and 2750 A with explosions of both methane and carbon monoxide. No significant absorption was found apart from the continuous absorption already described. The scatter of the experimental points was such that a peak of density 0.03 would have been just detectable. This would correspond to ca. 0.03% of the original free oxygen in a 2 CO:O₂ mixture at 15 cm. pressure.

Although there was no evidence of ozone absorption in the main part of the reaction zone, one series of experiments on the effect of pressure on the absorption at 2500 A in methane explosions suggested that a small quantity of ozone might be formed after the reaction was over, and the products were cooling. This was shown by the presence of a small amount of absorption about 10 m sec. (shown in fig. 4) after the main absorption peak. Although this phenomenon was not always reproducible, and, in some tests, was obscured by

electronic noise, a linear relationship between the pressure (p, in cms.) and the time (t, in milliseconds) which elapsed between the initial sharp rise in absorption and the appearance of the second peak suggested that it was not merely a random phenomenon. The equation of the straight line was

$$t = p + 4.0.$$

The optical density was of the order of 0.03, which would correspond to ca. 0.03% ozone.

Residual Absorption. In preliminary experiments with methane, the explosion tube not being heated, the absorption increased to a maximum and fell to about a third of the peak value in a very short time (by visual observation); the absorption then decreased to a steady value of about 10% after several seconds. This absorption was observed at wavelengths up to 4350 A, and it could be removed by pumping. As droplets were seen on the windows, scattering by the condensed products probably accounted for the observed absorption. Explosions of hydrogen under these conditions exhibited an additional feature. The first peak in absorption, which vanished above 2800 A, was very quickly followed by a second peak, with subsequent decrease to a constant absorption which again persisted to long wavelengths. This experiment will be referred to in the discussion of the evidence for the detection of hydrogen peroxide.

Rates of Decay of Absorption. Although there were differences in the appearance of the absorption, the rate of decay of the absorption after the peak obeyed a kinetic law which was similar for explosions of hydrogen at 2200 A, of carbon monoxide at 2300 A, and of methane at 2400 A. This was shown by plotting $\log (D)$ against t, where the time t was measured from the instant when the rate of decrease of absorption had reached a maximum value. The graphs obtained by this procedure are shown in fig. 5, while the point t_0 is indicated on fig. 6(a).

Fig. 5

The absorption associated with the CH radical at 3100 A was not sufficient for the application of the method.

Duration and Shapes of Absorption Curves. Many of the explosion absorption curves showed a composite character, which was revealed as the pressure was lowered. This is illustrated in fig. 6(c). As the effect was probably due to the flame travel not being symmetrical about the center of the tube, no further discussion of it will be made until more work has been done in spherical vessels. A number of typical curves are shown in fig. 6. At some wavelengths at which

Fig. 6

light was both emitted and absorbed, an emission peak appeared prior to the absorption one, as shown in fig. 6(b), for methane explosions, at 2700 A.

In any one set of conditions, the duration of emission was usually about half the time which elapsed before the absorption had become vanishingly small. The absorption and emission times obtained by the present method will be compared in a later publication with the data yielded by high-speed cinematography of the progress of the same flames. Briefly, however, it may be said that for hydrogen and methane explosions, the films indicate that the flames reached the ends of the tube in just under 1 msec., while absorption lasted for ca. 10 msec. Carbon monoxide flames took 20 - 40 ms. to travel to the ends of the tube, while absorption did not disappear for ca. 80 - 90 msec.

The time to reach maximum absorption did not appear to be related to the time of flame travel in the same manner in all the explosions. Thus, in explosions of hydrogen and methane, the time to maximum absorption was approximately twice that of flame travel, while in carbon monoxide explosions, the first steep rise in absorption only lasted one half to one quarter of the time of flame travel. Another distinction in appearance between the first two gases and carbon monoxide was the absorption in the former began to decay very soon after reaching the maximum absorption, while the carbon monoxide showed a much flatter portion between increase and decrease in absorption. This is illustrated in fig. 6(a) and (d).

Discussion

The nature of the various absorbing species will be considered first, and then the possibilities of the technique will be assessed. The first problem is to attempt to identify the molecules or radicals responsible for the absorption increasing to shorter wavelengths, which is found below 2800 Å. Although it might be due to hydrogen peroxide in the explosions of hydrogen and of methane, the absorption is of comparable intensity in carbon monoxide explosions in which the total hydrogen content is extremely small. Absorption in the latter explosions and also some of that in methane explosions might on the other hand, be ascribed to 'hot' carbon dioxide molecules, which have been postulated to take in the oxidation of carbon monoxide (Dr. A. O. Walsh, priv. comm.). However, the observation that the relation between absorption and wave number is identical for the explosions of the three gases studied (fig. 1) is an indication (though not a conclusive one) that the same absorbing substance is present in all three explosion mixtures. Clearly, the most likely molecule is oxygen, which is believed to absorb at high temperatures. Norrish and Porter, for example, found a very complex line absorption in the same region, with similar characteristics, when they flash-initiated hydrogen-oxygen explosions. The same spectrum was found when they replaced hydrogen by deuterium, bromine or chlorine, and they therefore concluded that oxygen was the absorber. Until direct evidence is obtained, the tentative conclusion will be made that hot oxygen was responsible for the main absorption observed in the present work.

The increase in absorption with rising pressure in the explosions of

hydrogen and of carbon monoxide could now be interpreted as follows. The intensity of absorption depends on the concentration of hot oxygen molecules, which is itself directly governed by the pressure and by the temperature, and, less directly, by the nature of the explosive gas. In addition, the temperature is known to affect the wavelength limit of the Schumann-Runge emission system, and the same is probably true of the absorption system. It might therefore be possible, if the fine structure were resolved, to relate the absorption quantitatively to the concentration of oxygen molecules and to the temperature.

The absorption by hot oxygen greatly increases the difficulty of attempting to detect hydrogen peroxide in explosions by U. V. absorption. If the hydrogen peroxide which was isolated in the chilled experiments on hydrogen - had all been formed in the gas phase, the expected optical density at 2300 Å would have been 0.21 for an initial pressure (at room temperature) of 15 cm. The observed value was more than double this, i.e. 0.44. If hydrogen peroxide were solely responsible, the only explanation would be that half of it decomposed before reaching the walls. The reverse situation was expected, however, since considerable amounts of the peroxide are probably formed on the cold walls. Furthermore, the shape of the observed $\log D$ vs. cm^{-1} plot differed from the published values of Holt, McLane and Oldenberg (1948) and of Urey, Dawsey and Rice (1929). The measured slopes of the absorption in the explosions (fig. 1) suggest that the main absorber was not hydrogen peroxide. However, the U.V. studies alone do not show conclusively the origin of hydrogen peroxide and some other technique, such as infra-red spectroscopy, must be applied.

Some indirect evidence of the formation of hydrogen peroxide is given by the preliminary experiments in which no heating jacket was used. With methane explosions, visual observation of the CRO trace suggested that up to about 3000 Å, the absorption very rapidly rose, fell by a third, then slowly decayed to the residual value of ca 10% absorption. The latter was observed at all wavelengths. Hydrogen explosions showed an additional feature, which consisted of a second absorption peak preceding the slow fall to the residual value. The second peak, as well as the residual, was observed at wavelengths up to 4350 Å. The final fall to a residual absorption has been shown to be due to the formation of condensate on the windows. The observed facts could be explained by suggesting that the second peak in hydrogen explosions is connected with the condensation of unstable hydrogen peroxide, whose rapid decomposition on the windows leads to a change in drop size and hence of the scattering of light. This is in agreement with the observation that much of the hydrogen peroxide chilled out (to -80°C or below) from hydrogen-oxygen explosions decomposes in less than a second, while no peroxide at all can be isolated if the reaction vessel is at room temperature (Everett).

Absorption by other species. No evidence was found to suggest that more than 0.03% of ozone was formed during the main part of the explosion process. It is just possible that mercury vapour was responsible, since some mercury lines appeared in emission in experiments carried out later; however, this is not considered probable. No definite conclusion about the role of ozone in explosions of carbon monoxide or of methane can be drawn, since it could be argued that its stationary concentration remains very low. Had ozone been detected, it might even have been an indication that it was an end product rather than an active intermediate. Nevertheless, although a low stationary concentration of intermediate is expected in a slow reaction or below an explosion limit, the instantaneous concentration might have been expected to increase during a branched chain explosion. This suggestion again is not conclusive, since it cannot be made quantitative at this stage. However, if the small additional absorption at 2550 Å observed after the main absorption (fig. 4) can be proved to be due to ozone, formed by the recombination of free oxygen atoms with each other or with oxygen molecules on cooling, then the evidence presented in this communication may be taken to suggest that ozone does not play a major part in the explosive oxidation of carbon monoxide.

The role of formic acid in the explosion of methane will not be discussed at this stage. It has been detected previously in the products of chilled methane explosions (Everett and Minkoff). Lack of reproducibility of the absorption of this compound is somewhat similar to the difficulties encountered in attempts to identify methyl peroxide in the products of methane explosions in vessels cooled to -180°C . It has not yet been possible to identify the factors which determine whether or not a peroxide shall be found, under apparently standard conditions. Although it is possible that the formic acid is due to a reaction of ozone with formaldehyde, it is strange that the absorption corresponds to a time of only a few milliseconds.

Finally, the potentialities of the method will be discussed. It has clearly been shown that events lasting 6 - 10 milliseconds can easily be followed and recorded, and that times of the order of 2% of this, i.e. 10^{-4} msec., can be resolved. There is no reason to suppose that much shorter times could not be followed, since the writing speed depends on the brightness of the oscilloscope spot, and this was not used to its full extent. The absence of timing marks is not a good feature, but this could be easily remedied in future work.

The shape of the reaction vessel used, i.e. a tube viewed axially with one flame front travelling toward the spectrometer while the other flame front travelled away from it, is not suitable for general studies. Wall effects, including loss of heat, must have been considerable, although the high extents of reaction (90-95% in explosions of hydrogen and of methane, and 80-90% in those of carbon monoxide) suggest that quenching was not of great importance. Nevertheless, it is clear that less equivocal information would be obtained if the explosions were in a spherical vessel. The effects

of the walls could then be assessed by using cylindrical tubes of varying diameters. The reason for using a cylindrical vessel in the present work is that the studies of the formation of hydrogen peroxide in chilled explosions (Everett and Minkoff, 1948; Everett, 1953) showed that yields were extremely sensitive to changes of shape or of vessel size. The vessel selected was therefore similar to those in which most of the previous work had been done.

A general criticism of the method of viewing through a flame is that only an average description is obtained of the various sections. The present technique, however, can be used to distinguish whether a certain absorbing species exists mainly in the flame front or in the hot gases left behind. The concentration of species in the flame front would rise very quickly, as soon as the flame front is established, to a value which remains approximately constant. When the flame is extinguished on reaching the end of the tube, the concentration would fall sharply to zero. If, on the other hand, the species were related to the hot gases, then its concentration would rise less rapidly, in a time of the order of magnitude of that of flame travel, and then decay, probably exponentially, at a rate controlled by the cooling of the gases. It is clear from the curves in Fig. 6(a) and (c), that the absorption observed in the explosions of hydrogen and of methane are of this latter type. The absorption of carbon monoxide explosions, Fig. 6(a) at first sight seems to indicate absorption connected with the flame front. This is not correct, since the rate of decay is still exponential. The approximately flat portion of the absorption trace is probably due to the much slower rate of movement of the flame (Everett and Minkoff, 1953), with the consequent absence of reheating effects in the bulk of the gas.

In conclusion, the method has the great advantage of attempting to relate quantitatively studies of absorption to such factors as pressure, composition, etc. The most useful results would be obtained if extremely short exposures of the whole absorption spectrum could also be recorded photographically, in order to reveal the existence of any unexpected band systems.

One of us (H. P. B.) is grateful for the award of a John Simon Guggenheim Memorial Fellowship.

REFERENCES

- Bullock and Silverman, S., 1953, JOSA
- Egerton, A. and Minkoff, G. J., 1942.
- Egerton, A., Everett and Minkoff, 1953.
- Everett, and Minkoff, G. J., 1948.
- Everett and Minkoff, G. J., 1949.
- Everett, 1953.
- Fabry, 1950.
- Norrish, and Porter, 1952, Proc. Roy. Soc.
- Norrish, and Porter and Thrush, 1953, Nature
- Oldenberg, O. and Broida, H. P., 1950, JOSA 40, 381.
- Urey, Dawsey, and Rice, 1929.

8. USE OF A VACUUM SPECTROGRAPH FOR COMBUSTION STUDY

W. R. S. Garton, Department of Astrophysics,
Imperial College, London

and

H. P. Broida,* National Bureau of Standards
Washington, D. C.

Since many hydrocarbon molecules have characteristic absorption spectra and large absorption coefficients in the far ultra-violet, it might be possible to investigate some reactions by following the concentration of one or several species during combustion. Small concentrations of oxygen completely absorb radiation below 1760 Å and therefore it is necessary to use a vacuum spectrograph to obtain the shorter wavelengths, and in addition only those reactions not involving molecular oxygen can be studied.

We have made some preliminary studies of flat diffusion flames of the type investigated by Wolfhard and Parker (1952). It was hoped that changes in the absorption spectra would be found by measuring the absorption from the fuel side to the oxygen side of the flame, and from such changes to learn something about the combustion process. These initial attempts have shown that, while the far ultra-violet might be profitably applied to combustion, much background study of hot gases will have to be completed before many definite conclusions can be made.

A rectangular burner 14mm by 25mm, with the inlet supply of gaseous fuel separated by a thin metal barrier from the oxygen, was completely surrounded by a stream of oxygen-free nitrogen and enclosed by a metal housing 30mm by 42mm with two lithium fluoride windows (transmitting to below 1200 Å). One window was sealed over the slit of a vacuum one meter normal incidence grating spectrograph and the other to a large Lyman hydrogen discharge tube. A one mm slit was used on the Lyman tube to limit the aperture of the light beam going to the spectrograph slit. The slits were parallel to the direction of the gas flow and to the flame. Exposure times of 4 minutes were sufficient for the entire spectral region from 1200 to 2550 Å. The burner was mounted on a rack and pinion, moving transversely across the light beam so that different portions of the flame could be observed.

Flames with three different fuels were observed - town gas, ethylene and hydrogen; all were burned with oxygen. In each case there was a continuous absorption that extended as far as 1925 Å; even as far as 9mm on the ethylene side of the flame there was continuous absorption below 1850 Å which was not caused by oxygen since Schumann-Runge system was not observed. On the oxygen side of the flame this oxygen system was clearly evident. Near the flame front the absorption extended to longer wavelengths than at either side. On the fuel side of the flame with both town gas and ethylene, an absorption consisting of fine structure extended from the continuous absorption to 2200 Å, the amount of absorption decreasing toward the center of the flame. In one plate taken with a flame of town gas and oxygen, the absorption bands of NO between 2000 and 2200 Å were detected. In the hydrogen flame a very weak group of 6 absorption bands were found between 1940 and 2200 Å, but these were not identified.

A careful check was made to determine the cause of the continuous absorption and to make certain that it was not due to some impurity in one of the gases. For example, spectra observed of hydrogen and the surrounding nitrogen showed that these gases did not absorb appreciably to the cut-off limit of the windows. Oxygen showed the Schumann-Runge system and the continuous absorption below 1760. The most probable cause of the observed continuous absorption during the burning is absorption by water vapour. Water at room temperature is known to absorb below 1830 Å and it is quite possible that hot water would absorb to longer wavelengths.

We were surprised not to see any evidence of the "pyrolysis" continuum such as that observed by Wolfhard and Parker¹ in their experiments with hydrocarbon flames. It is possible that our failure to detect this absorption is due to the Schlieren effect of the hot gas on the unfocused light beam. However it might be well to emphasize the difficulty of measuring continuous absorption near the short wavelength limit of a quartz spectrograph, which might cause the appearance of a stronger continuum than actually exists.

¹Wolfhard and Parker, Proc. Phys. Soc., A 65, 2(1952).

9. Development Work on the Noise Thermometer*

E. W. Hogue

The general objective of the project has been to design and construct a thermometer which will determine the ratio of two absolute temperatures by a method based on the noise thermometer of J. B. Garrison and A. W. Lawson at the Institute for the Study of Metals, University of Chicago¹; and to use the thermometer to provide independent values accurate to three places for temperatures in the region 1000°K to 1500°K for comparison with results obtained by other methods.

The noise thermometer is a null device for determining the ratio of two absolute temperatures by balancing the average values of the thermally generated voltage fluctuation, obtained after amplification, from two resistor elements maintained at the temperatures in question. (See fig. 9.1). In the use of this device, the value of one resistor is adjusted until a null is reached, indicating that the average value of the noise produced by it equals that from the other resistor. Then if the electrical time-constants R_1C_1 and R_2C_2 of the two resistors and their total respective associated shunt capacitances are made equal, the ratio of their temperatures is given by the inverse ratio of their DC resistances.

The block diagram in figure 9.1 shows the principal components of the noise thermometer. From the input (synchronous switch 1) to amplifier #4, it is basically the same as the original noise thermometer of this type built by Garrison & Lawson¹, but the remainder was devised at NBS in an effort to improve noise balance sensitivity by increasing both gain and averaging time. Electronic circuits are used to balance the average value of the noise fluctuation and to equalize the time constants of the resistor elements for the condition of noise balance. These operations involve the amplification of noise outputs from the resistors, the averaging of the separately amplified noise voltages over a time interval of 1/5 second; the subtraction of one average from the other; the averaging of the difference over a period of approximately 8 minutes; and the exhibition of this average difference on a meter or strip chart recorder. The principal balance is obtained using an amplification band of from 10KC to 60KC, (amplifiers 1, 2, & 3); and the equalization of time constants is carried out using a high-frequency, small relative bandwidth amplifier 20KC wide at 450KC (amplifier #6). The first three sections of the wide-band, low-frequency part of the thermometer serve to amplify the noise from each resistor element in succession by being rapidly switched (approximately 67 times per second by means of an electrically driven vibrating-reed switch) between the two elements. This amplification

*This work was supported in part by ONR and the Office of Basic Instrumentation.

raises the noise from approximately 2 microvolts rms to 20 volts average fluctuation amplitude. Half-wave rectification is then carried out by a linear diode detector, and is the first step necessary in the averaging process, producing a DC component proportional to the average amplitude of the noise level from each resistor. A second vibrating switch, operating in synchronism with the first, deposits charge through a common resistor R in each of two capacitors C_a and C_b , so that the voltages maintained as the capacitors are proportional to the average amplitudes of the noise voltages from the two resistor elements. The large time constant (1/5 second) of the charging resistor and each capacitor effectively filters out most of the high frequency components, leaving slowly fluctuating voltages indicating the average noise levels averaged over roughly 1/5 second. The difference between the voltages on the capacitors is the unbalance signal, and will average to zero over an infinite time for perfect balance. The precision with which the noise balance can be made depends upon the length of time over which this unbalance signal is averaged between adjustments of the resistor element toward balance. The 1/5 second time constant gives insufficient averaging time for the desired precision of 0.1% or better in temperature measurement. Also, calculations show that the d.c. component of $V_a - V_b$ for an unbalance equivalent to 0.1% in temperature is of the order of only a few millivolts. To provide extra gain, and a longer averaging time, a 67 cycle per second square-wave carrier having the unbalance signal $V_a - V_b$ for its envelope is generated by switching the high impedance input of amplifier #4 between C_a and C_b by means of synchronous switch #3. This amplifier raises the amplitude of the square-wave carrier by a factor of 30 or so, after which its envelope is recovered by a full-wave synchronous detector of the type shown in fig. 9.2, and is fed to a feed-back type integrating circuit such as is used in analogue computers, (see fig. 9.3). As far as its effect on the signal is concerned, this integrator behaves like a low-pass RC-filter having a time constant of 8 minutes, followed by a d. c. amplifier leaving a gain of 650. Because of a factor of two loss in the modulation-demodulation process, the total gain added after the diode detector is approximately 10,000. As a result, the unbalance signal corresponding to a 0.1% temperature measurement error appears at the output of the integrator in about 8 minutes as a steady voltage of approximately 25 volts. Superimposed on it is the random fluctuation remaining after passage of the initial 10 volt, 10 KC to 60 KC noise at the diode detector through the low-pass filter RC_a and RC_b and finally the very narrow low-pass "integrator". The fluctuation amplitude reduction resulting from the bandwidth reduction which follows the diode approximately equals the total gain following the diode so that the random component at the integrator output about equals that at the diode about 10 volts average amplitude.

Calculations, checked by experiment, indicate that for this noise thermometer to achieve a temperature measurement precision of 0.1%, a difference in the average value of the noise at the detector of one part in 4000 must be detectable. The DC component at the detector is approximately 10 volts; therefore, at the integrator output a steady voltage of $10 \times 1/4000 \times 10,000 = 25$ volts must be distinguishable in the presence of 10 volt (average amplitude) fluctuations.

In operation, the integrator output is continuously recorded on a chart to provide a record of the signal behavior during the averaging period. After each average, the integrator is readjusted to zero (the center of the chart). Several kinds of sensitivity measurements were made to determine what temperature measurement precision might be expected. The results showed that the circuit, exclusive of the first synchronous switch is capable of resolving noise average-amplitude differences of the order of a part in four thousand. This corresponds to a temperature measurement precision of 0.1% when the amplifier noise equals that of the input resistor elements. The time required to resolve such a small difference is 8 to 10 minutes. With the input synchronous switch in operation, it was impossible to achieve stability sufficient for precision better than 0.3% to 0.5%. Experience with the electrically driven synchronous switch system points to the necessity for mechanically driven switches of special design.

The most serious fundamental limitation of this type of noise thermometer for precise temperature measurements, is the requirement that the amplification characteristic (gain, noise, and bandwidth) of the input stages be independent of the source impedance presented to it. For example, if the reference resistor is maintained at 0°C and the other resistor is used as a thermometer element to measure temperatures near 1000°C, the impedance presented to the input stage changes by a factor of 4. The gain and noise level of this stage must, however, remain constant to better than one part in four thousand for measurement of temperature to 0.1%. Because of the improbability that this final requirement can be fulfilled, the method of noise thermometry just described has been abandoned as a possible high-temperature absolute standard. If the comparison resistor R_1 , which is maintained at the reference temperature, could be replaced by a noise generator having an internal impedance identical with that of the thermometer element this requirement would be eliminated. The result, would then not be a self-calibrating absolute thermometer as was the case when a resistor was used as the noise source because the noise from the generator would not be produced directly by thermal agitation. If, however, the mean-squared value of the noise from the generator were a unique, simple, and accurately known function of some easily and accurately measurable parameter of the generator; and if the amplitude vs. frequency spectrum, and statistical distribution of maxima of the generator noise were identical with that of thermal noise, a calibration curve of the generator could be made. One might ask what would be the advantage of such a method over the resistance thermometer or thermocouple since a calibration curve is required for all three. The answer lies in the nature of the function relating the measurable generator parameter to the Kelvin temperature on the one hand, as compared with the functions relating resistance and thermoelectric e.m.f. to Kelvin temperature on the other. If the generator noise has the same characteristics as thermal noise, then under conditions of noise thermometer balance, the mean-squared generator noise will be an exact linear function of the Kelvin temperature of the thermometer element; therefore, the form of the relationship between Kelvin temperature and generator parameter will be exactly that of the function relating mean-squared generator noise with generator parameter. It is felt that it might be possible to build a generator which duplicates thermal noise

sufficiently well and for which this function can be specified exactly for all values of generator noise by two or three calibration points; and therefore the relationship between generator measurable parameter and thermometer element Kelvin temperature could be expressed as a simple function completely determined for all temperatures by two or three calibration points. Because the curve is specified exactly, absolute temperatures well outside the range of calibration could be determined with certainty. This cannot be said for the resistance thermometer and the thermocouple. The curves for these devices are entirely empirical, dependent as they are on the physical properties of matter, so that the uncertainty of a measurement increases rapidly outside the range of calibration.

REFERENCES

1. "An Absolute Noise Thermometer for High Temperatures and High Pressures", J. B. Garrison and A. W. Lawson, Rev. Sci. Instr. Vol. 20, No. 11, 785-794, November, 1949.

Fig. 9.1

Noise Thermometer basic diagram.

Fig. 9.2

A synchronous detector.

Fig. 9.3

Miller integrator.

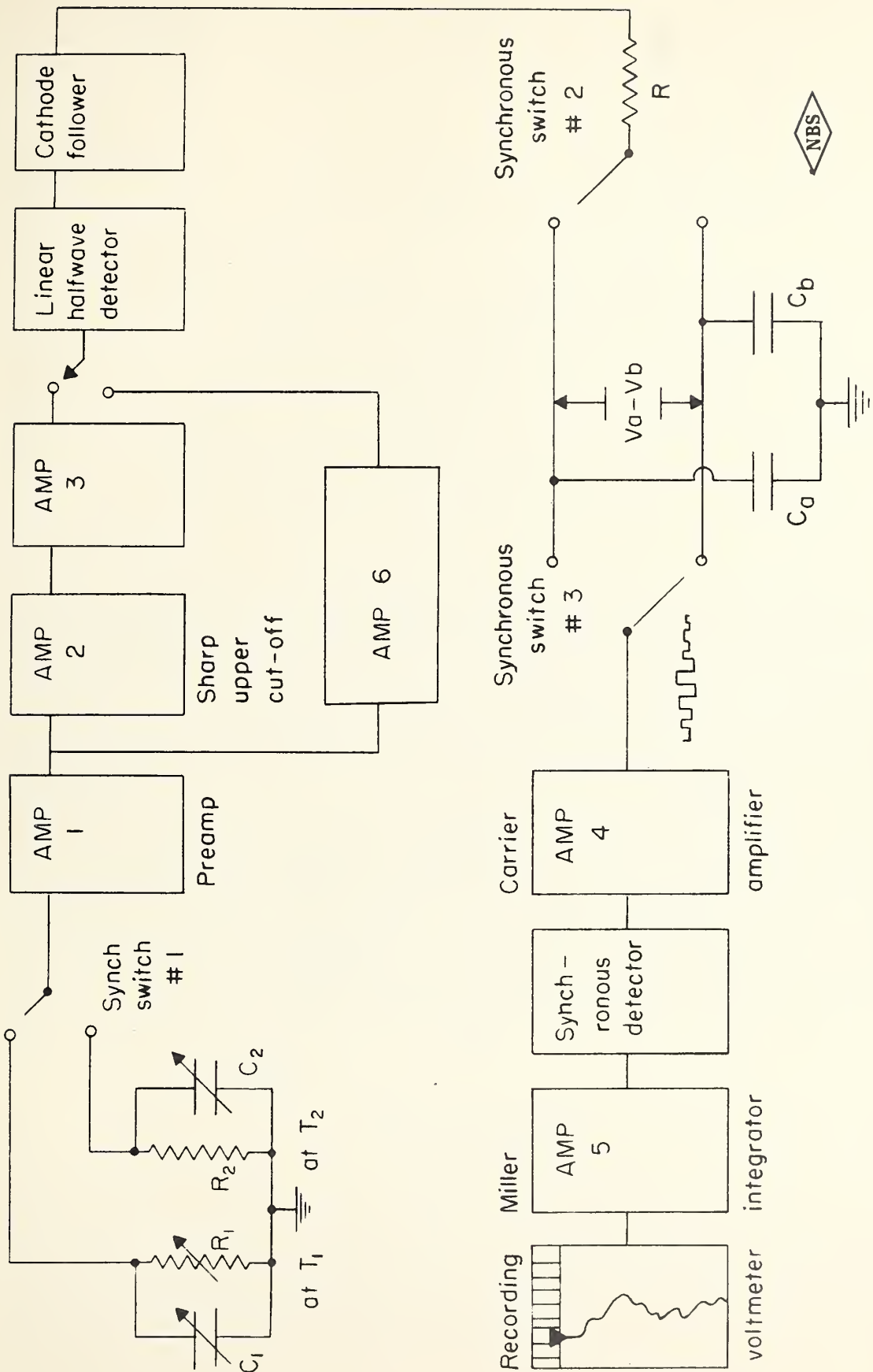


Figure 9.1

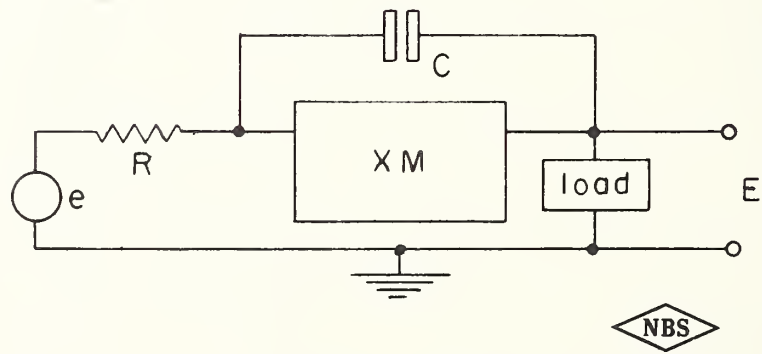
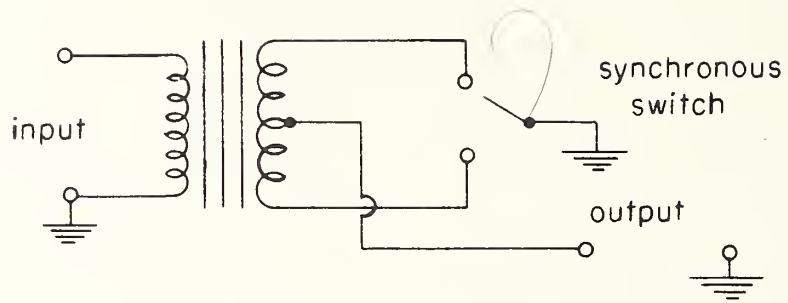


Figure 9.2 - 9.3

10. The Pyrometry Laboratory

John P. Evans

A. Since September, 1951, research and development work in the pyrometry laboratory has been centered around the projects listed below. These projects, except for the development of a new base-metal thermocouple which was sponsored by the U. S. Naval Engineering Experiment Station, were unsponsored.

1. Tantalum Tube Furnace: A furnace for general laboratory use consisting of a resistively heated tantalum tube insulated by tantalum and nichrome foil has been constructed. Provisions are made to operate the furnace in a vacuum or in an inert atmosphere. During initial runs to 1700°C, oil from the diffusion pump condensed on the water cooled walls of the furnace so that it was necessary to introduce a refrigerated baffle in the system between the pump and the furnace. The furnace will be used to determine the temperature-emf relations for high temperature thermocouple materials. It is so designed that temperatures may be measured with an optical pyrometer. The furnace is designed to attain temperatures of about 2500°C.

2. Copper Black Comparator Furnace: A furnace, consisting of an electrically heated copper block containing a number of wells, has been constructed for the intercomparison of platinum resistance thermometers and platinum versus platinum-rhodium thermocouples. The furnace is designed to operate in a vacuum or with an inert atmosphere. Longitudinal thermal gradients are minimized by heated end blocks and temperature differences between the various wells are not more than 0.01°C. The furnace has been operated to the freezing point of antimony (630.5°C) and has proven satisfactory for the primary calibration of thermocouples.

3. Black-body Radiation Source: The black-body radiator, consisting of an inductively heated graphite tube insulated by lamp black, has been used to determine the response of a photoelectric recording monochromator up to 2300°C. A neutral atmosphere of argon was found to give the best results. An adapter is being constructed to permit the calibration of total radiation pyrometers up to a temperature of 2300°C. Incorporated in the adapter is a gas tight chamber so that the effect of various types of atmospheres interposed in the path of radiation may be studied easily. Temperatures will be determined with an optical pyrometer.

4. Modified 1913 Reference Tables for Iron-Constantan Thermocouples:

An investigation was made of the characteristics of iron-constantan thermocouples typical of those being supplied to reproduce the standard temperature-emf relationship that was established commercially in 1913. Using the calibration of the thermocouple that most nearly matched the 1913 reference table over the range to which iron-constantan thermocouples usually are limited, a slightly different temperature-emf relationship was derived which is more nearly realizable by commercially available materials. [R. J. Rorrucini and H. Shenker, J. Res. N.B.S. 50, 229 (1953)].

5. Development of a New Base-Metal Thermocouple: Alumel wire, in chromel-alumel thermocouples, has failed in applications in which it was exposed to atmospheres containing sulfur or in which it was subjected to severe vibrations at high temperatures. Such failure has been ascribed to intergranular corrosion. A material to replace the alumel wire of chromel-alumel thermocouples was sought. It was found that a pencil-type chromel-alumel thermocouple is suitable for use in atmospheres containing sulfur up to 2000°F provided a silver shield is not used. A 310 stainless steel versus alloy 242 thermocouple is suitable for applications where severe vibrations or atmospheres containing sulfur are encountered.

6. Annealing of Platinum for Thermometry: Experiments were performed on the annealing of platinum wire in which the coefficient of resistance and thermal emf were used as criteria of the physical state of the metal. It was found that the platinum wire of the highest purity almost completely recovers its electrical properties at a temperature as low as 300°C, although a slight further recovery occurs with increase of annealing temperature up to 1450°C. On quenching heated wires in various gaseous media, changes in the electrical properties occur that are greater the more rapid the quenching and that are similar to the effect of strain. The electrical properties of dilute alloys of gold, silver, and copper in platinum were measured. Contrary to prediction, the copper and silver alloys were thermoelectrically positive to platinum at ordinary temperatures. Thus far, no impurity other than gold has been found to lower the thermoelectric power of platinum. [R. J. Corruccini, J. Res. N.B.S. 47, 94 (1951)].

B. Under consideration for future investigation are the following items. Only preliminary work has been done and these items are listed to show the fields in which interest lies.

1. High Temperature Thermocouples: The tantalum tube furnace described above (A-1) will furnish a means for calibrating very high temperature thermocouple materials, such as iridium vs. iridium-rhodium. The temperature-emf relationship for tungsten vs. tantalum and tungsten vs. molybdenum will be investigated first, and these materials will then possibly be used as intermediaries in the calibration of the iridium vs. iridium-rhodium.

2. Photoelectric Pyrometer: A means of replacing visual observation by photoelectric detection in the disappearing filament type optical pyrometer has been studied and appears feasible. The field of view would be scanned by a vibrating mirror and the image projected on a photomultiplier tube. The output signal of the tube would be used to detect a mismatch in brightness between the standard pyrometer lamp and the target area. The detector unit would be designed as an attachment to the laboratory standard optical pyrometer and little modification in the present instrument would be required.

11. Thermal Conductivities at High Temperatures

D. C. Ginnings and R. L. Nuttall

The thermal conductivity program consists of two parts, (1), the measurements on gases up to 500°C and 100 atmospheres pressure and (2), the measurements on liquids and solids up to 1000°C and one atmosphere pressure.

1. Gases: It was the purpose in these measurements to obtain as high an accuracy as possible at these high temperatures and pressures. The method used longitudinal heat flow downward from a "hot plate" through a thin (0.5mm) gas space to a "cold plate". A "guard ring" was used to protect the hot plate from heat flow other than to the cold plate. The heat transfer by radiation is accounted for by a "blank" experiment with the apparatus evacuated. The use of bright silver surfaces throughout minimizes radiation heat transfer. The apparatus used for these measurements has several advantages in precision work over other apparatus used in this field. First, using linear heat flow downward avoids the possibility of convection errors which may exist in radial heat flow. Second, the use of platinum resistance thermometers gives a temperature scale which is independent of the thermoelectric power of any thermocouples. Third, no spacer is used between the hot plate and the cold plate, the spacing between the two plates being determined in place by an absolute capacitance method.

The apparatus has been completed after many difficulties of which probably the most troublesome has been contamination of the platinum resistance thermometers in the blank experiments (evacuated) near 500°C. In spite of the difficulties, satisfactory conductivity measurements have been completed on pure nitrogen gas up to 500°C and 100 atmospheres pressure. These measurements are now being written up for publication. This program was supported initially by the National Advisory Committee for Aeronautics and later by the National Bureau of Standards.

2. Liquids and Solids: This program, sponsored by the Wright Air Development Center, was intended originally for measurements on liquids at high temperatures but because the apparatus was also suitable for measurements on solids, measurements have been made on two solids. The program can be divided into two parts, (a) the measurements on liquids and solids having relatively high thermal conductivities, and (b), the measurements on liquids having moderately low thermal conductivities.

a. Apparatus for high-conductivity liquids and solids.

This apparatus uses longitudinal heat flow downward through either a solid rod or a tube containing liquid. Heat is introduced electrically at the top of the sample and the resulting temperature gradient in the sample is measured by platinum vs. platinum-rhodium thermocouples. Radial heat loss from the sample is minimized by (1) providing a "guard" surrounding the sample with the same temperature gradient as the sample, and (2), providing as good insulation as possible between the sample and the guard. If a liquid sample is to be used, it is contained in a tube and a "blank" experiment must be made with no liquid in the tube to account for heat flow down the tube. This apparatus has been used on two solids, namely on molybdenum and molybdenum disilicide, the latter up to 800°C.

b. Apparatus for low thermal conductivity liquids

For these measurements, a radial heat flow apparatus is now under construction. The heat will flow through a thin layer (1/16") of the liquid which is contained between two coaxial silver cylinders. Calculations indicate that convection in this thin layer should be negligible. Temperatures will be measured by platinum vs. platinum-rhodium thermocouples. The upper temperature limit of this apparatus will be 900°C.

12. Heat Capacities at High Temperatures

T. B. Douglas and E. D. West

1. Drop Method

The NBS program for the measurement of heat capacities at high temperatures (up to 900°C, the limit of the present apparatus) emphasizes the highest accuracy compatible with the purity of the materials measured. Using apparatus which was developed at this Bureau and which is generally regarded as the most accurate of its type, the "drop" method has been used here continuously for the past nine years.

These measurements of heat capacity have served several different purposes. The results on aluminum oxide (synthetic sapphire) and n-heptane, two of the materials recommended by the U. S. Calorimetry Conference as standards of heat capacity in the high-temperature range, will be described in detail in publications to appear in the near future in Journal Research NBS. In addition, accurate measurements have been made on a number of materials that are useful as heat-transfer media at high temperatures (such as liquid salt mixtures and liquid alloys), and on certain solids useful because of their resistance to corrosion at high temperatures (such as molybdenum disilicide and several transition-metal alloys). Many of these results have been used also to evaluate critically and correlate the thermodynamic properties of these substances.

A previous report (NBS Report No. 1123, "Technical Report on High Temperature Thermodynamics") describes some of the work done up to the date of its publication, 1951. The publications listed below cover most of the unclassified work done since. In addition, abstracts of a few examples are included.

2. Adiabatic Method

The apparatus at NBS for high temperature "drop" calorimetry is being augmented by an adiabatic calorimeter designed to measure heat capacity and heats of transition in the range 30 to 600°C with an accuracy of a few tenths of a per cent. This calorimeter will be used for materials which do not easily reach reproducible states at the ice point and are therefore difficult or impossible to investigate with the drop calorimeter. It offers the advantage that measurements can be made over small temperature intervals, permitting a more detailed determination of heats of transition and rapidly changing heat capacities. The first work will be done on sulfur, which assumes various solid states at 0°C, depending on the temperature of the liquid before quenching.

The calorimeter consists of an inner sample container of suitable material screwed to a heavy silver ring which also supports three thin silver shields. The shields reduce radiative heat transfer and attenuate temperature gradients on the container so that the outer shield presents the same surface temperature distribution to the surroundings whether the container is full or empty. Heaters and thermocouples are attached to the silver ring. The absolute temperature is measured with a platinum resistance thermometer placed in the center of the calorimeter.

The calorimeter is surrounded by a jacket consisting of a similar system of four thin silver shields attached to a heavy silver ring whose temperature is matched to that of the silver ring in the calorimeter by means of a ten junction thermopile. The heat accounting method will depend not on eliminating all significant temperature gradients but on matching in empty or "blank" experiments the small gradients produced in the experiments with the container filled. Since heat transfer in the experimental range is largely by radiation, the apparatus will not be evacuated but will be operated in an argon atmosphere.

The bulk of the heat lost to the room will be supplied by nichrome heaters fixed in a closed aluminum cylinder surrounded by insulation.

The major parts of the apparatus have been built in the shop and assembly has been started. Auxiliary equipment for measuring electric power, time, and temperature and for evacuating the container has been set up. It is estimated that assembly of the apparatus will be completed and measurements made on sulfur in 1954.

Recent Publications

Heat capacity standards for the range 14 to 1200°K (D.C. Ginnings and G. T. Furukawa), Jour. Amer. Chem. Soc. 75, 522, 6359 (1953).

**Calorimetric determination of the half-life of polonium (D. C. Ginnings, A. F. Ball, and D. T. Vier¹), J. Research NBS 50, 75 (1953).

**Heat capacity of potassium and three potassium-sodium alloys between 0° and 800°, the triple point and heat of fusion of potassium (T. B. Douglas, A. F. Ball, D. C. Ginnings, and W. D. Davis²), Jour. Amer. Chem. Soc. 74, 2472 (1952).

*The heat capacity of lithium fluoride from 0° to 900°C (T. B. Douglas and J. L. Dever), Wright Air Development Center Technical Report 53-201, Part 1 (1953).

**A cryoscopic study of the solubility of uranium in liquid sodium at 97.8°C (T. B. Douglas), AEC Document 3254 (1951); J. Research NBS (1954).

*The heat capacity of anhydrous sodium hydroxide from 0° to 700°C (T. B. Douglas and J. L. Dever), Wright Air Development Center Technical Report 53-201, Part 2 (1953).

*The heat capacity of molybdenum disilicide from 0° to 900°C (T. B. Douglas and W. M. Logan), Wright Air Development Center Technical Report 53-201, Part 3 (1953).

Heat capacity of four alloys: Nichrome V and Stainless Steels types 347 and 446, 0° to 900°C; Monel, 0° to 300°C (T. B. Douglas and J. L. Dever), NBS Report 2302 (1953).

**Heat capacity of the eutectic mixture of lithium chloride and potassium chloride from the eutectic temperature to 800°C (T. B. Douglas and J. L. Dever), NBS Report 2303 (1953).

**The heat capacity of lead from 0° to 900°, and the heat of fusion; the heat capacity of the lead-bismuth eutectic alloy from 150° to 800°C (T. B. Douglas and J. L. Dever), NBS Report 2544 (1953).

**The heat capacity of lithium from 25° to 900°C; the heat of fusion and the triple point; thermodynamic properties of the solid and liquid (T. B. Douglas, L. F. Epstein², J. L. Dever, and W. H. Howland²), NBS Report 2879 (1953).

*Sponsored by the U. S. Air Force, Wright Air Development Center.

**Sponsored by the U. S. Atomic Energy Commission.

¹Los Alamos Scientific Laboratory, University of California, Los Alamos, N. M.

²Knolls Atomic Power Laboratory, General Electric Co., Schenectady, N. Y.

Calorimetric Properties of Normal Heptane from 0° to 520°K.

T.B. Douglas, G.T. Furukawa, R.E. McCoskey, and A.F. Ball

Precise measurements of the heat capacity of solid and liquid n-heptane from 20° to 523°K are described. An adiabatic calorimeter, with which was determined also the triple point and heat of fusion, was used from 20° to 370°K, whereas a drop method was used with a Bunsen ice calorimeter from 273° to 523°K. These two series of heat-capacity measurements and three other series of independent values show a maximum difference of approximately 0.25 percent in the range 50° to 370°K. Besides the heat capacity, the enthalpy, entropy, and Gibbs free energy of the solid and liquid at saturation pressures from 0° to 520°K are derived and tabulated. The same properties of the ideal gas from 298° to 470°K also are derived by making use of published precise measurements of gaseous heat capacity, heat of vaporization, and the normal boiling point. Interconsistency of the values of the various thermal properties is shown by the fact that the vapor pressures calculated from these values agree with those precisely measured by other investigators between 299° and 372°K to within ± 0.1 percent.

The Heat Capacity of Sodium Hydroxide from 0° to 700°C

(Sponsored by the U. S. Air Force, Wright Air Development Center)

T. B. Douglas and J. L. Dever

Samples of sodium hydroxide, whose purity as indicated by analyses was approximately 99.3 percent, were sealed in pure silver. Cryoscopic measurements indicated a transition temperature of 293°C. Using a drop method and a Bunsen ice calorimeter, the enthalpy change between 0° and each of eleven temperatures up to 700°C was measured. With reasonable simplifying assumptions, the thermal measurements near the freezing point were used to correct for the impurity, giving values for the melting point and heats of transition and fusion of the pure compound. The heat capacity derived for the liquid is estimated to be correct within ± 2 percent. Values of heat capacity, entropy, relative enthalpy, and relative free energy are tabulated at regular intervals from 298° to 1000°K.

The Heat Capacity of Sodium Hydroxide from 0° to 700°C

(Sponsored by the U.S. Air Force, Wright Air Development Center)

T.B. Douglas and J. L. Dever

Samples of sodium hydroxide, whose purity as indicated by analyses was approximately 99.3 percent, were sealed in pure silver. Cryoscopic measurements indicated a transition temperature of 293°C. Using a drop method and a Bunsen ice calorimeter, the enthalpy change between 0° and each of eleven temperatures up to 700°C was measured. With reasonable simplifying assumptions, the thermal measurements near the freezing point were used to correct for the impurity, giving values for the melting point and heats of transition and fusion of the pure compound. The heat capacity derived for the liquid is estimated to be correct within ± 2 percent. Values of heat capacity, entropy, relative enthalpy, and relative free energy are tabulated at regular intervals from 298° to 1000°K.

Thermodynamics of the Liquid System Sodium-Potassium from 0° to 800°C

T. B. Douglas

The available published data on the solid-liquid and liquid-vapor phase equilibria are combined with heat-capacity data determined recently at the National Bureau of Standards. From these are derived equations of moderate accuracy for the free energy, heat content, and entropy of liquid sodium-potassium solutions, relative to the pure liquid elements, at one atmosphere pressure and over the temperature range 0° to 800°C. Numerical uncertainties are estimated and assigned to the results. These properties can all be derived simply from the equation

$$F - F_{\text{ideal}} = \left[(1201 - 18200/T - 0.692T) - (1282 - 1.192T) N_k + (1183 - 1.102T) N_k^2 \right] N_{\text{Na}} N_k,$$

which gives the free energy at T°K (in calories per gram-atom of solution) in excess of that of a hypothetical ideal solution of the same composition (atomic fractions N_{Na} and N_k). The free-energy deviations from ideality, which are positive throughout this temperature range, are fairly large near 0°C. The calorimetrically measured values of one recent investigation elsewhere agree closely with the calculated heats of solution.

Heat Capacity of Lithium from 25° to 900°C.

The Triple Point and Heat of Fusion.

Thermodynamic Properties of the Solid and Liquid.

(Sponsored by the U. S. Atomic Energy Commission)

T.B. Douglas, L.F. Epstein, J.L. Dever, and W.H. Howland

Lithium was distilled at 650°-700°C in vacuum and sealed in stainless steel type 347. From chemical analysis the purity of the first sample was 99.98 atomic % and that of the second sample, obtained with the still in vacuum, was approximately 99.99 atomic %. The melting curves, which are consistent with these analyses, gave a triple point of 180.54°C. Using a Bunsen ice calorimeter and a drop method, the relative enthalpy was measured from 0 to 900°, yielding values of the heat capacity of the liquid estimated to be accurate to ± 0.3 percent. The observations were combined with adjusted published low-temperature heat capacities and vapor pressures at high temperatures, with use of the Sackur-Tetrode equation, to determine the thermodynamic properties of the solid and liquid from 298° to 1200°K. A value of 38800 cal. per gram-atom was derived for the cohesive energy of the metal.

Thermodynamics of the Liquid System Sodium-Potassium from 0° to 800°C

T. B. Douglas

The available published data on the solid-liquid and liquid-vapor phase equilibria are combined with heat-capacity data determined recently at the National Bureau of Standards. From these are derived equations of moderate accuracy for the free energy, heat content, and entropy of liquid sodium-potassium solutions, relative to the pure liquid elements, at one atmosphere pressure and over the temperature range 0° to 800°C. Numerical uncertainties are estimated and assigned to the results. These properties can all be derived simply from the equation.

$$F - F_{\text{ideal}} = \left[(1201 - 18200/T - 0.692T) \right. \\ - (1282 - 1.192T) N_k + (1183 \\ \left. - 1.102T) N_k^2 \right] N_{\text{Na}} N_k,$$

which gives the free energy at T°K (in calories per gram-atom of solution) in excess of that of a hypothetical ideal solution of the same composition (atomic fractions N_{Na} and N_k). The free-energy deviations from ideality, which are positive throughout this temperature range, are fairly large near 0°C. The calorimetrically measured values of one recent investigation elsewhere agree closely with the calculated heats of solution.

THE NATIONAL BUREAU OF STANDARDS

Functions and Activities

The functions of the National Bureau of Standards are set forth in the Act of Congress, March 3, 1901, as amended by Congress in Public Law 619, 1950. These include the development and maintenance of the national standards of measurement and the provision of means and methods for making measurements consistent with these standards; the determination of physical constants and properties of materials; the development of methods and instruments for testing materials, devices, and structures; advisory services to Government Agencies on scientific and technical problems; invention and development of devices to serve special needs of the Government; and the development of standard practices, codes, and specifications. The work includes basic and applied research, development, engineering, instrumentation, testing, evaluation, calibration services, and various consultation and information services. A major portion of the Bureau's work is performed for other Government Agencies, particularly the Department of Defense and the Atomic Energy Commission. The scope of activities is suggested by the listing of divisions and sections on the inside of the front cover.

Reports and Publications

The results of the Bureau's work take the form of either actual equipment and devices or published papers and reports. Reports are issued to the sponsoring agency of a particular project or program. Published papers appear either in the Bureau's own series of publications or in the journals of professional and scientific societies. The Bureau itself publishes three monthly periodicals, available from the Government Printing Office: The Journal of Research, which presents complete papers reporting technical investigations; the Technical News Bulletin, which presents summary and preliminary reports on work in progress; and Basic Radio Propagation Predictions, which provides data for determining the best frequencies to use for radio communications throughout the world. There are also five series of nonperiodical publications: The Applied Mathematics Series, Circulars, Handbooks, Building Materials and Structures Reports, and Miscellaneous Publications.

Information on the Bureau's publications can be found in NBS Circular 460, Publications of the National Bureau of Standards (\$1.25) and its Supplement (\$0.75), available from the Superintendent of Documents, Government Printing Office. Inquiries regarding the Bureau's reports and publications should be addressed to the Office of Scientific Publications, National Bureau of Standards, Washington 25, D. C.

9

